GEOLOGICAL HAZARDS AND ENGINEERING GEOLOGY MAPS
OF HOSAINA NB 37-2

EXPLANATORY NOTES

Debebe Nida and **Yekoye Bizuye** *(Compilers)*
Vladislav Rapprich *(Editor)*

The Main Project Partners

The Czech Development Agency (CzDA)
cooperates with the Ministry of Foreign Affairs on the establishment of an institutional framework of Czech development cooperation and actively participates in the creation and financing of development cooperation programs between the Czech Republic and partner countries.
www.czda.cz

The Geological Survey of Ethiopia (GSE)
is accountable to the Ministry of Mines and Energy, collects and assesses geology, geological engineering and hydrogeology data for publication. The project beneficiary.
www.gse.gov.et

The Czech Geological Survey
collects data and information on geology and processes it for political, economical and environmental management. The main contractor.
www.geology.cz

AQUATEST a.s.
is a Czech consulting and engineering company in water management and environmental protection. The main subcontractor.
www.aquatest.cz

Acknowledgment

Contents

List of Figures

List of Tables

Under Separate Cover *(attached CD)*

Maps:
Engineering geology map of Hosaina NB 37-2 – full size and A3 size
Geological hazards map of Hosaina NB 37-2 – full size and A3 size

Extended Summary

The Hosaina map sheet (NB 37-2) at the scale of 1:250,000 is located in Southeastern Ethiopia covering an area of 17,281 km². The area is a part of the Oromia and Southern Nations, Nationality and People (SNNPR) regional states, its population exceeds 5.3 million people and it is moderately to highly cultivated.

Elevation in the study area copies its main geomorphological parts represented by the Rift Valley, Eastern Highlands, Western Highlands and gorges of Gibe and Omo. Elevations vary between 1,580 and 1,700 m a.s.l. on the rift valley floor, whereas along the escarpment the elevation rises to about 2,600 m a.s.l., and the edge of the plateau is flanged by high volcanic complexes with elevation from 2,970 to 3,550 m a.s.l. The area is part of the Omo-Gibe, Wabe Shebele and Rift Valley Lakes basins. The rainy season is bimodal from April to May and from July to September; the annual mean rainfall was adopted as being 1,100 mm/year for the Hosaina area. Winds blow predominantly from the west. There are three principal permanent rivers (Bilate, Djidu, Katar) and large lakes include Ziway, Langano, Abijata, Shalla and Hawasa.

The area investigated is influenced by endogenous as well as exogenous hazardous geological phenomena and processes. The endogenous geological hazards comprise seismic and volcanic activity. The seismic activity is associated with the Main Ethiopian Rift manifested by a network of normal faults. Unfortunately, there is lack of data on the precise location of earthquakes reaching a magnitude of up to 6.5. For this reason, seismically active faults cannot be identified within the observed tectonic network. Earthquakes would cause damage to buildings constructed in areas with thick accumulations of sediments. Large volumes of soft rock amplify seismic effects. The volcanic activity is represented by composite ("central") rhyolitic volcanoes and a field of monogenetic basaltic volcanoes. Activity of the rhyolitic volcanoes and volcanic complexes – Alutu and Corbetti (consisting of Chabi and Wendo Koshe cones) – includes effusions of obsidian lavas and explosive eruptions emitting large amounts of pumice. Monogenetic volcanic fields, such as Butajira volcanic field, East Ziway volcanic field, Bilate volcanic field and Hawasa-Shalla volcanic field, comprise numerous basaltic scoria cones with associated lava flows and, much less frequently, also maars. Individual eruptions affect a limited area but these cones are scattered and widespread. The main problem in assessing the volcanic hazard remains the critical lack of historical or geochronological data on Holocene eruptions. None of the volcanoes on the Hosaina map sheet have a historical record of eruptions and prior to our work no Holocene eruption had been analytically dated. The radiocarbon analysis of the paleosoil buried by the Wendo Koshe pumice suggests this rhyolitic Plinian eruption took place in about 400 BC.

Tectonic activity creates dynamic morphology with steep scarps prone to rock-fall, toppling, debris flows and landslides. Zones with frequent rock-fall features follow the scarps of the Main

Ethiopian Rift. The zone affected strongly by rock-fall is associated with the southern slope of Weransa Ridge between Shashemene and Hawasa. Two pronounced debris flows occurred on the western scarps of the Main Ethiopian Rift about 30 km north of Hosaina. The most extensive landslide area can be found in the Gibe Gorge. Numerous smaller landslides were documented on the scarps around Wendo Genet. One of the most serious environmental problems of Ethiopia remains erosion and degradation of soil. Areas with intense soil erosion were mapped and features triggering and enabling the erosion identified. Light sandy soils developed upon Late Pleistocene rhyolitic ignimbrites are extremely prone to erosion. Large areas affected by sheet erosion occur in the western part of the rift and around Pleistocene calderas. Streams and creeks with high flow rate are frequently responsible for gully erosion, namely during the rainy season. In addition, alluvial fans of larger streams and rivers are characterized by rapid sedimentation in particular during the rainy season. Lowlands and depressions frequently formed in calderas or on tectonically subsided blocks lacking drainage may be affected by inundations. Such areas can be found in Cheleleka and on the foothills of the western scarp of the Main Ethiopian Rift.

Rhyolitic volcanic rocks which erupted along the Main Ethiopian Rift are rich in fluorine. As the fluorine is not fixed in stable minerals (e.g., apatite), it is easily leachable, especially from pumice deposits with a large reaction surface. As a consequence, water resources in thick Holocene pumiceous deposits are strongly contaminated by fluorine, causing fluorosis if consumed.

Introduction

Background

Nature manifests its destructive power in many ways in Southern Ethiopia. There are not many regions in the world where such a wide spectrum of natural hazards is present. Ethiopia is crosscut by the Main Ethiopian Rift - a zone of active spreading associated with intense seismic and volcanic activity. The fault scarps are prone to slope deformations and loose pyroclastic deposits which are easily eroded. Ethiopia is also endangered by sheet erosion and several areas within the rift lacking drainage are prone to inundation. The topography together with the increasing population aggravates the environmental problems. It is therefore important to compile a map of natural hazards to be able to propose and implement appropriate measures to protect inhabitants and infrastructure. In this context a geohazard investigation was performed in the area of the Hosaina sheet, which comprises most of the types of geological hazards, in 2012 and 2013 by the Geological Survey of Ethiopia with the assistance of experts from the Czech Geological Survey. The work was conducted in the framework of bilateral cooperation between the Czech and Ethiopian governments, where the participation of the Czech experts was financed by the Czech Development Agency in the framework of the Czech Republic Development Assistance Program. Participation of the Ethiopian professionals was financed by the Ethiopian government. This report deals with the assessment of the characteristics of engineering geology and geological hazards acquired during the desk and field work and discussion between stakeholders and the joint Czech-Ethiopian team of professionals.

Objective and Scope

Geological hazards endanger most of Ethiopia's population. To enable ongoing development of the country, better knowledge of geological hazards and the limits they represent for land-use and construction is crucially needed. The main objectives of the study for geohazard mapping were to identify individual types of geological hazards and to map the extents of zones influenced by these hazardous processes. The work covers the interpretation of aerial photos and satellite images, meteorological and geological data analysis, collection of representative rock and soil samples for geological, structural and geochronological analysis, and evaluation of geohazard distribution within the area. The geohazard investigation of the Hosaina map sheet is part of the project entitled "**Capacity building in Environmental Geology – Mapping of Geo-risks including Hydrogeological Condition in Dila and Hosaina areas, Ethiopia**" that was conducted between 2012 and 2013 to reduce undesirable effects of geological processes on human society and the environment.

In order to achieve the main objectives, a number of tasks were undertaken at different levels having unique specific objectives that led to the final compilation of the geohazard map and completion of the explanatory notes. These specific objectives are as follows:

- To identify young faults with the potential of ongoing seismic activity and thick accumulations of sediments potentially amplifying seismic effects
- To identify potentially hazardous volcanoes, areas endangered by these volcanoes, their eruptive styles, eruption frequencies and the time since their last eruption
- To define zones prone to slope deformation
- To define areas endangered by sheet erosion and identify the principal features triggering the degradation of soil
- To identify the source of fluorine in the groundwater

The desktop study and field work were carried out by mixed groups of Ethiopian and Czech geologists. The geochronological analyses were carried out in Hungary and Poland. Final assessment and publication of the map were carried out by a joint Czech-Ethiopian team of professionals. The names of participating experts are shown in Tab. 1.1.

Tab. 1.1 Team members

Name	Institution	Participation field
Vladislav Rapprich	Czech Geological Survey	Volcanology, project leader, main editor
Leta Alemayehu	Geological Survey of Ethiopia	Engineering geology, project coordinator
Petr Kycl	Czech Geological Survey	Engineering geology, landslides
Yekoye Bizuye	Geological Survey of Ethiopia	Engineering geology, compiler of the engineering geology map
Tomáš Hroch	Czech Geological Survey	Geomorphology, erosion and sedimentation
Kryštof Verner	Czech Geological Survey	Structural geology
Jiří Málek	Institute of Rock Structure and Mechanics, Czech Academy of Sciences v.v.i.	Seismology
Veronika Kopačková	Czech Geological Survey	Remote sensing
Jan Mišurec	Czech Geological Survey	Remote sensing
David Čížek	Czech Geological Survey	GIS
Petra Hejtmánková	Czech Geological Survey	GIS
Jiří Šíma	AQUATEST a.s.	Hydrogeology
Craig Hampson	AQUATEST a.s.	English editing
Debebe Nida	Geological Survey of Ethiopia	Engineering geology
Yewubinesh Bekele	Geological Survey of Ethiopia	Engineering geology
Tsigehana Tesema	Geological Survey of Ethiopia	Geomorphology
Ezra Tadesse	Geological Survey of Ethiopia	Geophysics
Firdawok Legesa	Geological Survey of Ethiopia	Geophysics
Habtamu Bewket	Geological Survey of Ethiopia	Structural geology
Zoltán Pécskay	Hungarian Academy of Sciences	Geochronology

1. *Basic Characteristics of the Area*

1.1 Location and Accessibility

The study area is located in Southern Ethiopia, in the part of the Main Ethiopian Rift and adjacent eastern and western Ethiopian Plateau. Geographically, the study area is bounded from north to south by latitudes 8°00′ N and 7°00′ N, and from west to east by longitudes 37°30′ E and 39°00′ E. The area covers more than 17 thousand square kilometers of the topographic map sheet of Hosaina (NB 37-2) at a scale of 1:250,000. The location of the map is illustrated in Fig. 1.1. The sheet is bounded by the Akaki Beseka sheet to the north, the Asela sheet to the east, Dila sheet to the south and by Jima sheet to the west.
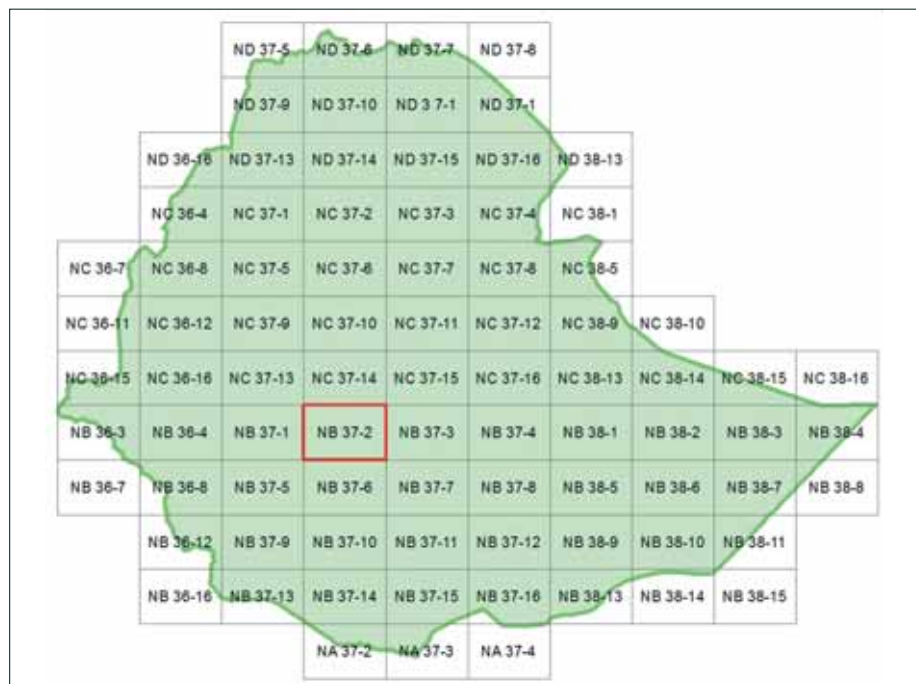
Fig. 1.1 Location map
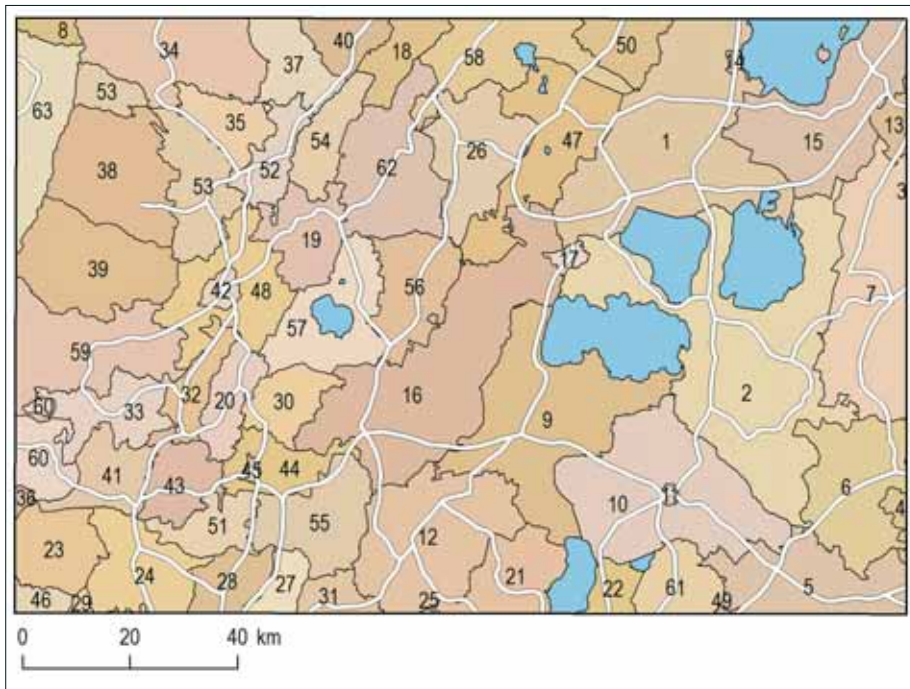
Fig. 1.2 Administrative zones and main roads:
1) Adami Tulu Jido Kombolcha; 2) Arsi Negele; 3) Digeluna Tijo; 4) Gedeb Asasa; 5) Kofele; 6) Kore; 7) Munesa; 8) Sekoru; 9) Shala; 10) Shashemene; 11) Shashemene Town; 12) Siraro; 13) Tiyo; 14) Ziway Town; 15) Ziway Dgda; 16) Alaba; 17) Alge Tec College; 18) Alicho Woriro; 19) Analemmo; 20) Angacha; 21) Hawasa Zuriya; 22) Hawasa Town; 23) Bolossa Bonibe; 24) Bolossa Sore; 25) Boricha; 26) Dalocha; 27) Damot Gale; 28) Damot Pulasa; 29) Damot Sore; 30) Daniboya; 31) Deguna Fango; 32) Doyo Gena; 33) Duna; 34) Enemor Ener; 35) Enidguagn; 36) Gena Bosa; 37) Geta; 38) Gibe; 39) Gombora; 40) Gumer; 41) Hadaro Tunito; 42) Hosaina; 43) Kacha Bira; 44, 45) Kedida Gamela; 46) Kindo Koyisha; 47) Lanifaro; 48) Lemmo; 49) Malga; 50) Mareqo; 51) Merab Badawocho; 52) Mirab Azernet Berbere; 53) Misha; 54) Misrak Azernet Berbere; 55) Misrak Badawocho; 56) Sankura; 57) Shashago; 58) Silite; 59) Soro; 60) Tibaro; 61) Wendo Genet; 62) Wilbareg; 63) Zeme Special.

The area can be accessed by the road connecting the capital city of Addis Ababa with Butajira – Hosaina – Sodo – Arba Minch and Mojo – Ziway – Shashemene – Hawasa – Dila and the main Nazareth – Assela – Shashemene asphalt roads. Other asphalt roads connect Butajira with Ziway, Shashemene – Alaba Kulito – Sodo and Wulbareg – Alaba Kulito. The all-weather gravel roads within the study area are in good condition and the area is accessible for mapping work at the scale of 1:250,000, except in the deep gorges of the Gibe Valley. Most of the central-eastern part (both rift floor and escarpment) up to Kubsa Mount can be accessed via the all-weather gravel road that branches off from the main Ziway – Shashemene asphalt road near Dole town and connects the towns of Goljota, Degaga and Kersa. Kersa is 49 km from the main asphalt road. The southwestern part of the area can be accessed via the main Hosaina – Sodo asphalt road.

The northwestern part, especially the Gibe River gorge is accessed through the all-weather road, starting from Hosaina to the north driving 22 km to reach Lera town which is situated on the western plateau. From Lera town to Kose further westward there is an 26 km all-weather road covering rolling topography. From Homecho down to Gibe River gorge there is a very difficult unpaved path.

Basic Characteristics of the Area

The Ethiopian Electric Power Authority constructed an asphalt road fromfrom Kose to the river for the Gibe hydropower project II and this road helps to access the river bed and to cross to the other side of the river section towards Fofa town. The main accessible roads are shown in Fig. 1.2.

1.2 Population and Settlements

The Hosaina map sheet is located within the Oromia and SNNP regional states. Most of the dwellers are Oromo people. Permanent settlement is concentrated along old asphalt roads, where the biggest towns Hawasa, Shashemene and Hosaina are located.

The eastern part of the study area is inhabited by Oromo people. Population settlement is mostly limited to the towns and villages. The western part of the study area is inhabited by different ethnic groups of the southern peoples. The northwest part is inhabited mostly by Muslim Siltis. The central western part is inhabited by Hadiyas and the south west is inhabited by Kembata people. The Amhara people are also found in the study area, mostly limited to the main towns of Ziway, Hosaina, Hawasa and Shashemene.

There are 11 Zones, 61 Weredas and Hawasa City Administration within the mapped area (Fig. 1.2); however, some are not located entirely within the boundary of the map sheet. The total Weredas population and the percentage of the area within the map sheets were used to calculate the total number of people living in the mapped area. Tab. 1.2 shows the population in the different Weredas within the mapped area.

Tab. 1.2 Population in the study area

| Region | Zone | Wereda | Wereda area in mapped area | | Total population | Assessed population in mapped area |
			[km²]	[%]		
Oromia	Arsi	Digluna Tijo	0.4	0.04	162,579	69
Oromia	Arsi	Munesa	646	60	192,628	116,159
Oromia	Arsi	Tiyo	60	10	100,237	9,932
Oromia	Arsi	Ziway/Town	11	100	53,841	53,841
Oromia	Arsi	Ziway Dugda	557	49	139,248	68,857
Oromia	East Shewa	Adami Tulu	980	90	164,234	147,067
Oromia	Jima	Sokoru	49	5	157,701	7,731
Oromia	West Arsi	Arsi Negele	1,281	100	303,223	303,223
Oromia	West Arsi	Gedeb Asasa	33	3	216,494	6,204
Oromia	West Arsi	Kofele	407	62	206,912	127,571
Oromia	West Arsi	Kore	430	86	119,643	102,575
Oromia	West Arsi	Shalla	758	100	17,277	17,277
Oromia	West Arsi	Shashemene Zuria	768	100	284,399	284,399
Oromia	West Arsi	Shashemene/ Town	11	100	123,877	123,877

Basic Characteristics of the Area

Tab. 1.2 Population in the study area (part 2)

Region	Zone	Wereda	Wereda area in mapped area		Total population	Assessed population in mapped area
			[km²]	[%]		
Oromia	West Arsi	Siraro	594	99	167,785	166,354
SNNP	Alaba Spec. Wereda	Alaba	995	100	270,892	270,892
SNNP	Hawasa C.A.	Hawasa C.A.	157	52	328,875	170,336
SNNP	Dawro	Genabosa	922	1	99,113	1,428
SNNP	Gurage	Enemorna Ener	915	48	192,907	93,270
SNNP	Gurage	Endegagn	151	100	56,291	56,291
SNNP	Gurage	Geta	202	95	79,284	75,716
SNNP	Gurage	Gumer	233	53	92,143	48,557
SNNP	Gurage	Mareko	252	61	75,098	45,855
SNNP	Hadiya	Analimo	224	100	82,651	82,651
SNNP	Hadiya	Duna	222	100	140,588	140,588
SNNP	Hadiya	Gibe	448	100	12,579	12,579
SNNP	Hadiya	Gomibora	462	96	106,321	101,986
SNNP	Hadiya	Hosaina	40	100	94,727	94,727
SNNP	Hadiya	Lemo	354	100	13,581	13,581
SNNP	Hadiya	Merab Badwacho	150	100	95,694	95,694
SNNP	Hadiya	Misha	363	100	146,592	146,592
SNNP	Hadiya	Misrak Badawacho	308	100	166,342	166,342
SNNP	Hadiya	Shashago	315	100	120,141	120,141
SNNP	Hadiya	Soro	706	63	219,159	137,374
SNNP	Kembata Tembaro	Angacha	153	100	101,991	101,991
SNNP	Kembata Tembaro	Deniboya	163	100	96,035	96,035
SNNP	Kembata Tembaro	Doyo Gena	131	100	91,186	91,186
SNNP	Kembata Tembaro	Hadero Tunito	190	100	117,282	117,282
SNNP	Kembata Tembaro	Kacha Bira	189	100	133,132	133,132

Tab. 1.2 Population in the study area (Part 3)

Region	Zone	Wereda	Wereda area in mapped area [km²]	Wereda area in mapped area [%]	Total population	Assessed population in mapped area
SNNP	Kembata Tembaro	Kedida Gamela	176	100	103,028	103,028
SNNP	Kembata Tembaro	Durame/Town	14	100	3,312	3,312
SNNP	Kembata Tembaro	Tembaro	340	47	122,126	57,618
SNNP	Sidama	Hawasa Zuria	305	78	142,085	111,388
SNNP	Sidama	Boricha	588	1	287,878	1,631
SNNP	Sidama	Malga	207	3	12,618	344
SNNP	Sidama	Wondo Genet	226	78	182,648	142,497
SNNP	Silti	Alicho Werero	263	52	105,736	55,243
SNNP	Silti	Dalocha	351	100	103,954	103,954
SNNP	Silti	Lanfuro	446	100	135,182	135,182
SNNP	Silti	Merab Azernet	151	100	68,746	68,746
SNNP	Silti	Misrak Azernet	168	100	5,792	5,792
SNNP	Silti	Sankura	277	100	97,502	97,502
SNNP	Silti	Silti	510	69	20,576	14,235
SNNP	Silti	Wulbareg	448	100	91,765	91,765
SNNP	Wolayta	Boloso Bonibe	272	82	100,626	82,481
SNNP	Wolayta	Boloso Sore	303	97	232,641	225,860
SNNP	Wolayta	Damot Gale	256	34	17,757	6,034
SNNP	Wolayta	Damot Pulasa	165	88	12,117	10,614
SNNP	Wolayta	Damot Sore	181	10	116,227	11,292
SNNP	Wolayta	Deguna Fanigo	402	21	110,854	23,447
SNNP	Wolayta	Kindo Koyisha	526	9	120,758	11,365
SNNP	Yem Spec. Wereda	Yem Spec. Wereda	648	46	93,789	43,209
Total						5,355,901

Source: Population by Zone, Central Statistics Authority Statistical Abstract (2012)

Basic Characteristics of the Area

Based on the data provided by the Central Statistics Authority, the total population is assumed to be 5,355,901; however, this figure could in reality be several thousand higher. The urban population comprises about 40 % (Hawasa with 328,875 inhabitants is the biggest urban settlement in the area) and the remaining 60 % of the population lives in rural areas. The population is increasing by 2.6 % in Oromia and 2.8 % in SNNPR, respectively. The life expectancy at birth is 49 years for males and 51 years for females (WHO, 2006). As in most developing countries, Ethiopia's main health problems are communicable diseases caused by poor sanitation and malnutrition. Mortality and morbidity data are based primarily on health facility records which show that the leading causes of hospital deaths are dysentery and gastroenteritis, tuberculosis, pneumonia, malnutrition and anemia, and liver diseases including hepatitis, tetanus, and malaria. The situation is complicated by the fact that Ethiopia's population mainly lives in rural areas (84 %) where access to healthcare is more complicated than in urban areas.

The majority of the rural population of the region practices crop production which is in some areas highly developed and commercial plantations are common. The agriculture in the SNNPR is small scale subsistence farming, producing products mostly for family consumption. The contribution of industry as well as services has increased over the last decade indicating the structural transformation of the economy from agriculture toward industry and services. Oromia made the largest industrial contribution to Ethiopia's economy, with an estimated 60 % of foreign exchange earnings. The largest proportion of Ethiopia's export commodities originates in Oromia, including the following products: coffee, oilseeds, leather products, fruits and vegetables, flowers, gold, etc.

1.3 Land Use and Land Cover

Poor land use practices, improper management systems and lack of appropriate soil conservation measures have played a major role in causing land degradation problems in the country. Because of the rugged terrain, the rates of soil erosion and land degradation in Ethiopia are high. Setegn (2010) mentions the soil depth of more than 34 % of the Ethiopian territory is already less than 35 cm, indicating that Ethiopia loses a large volume of fertile soil every year and the degradation of land through soil erosion is increasing at a high rate. The highlands and some part of Rift Valley floor are now so seriously eroded that they will no longer be economically productive in the foreseeable future.

The land and water resources are in danger due to the rapid growth of the population, deforestation and overgrazing, soil erosion, sediment deposition, storage capacity reduction, drainage and water logging, flooding, and pollutant transport. In recent years, there has been an increased concern over climate change caused by increasing concentrations of CO_2 and other trace gases in the atmosphere. Major effects of climate change include alterations in the hydrologic cycles and changes in water availability. Increased evaporation combined with changes in precipitation characteristics has the potential to affect runoff, frequency and intensity of floods and droughts, soil moisture, and water supplies for irrigation and generation of hydroelectric power.

The effect of human interference on the physical environment is great because the high population growth rate and migration have resulted in people searching for additional farmland by clearing the existing small patches of vegetation cover; farming is also practiced on slopes which aggravate the erosion rate. Sheet and gully types of soil erosion are mainly observed.

Land cover includes cultivated land (large scale farms and family farms with different rates of cultivation), vegetation (shrub lands and natural forest, grassland riparian vegetation, swamp), manmade features (urban or built-up areas), rocky outcrops, bare sand/soil and water bodies.

Basic Characteristics of the Area
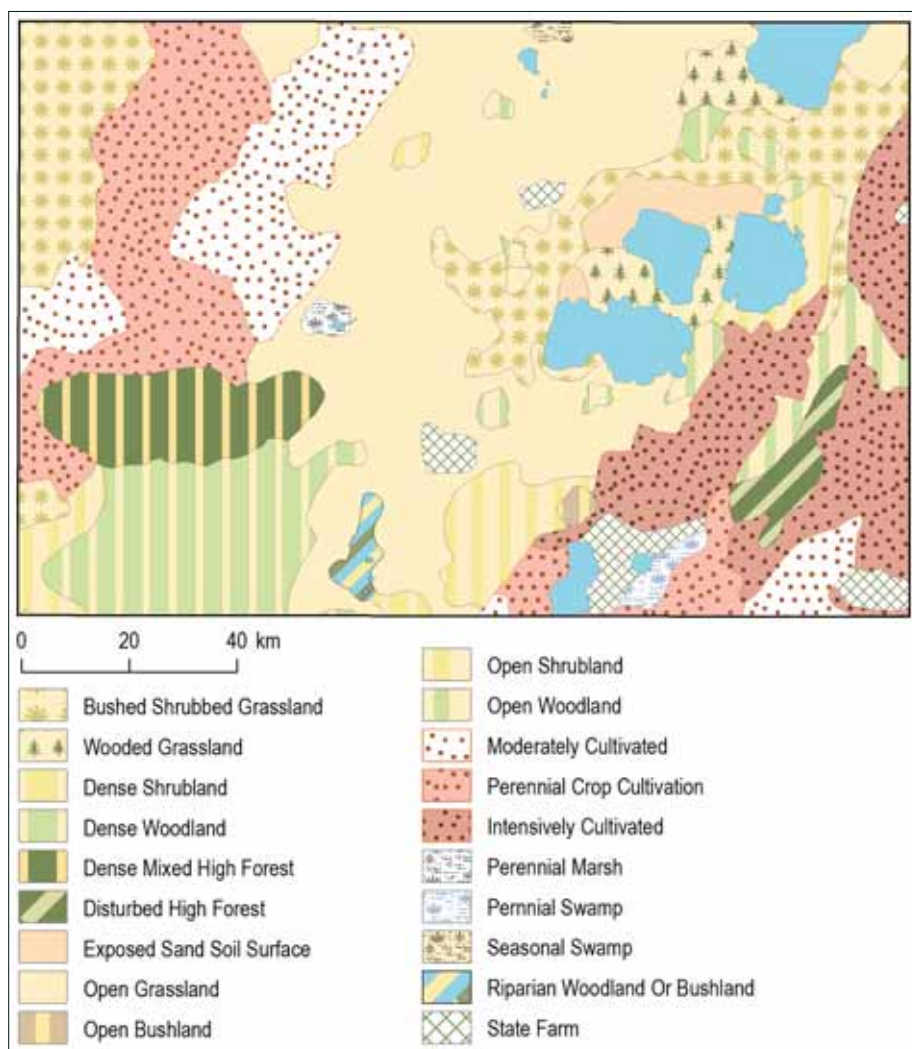
Fig. 1.3 Land cover

Land cover is shown in Fig. 1.3. The land use is characterized according to FAO (2000) by the arrangements, activities and inputs people undertake in a certain land cover type to produce, change or maintain it.

Land use information is derived from land cover maps and provides land use classes. It shows that only a negligible part of the Hosaina area is not cultivated. The floor of the Rift Valley is used for irrigation to plant different types of vegetation and fruits. This land use classified as "Intensive Annual Crop Production" describes all the areas where the cultivation of annual crops (cereals, pulses, oilseeds and vegetables) takes place. "Intensive Perenial and Annual Crop Production"
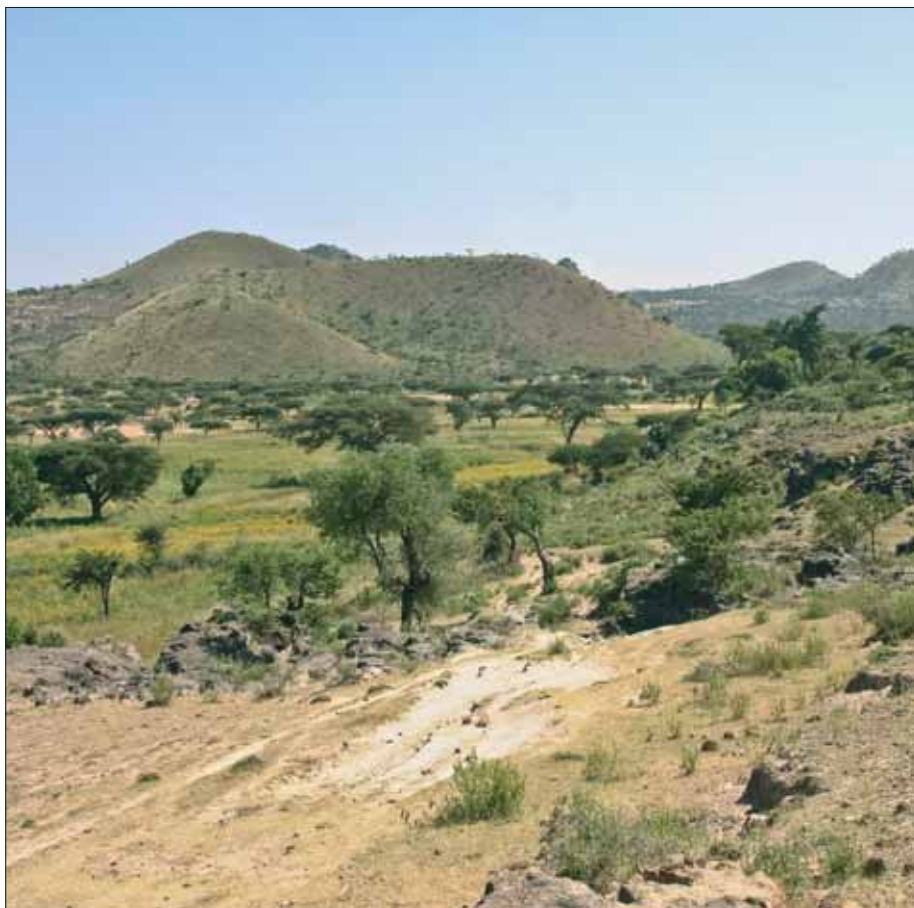
Fig. 1.4 Bush grassland and poorly vegetated scoria cones east of Lake Ziway

describes areas of mixed agriculture where both perennial (enset, coffee, chat, fruit trees, bananas, etc) and annual crops are the main source of income. "Pastoral-Grazing and Browsing with some fuelwood production" is extensive throughout the area and ranges from afro-alpine vegetation in Arsi in the north-east to woodland, shrubland, wooded grassland and even bare land with some vegetation in the centre and south of the area.

Vegetation

The vegetation cover of an area helps to minimize water loss and soil degradation. The type of vegetation and its distribution in the area varies mainly based on temperature, altitude, soil type and humidity and/or precipitation. The population density is also an important factor for vegetation cover. Most of the Hosaina map sheet is covered with agricultural land. The vegetation types are varied from place to place. Eucalyptus trees, Junipers, Hagenia abyssinica, Podocarpus grcilior (zigba), and Vernonia amygdalina (bisana) are common on the highland plateaus. The low land area especially the rift floor is dominated by acacia 'girar', thorn bushes, small shrubs and

Basic Characteristics of the Area

Fig. 1.5 Relics of forest and re-forestation in the area of Mt. Ambericho
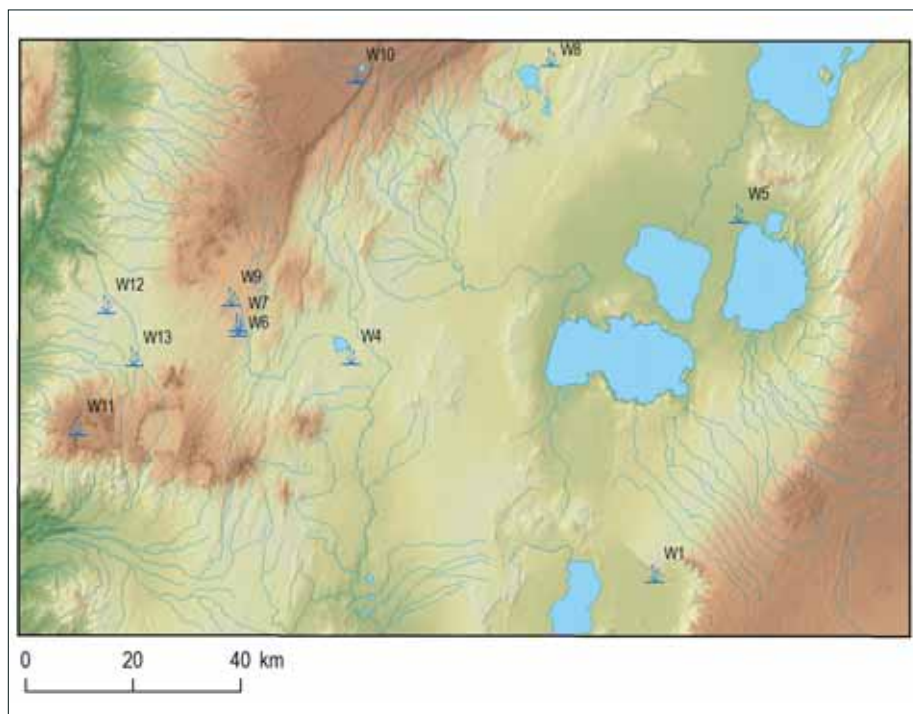
Fig. 1.6 Sketch map of documented wetlands

many undifferentiated ever green plants. Natural vegetation can be classified as forest (Wondo Genet area), woodland and savanna regions.

Cultivation and deforestation have considerably changed the natural vegetation cover over much of the area, aggravating the rates of weathering and erosion.

During the field campaigns, several wetland areas (Fig. 1.6) were documented in the area providing a specific biotope for conserving a wide range of animal life.

Fig. 1.7 Open to bushed grassland to the east of Lake Ziway

Basic Characteristics of the Area

2. *2. Selected Physical and Geographical Settings*

The entire study area is located in the Rift Valley, the adjacent rift escarpment and parts of the eastern and western Ethiopian Plateau dissected by river valleys and the more pronounced Gibe and Omo gorges.

2.1 Geomorphology

The geomorphology of the area is highly variable and is generally the result of repeated volcanic and tectonic events with the associated erosion of volcanic rocks and deposition processes. The principal feature of the Main Ethiopian Rift (hereinafter referred to as MER) is the graben, a block limited by normal faults in which the floor of the valley has become vertically displaced with
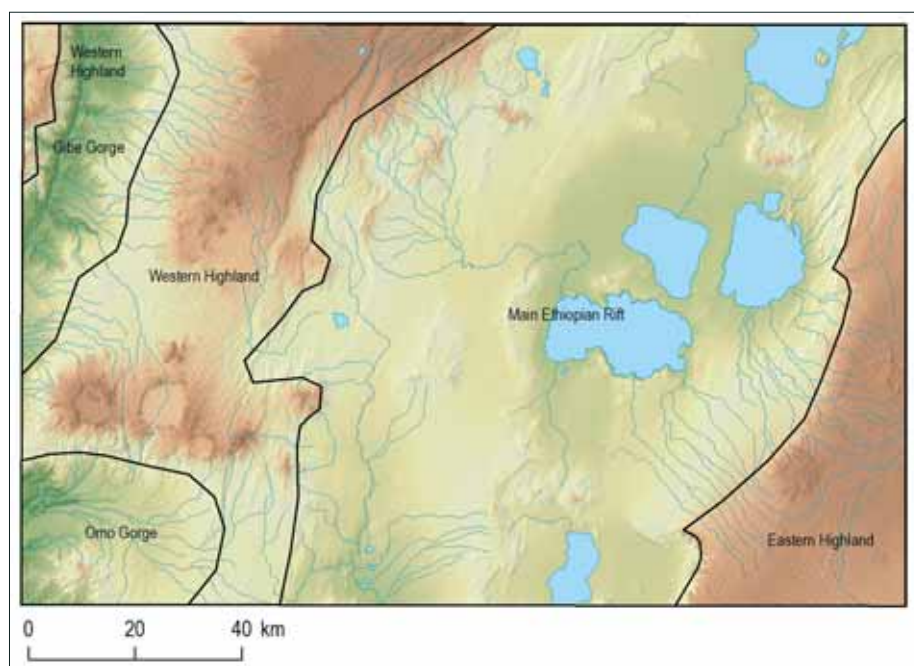
Fig. 2.1 Generalized geomorphological units

respect to the valley sides. The tectonic activity and lithological variation in the area also partly or wholly control the drainage density and drainage pattern. Most of the river channels follow the young lineaments and discharge their water into lakes at the bottom of the rift. The most distinct geomorphological units are shown in Fig. 2.1.

Elevation in the study area copies its main geomorphological parts and is between 1,580 to 1,700 m a.s.l. on the MER floor, rising along the escarpment to an elevation of about 2,600 m a.s.l. The edge of the plateau is flanged by high volcanic complexes with an elevation from 2,970 to 3,550 m a.s.l. A detailed description of the main geomorphological categories is as follows:

MER floor (Lake Langano 1,584.33 m a.s.l. –Lake Hawasa 1,690 m a.s.l.) covering 10,245 km^2 (56 %) is located in the central part of the map. Sedimentary formations, located throughout the whole rift floor, form a flat plain and are eroded along river/wadi banks and dominant Late Pleistocene to Holocene volcanic structures (Fig. 2.2). The area between the lakes of Ziway and Hawasa is almost flat in the valley bed with several mounds of hills in the west and volcanic bodies. The hills are mostly in the shape of cone or semi-conical crests that leave the traces of past volcanic activity.

Fig. 2.2 Chabi Volcano rising above the Lake Hawasa

Rift Escarpment (1,600–2,600 m a.s.l.) covering 2,698 km^2 (15 %) rises on both edges of the rift connecting its bottom with the eastern and western highlands. The margins of the rift are characterized by a few widely spaced faults with very large vertical displacements to the rift floor. The eastern margin is well developed and is defined by a more or less continuous system of faults, whereas the western border is marked by only a few major faults in the Gurage Mountains. The tectonic escarpment itself is formed by a narrow strip of blocks but for the hydrogeological assessment this narrow strip was enlarged up to the main water divide bounding the Rift Valley Lakes basin.

Fig. 2.3 Numerous waterfalls and cascades can be found on the edge of the Rift Escarpment

Eastern and western highlands – plateau (2,600–3,550 m a.s.l.) covering 5,355 km² (29 %) in the eastern and western part of the map sheet. The landform in this region is a result of major regional tectonics and associated volcanism. In addition, residual landforms also dominate this region due to the weathering of volcanic landforms and products. The Gibe and Omo gorges are found in the north and south of the western corner of the study area forming a deep valley cut in the western highlands, representing about 7 % of the highlands area. The highest peak of Mt. Kubsa (3,550 m a.s.l.) is located on the edge of the eastern plateau.

Selected Physical and Geographical Settings

2.2 Climatic Characteristics

The area is climatically highly variable and is mainly characterized by the subtropical Weina Dega on the rift floor and the temperate to humid Dega climatic zones on the escarpment and the adjacent highlands. The highest peak of Mt. Kubsa is characterized by the sub-alpine Wurch and the bottom of the Gibe and Omo gorges is characterized by the arid Kola climatic zone. The rainy season within the area passes from March to May and from July to October. The mean annual rainfall is about 1,100 mm. The mean annual temperature is about 20°C. The weather of the Hosaina map sheet is mainly controlled by the seasonal migration of the inter-tropical convergence zone (ITCZ), which is conditioned by the convergence of trade winds of the northern and southern hemispher and the associated atmospheric circulation.

2.2.1 Climatic Zones and Measurements

The climatic conditions of Ethiopia are mostly dominated by altitude. According to Daniel Gamatchu (1977) there are wide varieties in climatic zones. Climatic zones defined by Javier Gozálbez and Dulce Cebrián (2006) and Tesfaye Chernet (1993) are shown in Tab. 2.1. Climatic zones of the project area defined based on elevation and precipitation depth are shown in Fig. 2.4.

Tab. 2.1. Ethiopian climate classification

Name / Altitude / Mean annual temperature	Precipitation below 900 mm	Precipitation between 900 and 1,400 mm	Precipitation above 1,400 mm
High Wurch (Kur) above 3,700 m below 5 °C			**Afro-alpine** meadows of grazing land and steppes, no farming *Helichrysum, Lobelia*
Wurch (Kur) 3,200–3,700 m 5–10 °C		**Sub-afroalpine** barley *Erica, Hypericum*	**Sub-afroalpine** barley *Erica, Hypericum*
Dega 2,300–3,200 m 10–15 °C		**Afro-mountain (temperate)** forest – woodland barley, wheat, pulses *Juniperus, Hagenia, Podocarpus*	**Afro-mountain** (temperate) bamboo forest barley, wheat, nug, pulses *Juniperus, Hagenia, Podocarpu, bamboo*
Weina Dega 1,500–2,300 m 15–20 °C	**Savannah** (sub-tropical) wheat, teff, some corn acacia savannah	**Shrub-savannah** (sub-tropical) corn, sorghum, teff, enset, nug, wheat, barley *Acacia, Cordia, Ficus*	**Wooded savannah** (sub-tropical) corn, teff, nug, enset, barley *Acacia, Cordia, Ficus, bamboo*
Kolla 500–1,500 m above 30 °C	**Tropical** sorghum and teff acacia bushes	**Tropical** sorghum, teff, nug, peanuts *Acacia, Cordia, Ficus*	**Wet tropical** mango, sugar cane, corn, coffee, oranges *Cyathea, Albizia*
Bereha below 500 m above 40 °C	**Semi-desert and desert** crops only with irrigation thorny acacias, *Commiphora*		

Remark: after Javier Gozálbez and Dulce Cebrián (2006), Tesfaye Chernet (1993)

Fig. 2.4 Climatic zones

Legend:
- Sub-afroalpine (Wurch)
- Temperate (Dega)
- Subtropical (Weina Dega)
- Tropical (Kolla)

0   20   40 km
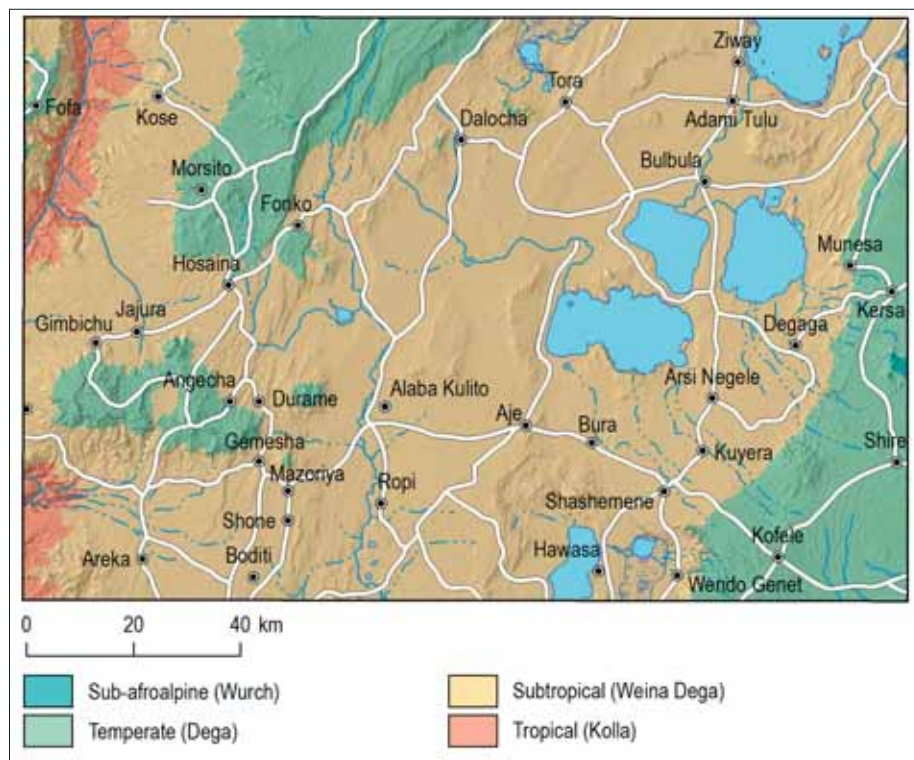
The outstanding modern quantitative climatic classification of Koeppen (1989) defines the climatic types according to the values of temperature and precipitation regardless of the geographic location of the region. Criteria for classification of principal climatic types in a modified Koeppen system are based on mean annual and mean monthly precipitation and temperature values. The actual application of the Koeppen system to climatological statistics shows that the Ethiopian climate is grouped into three main categories, each divided into three or more types making a total of 11 principal climatic types. The Rift Valley bottom belongs to the Bsh – hot semi-arid climate and Aw – tropical climate with distinct dry winters, whereas the plateau area belongs to the Cwb – warm temperate rainy climate with dry winters.

Tab. 2.2 Mean and extreme monthly temperature [°C] of Hawasa (Part 1)

	Mean	Mean Max	Mean Min	M max	M min
Jan	19.4	28.5	10.4	31	7
Feb	20.4	29.1	11.7	32	7
Mar	20.9	29.2	12.6	32	10
Apr	20.8	27.9	13.6	31	10

Tab. 2.2 Mean and extreme monthly temperature [°C] of Hawasa (Part 2)

	Mean	Mean Max	Mean Min	M max	M min
May	20.2	26.6	13.8	28	12
Jun	19.5	25.1	13.9	27	12
Jul	18.8	23.6	14.0	25	13
Aug	18.9	24.1	13.7	26	11
Sep	19.0	25.0	13.1	27	12
Oct	19.0	26.4	11.7	29	9
Nov	18.4	27.5	9.3	30	7
Dec	18.6	27.9	9.3	30	4
Average	19.5				

There are a large number of meteorological stations operated by the Meteorological Institute and WMO within the mapped area and several others are located in the near surroundings. The mean annual ambient air temperature of Hawasa is 19.5 °C (Tab 2.2). Minimum, maximum and mean temperatures were calculated from the original data supplied by NMSA (National Meteorological Survey Agency). The monthly minimum and maximum temperatures measured during 1972–2000 are 4 °C and 32 °C, respectively. The hottest and coldest months are March and November, respectively (Tab. 2.2).

2.2.2 Wind speed and direction

An important factor controlling the deposition of pyroclastic material is wind. The wind speed is high from January to July and the lowest is recorded during October in Hawasa. The mean annual wind speed in Hawasa is given in Tab. 2.3. According to the measured data, the prevailing wind

Tab. 2.3 Wind speed in Hawasa (part 1)

	Wind speed [m/s]		
	Mean	Min	Max
Jan	1.1	0.1	1.7
Feb	1.2	0.1	1.7
Mar	1.2	0.2	1.7
Apr	1.1	0.1	1.6
May	1.1	0.1	1.8
Jun	1.3	0.1	1.8
Jul	1.1	0.1	1.5
Aug	1.0	0.1	1.4

Tab. 2.3 Wind speed in Hawasa (part 2)

	Wind speed [m/s]		
	Mean	**Min**	**Max**
Sep	0.9	0.1	1.9
Oct	0.8	0.1	1.1
Nov	0.9	0.1	1.4
Dec	1.0	0.1	1.7
Average	1.0	0.1	1.5

directions differ significantly in the northern and southern part of the map sheet (Fig. 2.5 and 2.6). In Hawasa the winds blow dominantly from the west from October until April and from the west, southwest and south from May until September (Fig. 2.5). The prevailing wind direction can be also documented from the distribution of air-fall tephra from Wendo Koshe Volcano, which is deposited mostly to the east of the source vent. On the other hand, two seasons of completely
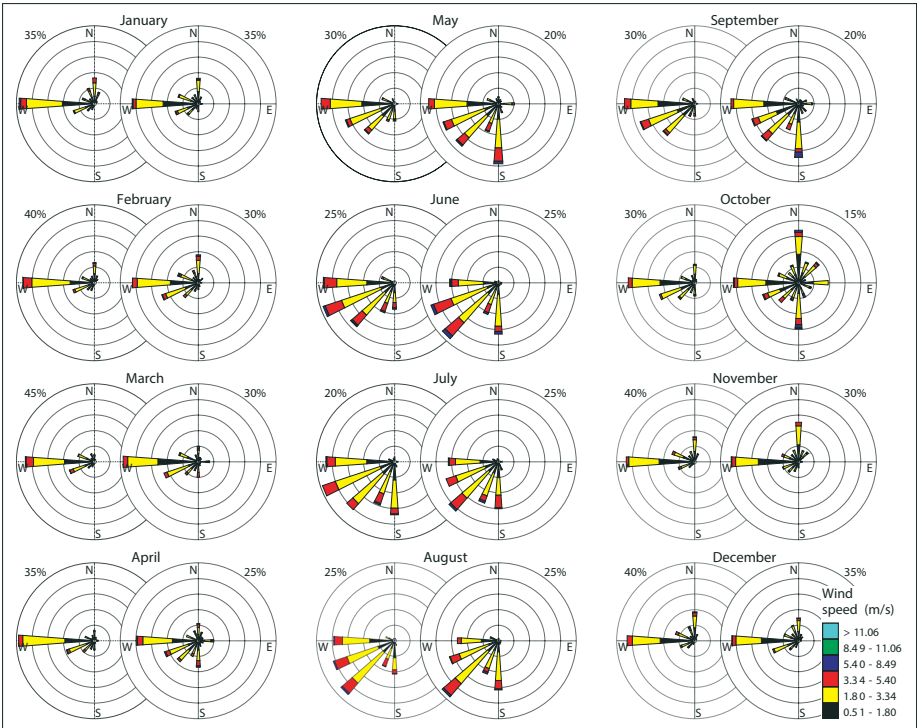
Fig. 2.5 Wind-rose diagrams for Hawasa station, data for each month represent wind distribution at 12:00 hours (left) and 15:00 hours (right) (based on 1987–2003 data by the Ethiopian National Meteorological Agency). Concentric circles represent percentages in the distribution of wind direction (the highest value given next to the diagram for each month and time).
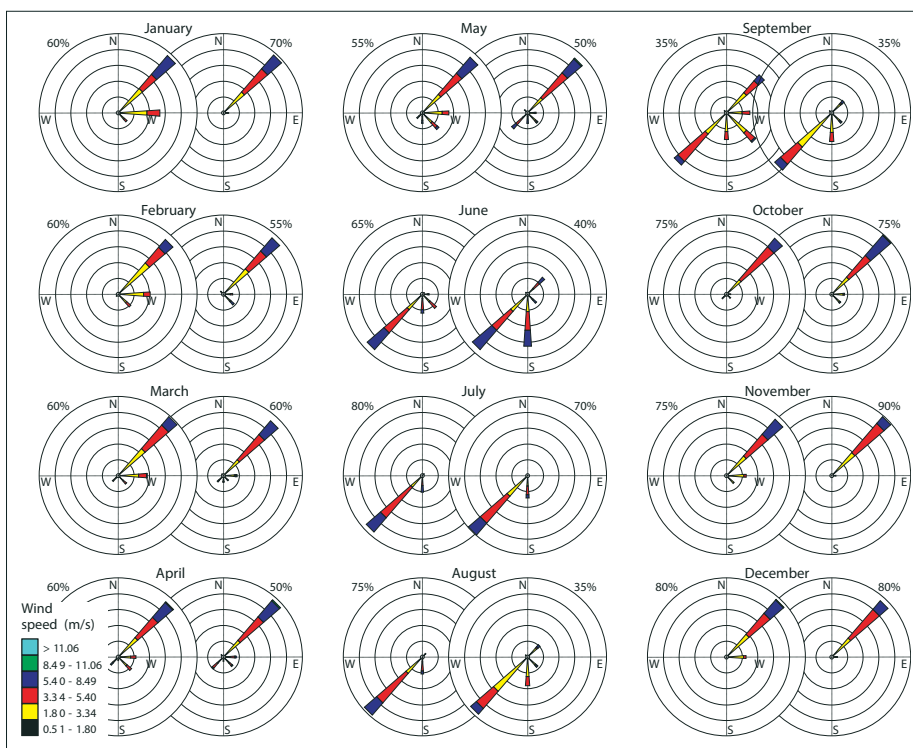
Fig. 2.6 Wind-rose diagrams for Ziway station, data for each month represent wind distribution at 12:00 hours (left) and 15:00 hours (right) (based on 1987–2003 data by the Ethiopian National Meteorological Agency). Concentric circles represent percentages in the distribution of wind direction (the highest value given next to the diagram for each month and time).

opposite wind direction can be identified in Ziway. From October until May, the wind mainly blows from northeast (50–90%). In June, the wind direction switches to the southwest until August, whereas during September both directions as well as wind from the south and southeast appear. The strongest winds (over 8.5 m/s) occur in Ziway during April–May, blowing from the northeast.

2.2.3 Precipitation

The Ethiopian territory is divided into four zones marked as A, B, C, and D, each of them with different precipitation patterns. The seasonal classification and precipitation regimes of Ethiopia (after NMSA, 1996) are characterized in Tab. 2.4.

The mapped area belongs to zone A which is characterized by four distinct seasons and by bimodal precipitation patterns with two peaks, the first occurring in March–May and the second September–November. The importance of rain during April is more in the southwest of the sheet. Precipitation patterns in selected stations are shown in Fig. 2.7.

The average amounts of annual rainfall vary with an up to 5-fold difference (500–2,600 mm). This is relatively large but there is a relatively small difference in the minimum and maximum rainfall

Tab. 2.4 Characterization of the precipitation pattern in Ethiopia

Zone	Precipitation pattern
A	This region mainly covers the central and central eastern part of the country. It is characterized by three distinct seasons, and by bimodal precipitation patterns with small peaks in April and the main rainy season during mid June to mid September with peaks in July.
B	This region covers the western part of the country. It is characterized by a single precipitation peak. Two distinct seasons, one being wet and the other dry, are encountered in this region. The analysis of mean monthly precipitation patterns shows that this zone can be split into southwestern (b1) with the wet season during February/March to October/November, western (b2) with the wet season during April/May to October/November, and northwestern (b3) with the wet season from June to September.
C	This region mainly covers the southern and southeastern parts of the country. It has two distinct precipitation peaks with a dry season between. The first wet season is from March to May and the second is from September to November.
D	The Red Sea region in the extreme northeastern part of the country receives diffused precipitation with no distinct pattern; however, precipitation occurs mainly during the winter.

amounts at the individual stations. The average difference between the minimum and maximum for the Rift Valley Lakes basin is 62.4 % and it varies from 24 to 85 %. This shows that drought problems are chronic in the Rift Valley Lakes basin; however, the basin is not classified as a drought prone
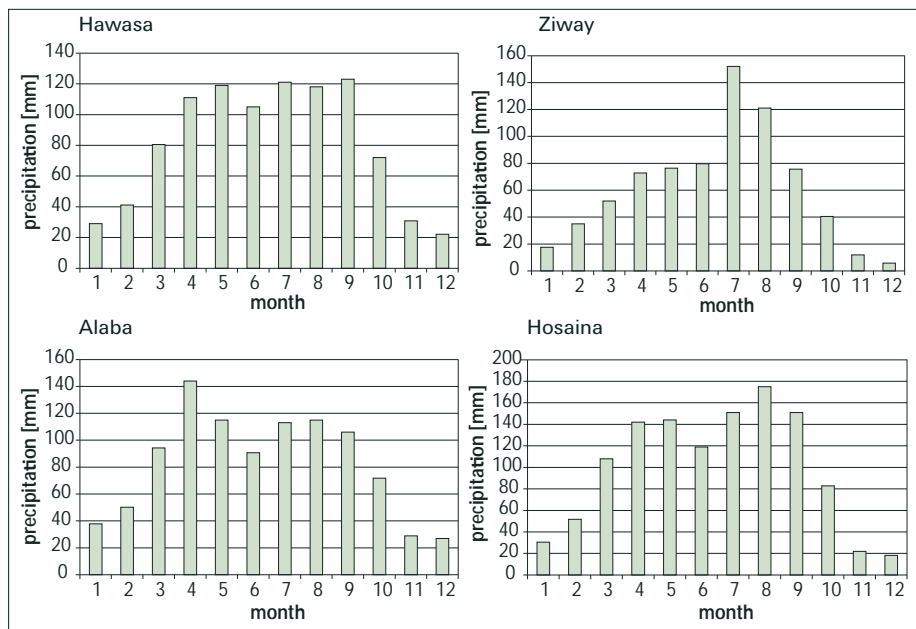
Fig. 2.7 Precipitation pattern in Hawasa, Ziway, Alaba, and Hosaina meteo-stations

area. The study of NMSA (1996) considers an occurrence of meteorological drought when seasonal rainfall over a region is less than 19 % of its mean. In addition, a drought is classified as moderate and severe if seasonal rainfall deficiency is between 21–25 % and more than 25 %, respectively.

Since the data periods covered differ considerably from station to station, the maximum and minimum levels of precipitation naturally appear in different years. However, based on the collected data, the maximum annual precipitation occurs in 1997 (in 9 stations), and in 2010 (in 8 stations), and the minimum annual precipitation occurs in 1999 (in 11 stations) and in 1984 and 2002 (in 8 stations). The maximum and minimum levels of annual precipitation recorded were 5,152 mm (at Aje station) and 211 mm (at Erbore station), showing a 20-fold difference. The difference between the maximum and minimum levels of precipitation from the data of a single station ranges from 247 mm (at Kulumsa station) to 4,104 mm (at Aje station). In terms of the ratio, it is within the range of 1.34 (at Kulmusa) to 8.94 (at Wolaita Sodo station).

2.3.4 Climate Change

Current climate change poses a significant challenge to Ethiopia by affecting food security, water and energy supply, poverty reduction and sustainable development efforts, as well as by causing natural resource degradation and natural disasters. For example the impacts of past droughts such as those of 1972/73, 1984 and 2002/03 are still fresh in the memories of many Ethiopians. Floods in 2006 caused substantial loss to human life and property in many parts of the country. In this context, planning and implementing climate change adaptation polices, measures and strategies in Ethiopia will be necessary.

The agricultural sector is the most vulnerable to climate variability and change. In terms of livelihoods, small scale rain-fed subsistence farmers and pastoralists are the most vulnerable.

In recent years the environment has become a key issue in Ethiopia. The main environmental problems in the country include land degradation, soil erosion, deforestation, loss of biodiversity, desertification, recurrent drought, flooding, and water and air pollution.

The major adverse impacts of climate variability in Ethiopia include:
• Food insecurity arising from the occurrence of droughts and floods.
• Outbreaks of diseases such as malaria, dengue fever, water borne diseases (such as cholera, dysentery) associated with floods and respiratory diseases associated with droughts.
• Heavy rainfalls which tend to accelerate land degradation.
• Damage to communication, road and other infrastructure by floods.

The other climate related hazard that affects Ethiopia from time to time is flooding. Major floods occurred in different parts of the country in 1988, 1993, 1994, 1995, 1996 and 2006. All of them caused loss of life and property. The DPPA estimate is about 199,000 critically affected people due to the flood in the country. For example in 2006 flooding in the main rainy season (June–September) caused the following disasters (NMA, 2006):
• More than 250 fatalities and about 250 people unaccounted for in Dire Dawa flood.
• More than 10,000 people in Dire Dawa became homeless. Over Dire Dawa, the loss in property is estimated in the order of millions of dollars.
• More than 364 fatalities in Southern Omo and more than 6,000 (updated to 8,350 after August 15) people were displaced over Southern Omo, where around 14 villages were flooded. More than 900 livestock drowned over South Omo. In addition, 2,700 heads of cattle and 760 traditional silos were washed away (WFP).
• More than 16,000 people over West Shewa were been displaced.
• Similar situations also occurred over Afar, Western Tigray, Gambella Zuria and over the low lying areas of Lake Tana. About 10,000 livestock encircled by river floods in Afar.

The impact of climate change on the water resources of the RVLB has been assessed by Halcrow using a climate change scenario based on the outputs of Global Circulation Models (GCMs) and scenarios used in other climate change studies for Ethiopia. This study used a hypothetical increase in temperature of +2 °C resulting in a 10 % increase of evapotranspiration but a 10 % decrease of rainfall over the period of 30 years; a relatively high impact scenario. For this climate change scenario the results from the regional flow model show a 24 % reduction in the total annual flow in rivers compared to present day runoff. The impact of climate change will be more serious in lakes Ziway, Abijata and Langano and the total average annual inflow into Lake Ziway is predicted to decrease by between 19 % and 27 % due to decreasing inflows in the main rainy season (June–September).

2.4 Hydrology of the Area

The Hosaina area is found mainly within the Rift Valley Lakes, Wabe Shebelle and Omo-Gibe basins. The principal river basins of the area are shown in Fig. 2.8.
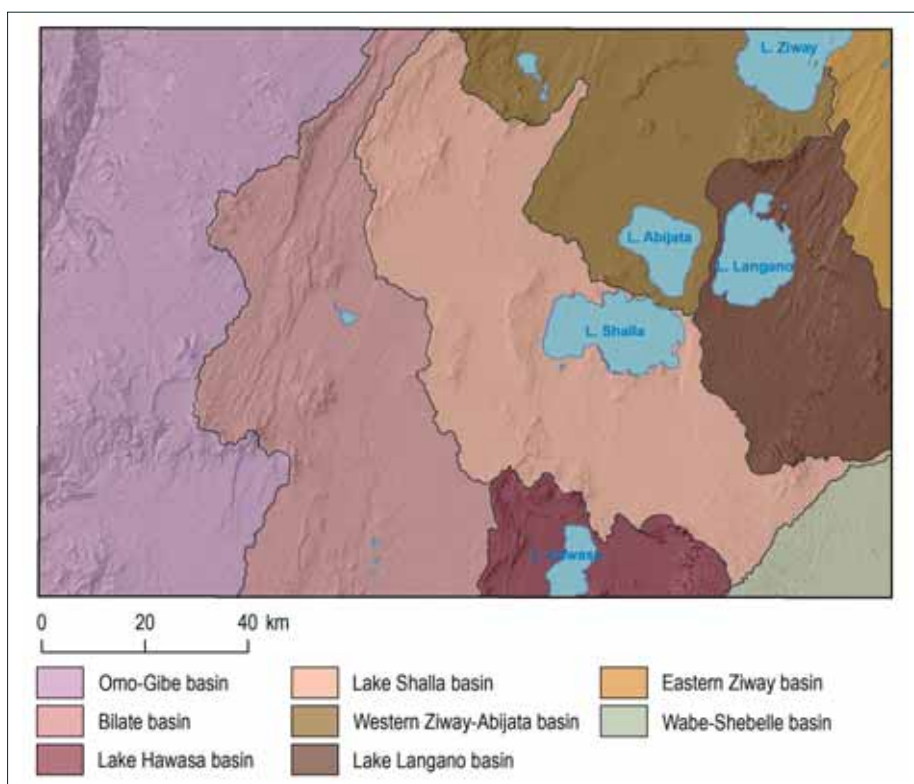
Fig. 2.8 The principal river basins of the area

2.4.1 Surface Water Network Development

The Hosaina topographic map sheet is divided by the main surface water divide and the largest part in the eastern and central part of the sheet belongs to the Rift Valley Lakes basin, the western part belongs to the Omo-Gibe basin and southeastern corner belongs to the Wabe Shebelle basin.

The Omo-Gibe basin covers 4,847 km^2 of the sheet. The basin is drained by small rivers flowing from the main water divide in a western and/or northwestern direction which join the Gibe River as its left tributaries. The Gibe River itself is a left tributary of the Omo River which briefly appears on the map sheet in the southwestern corner.

The Wabe Shebelle basin covers 508 km^2 of the sheet. The basin is drained by small streams (Siti, Combolcha, Goffer) forming left tributaries of the upper reach of the Wabe Shebelle River. These small rivers flow from the main water divide in a southeastern direction to join the Wabe Shebelle River.

The Rift Valley Lakes basin (RVLB) covers 12,945 km^2 of the sheet. The RVLB is a closed basin and surface water is drained by small rivers into its lakes and marshes which form the drainage for collected water. Four of the seven main lakes of the RVLB are terminal in themselves, and those which are not (Ziway, Langano and Abaya) flow into terminal lakes and are thus part of a terminal lake system. Halcrow (2008) supposes groundwater outflows from RVLB but there is no real evidence for this and at this time there is little data to support the hypothesis. The Ziway – Shalla and the Abaya – Chamo – Chew sub-basins are grouped as one because these lake complexes and river systems are spatial and temporally strongly interlinked. Significant inflow on the map sheet is formed by the rivers Meki (180 Mm^3/year) and Katar (300 Mm^3/year); the Bilate River has an estimated inflow of 830 Mm^3/year to the south into Lake Abaya.

2.4.2 River Flow Regime

There are a large number of river gauging stations within the RVLB, Wabe Shebele and Omo-Gibe basins. Some of them are operational but many of the stations have no data. On the Hosaina sheet there are 15 registered gauging stations and 5 lake level monitoring stations. Other river gauging stations are within the neighboring sheets and data from these stations were also calculated for the assessment of surface as well as baseflow values. Records from all stations reflect the fact that the river discharge is directly proportional to the intensity of rainfall within the basin. There is a high discharge fluctuation between the wet and dry seasons of the year. The first high flow period is usually from April to May, the highest flow period is from June to October and the peak flow for

Tab. 2.5 Runoff data (Part 1)

Map ID	River	Station	Mean flow [m^3/s]	Annual flow [mm]	Annual precip. [mm]	Area [km^2]	Specific runoff [l/s.km^2]	Dominant Aquifer
3	Dedaba	Nr Kuyera	1.04	201	1,070	163	6.4	Volcanic/ esc
4	Djidu	Children's Well	5.72	101	1,083	1,794	3.2	
6	Gedemso	Nr Lake Langano	2.41	1,463	924	52	46.3	Volcanic/ esc
21	Tinshu Dedaba	Nr Kuyera	0.41	126	1,071	103	4.0	
11	Guta /Melka Oda	Nr Melka Oda	0.32	135	1,101	75	4.3	
2	Bilate	Nr Alaba	11.06	174	1,131	2,009	5.5	
15	Wesha	Wondo Genet	0.63	497	1,139	40	15.8	Volcanic/ esc
13	Weira	Nr Hosaina	7.31	442	1,265	522	14.0	Volcanic/ esc

Selected Physical and Geographical Settings

Tab. 2.5 Runoff data (Part 2)

Map ID	River	Station	Mean flow [m³/s]	Annual flow [mm]	Annual precip. [mm]	Area [km²]	Specific runoff [l/s.km²]	Dominant Aquifer
7	Guder	Nr Hosaina	1.18	247	1,270	151	7.8	Volcanic/esc
1	Batena	Nr Hosaina	1.20	533	1,259	71	16.9	
14	Butara / Werka	Nr Wondo Genet	0.26	200	1140	41	6.3	Volcanic/esc
16	Sokie	Nr Ajora Falls	1.96	ND	1250	ND	ND	Volcanic/plat
17	Ajanchon	Nr Areka	1.17	121	1,250*	306	3.8	Volcanic/plat
18	Shopa	Nr Areka	1.45	2,408	1,250*	19	76.3	Volcanic/plat
19	Weibo	Nr Areka	1.75	23	1,250*	2,368.4	0.73	Volcanic/plat
20	Sana	Nr Tunto	3.53	51	1,250*	2,190	1.6	Volcanic/plat
81007	Ashebeka / Upper Tim	Nr Digelu	0.17	44	975	122	1.4	
81008	Ashebeka / Lower Tim	Nr Sagure	0.84	102	941	261	3.2	
81009	Wolkessa	Nr Asela	0.29	915	1,087	10 (31)	29.0 (9.4)	
81010	Gushe / Ashebeka	Nr Sagure	1.57	539	888	92	17.1	
81011	Katar	Nr Fete	11.33	184	917	1,945	5.8	
81018	Meki	Meki village	8.96	146	1,021	1,943	4.6	
81019	Katar	Abura	12.47	128	934	3,077	4.1	
81025	Chiufa	Nr Arata	1.47	134	1,051	347	4.2	
82032	Rinzaf	Butajira	0.85	389	1,126	69	12.3	

*Approximation from Halcrow (2008) Isohyetal map; ND = not defined

all rivers is usually recorded in August. The period from December to March is characterized by low flow when most of the smaller rivers are completely without water. Different patterns are also known within the map area and its close surroundings. Runoff data are summarized in Tab. 2.5.

Measured discharge of the Bilate River at the Alaba river gauge in the period from 1980 to 2007 is shown in Fig. 2.9. The figure shows that the flow is relatively regular; however, the total value of annual flow and particularly maximal monthly flow can vary substantially from year to year. The lowest daily discharge of 0.036 m³/s (February and March, 1981) and the highest daily discharge of 118.775 m³/s (15th of May, 2007) were recorded at the river gauge. The calculated mean annual flow of 12.032 m³/s for the Kuyera station represents flow generated mainly in the western highlands where the Bilate River rises (originates) and which receives the highest precipitation within the basin.
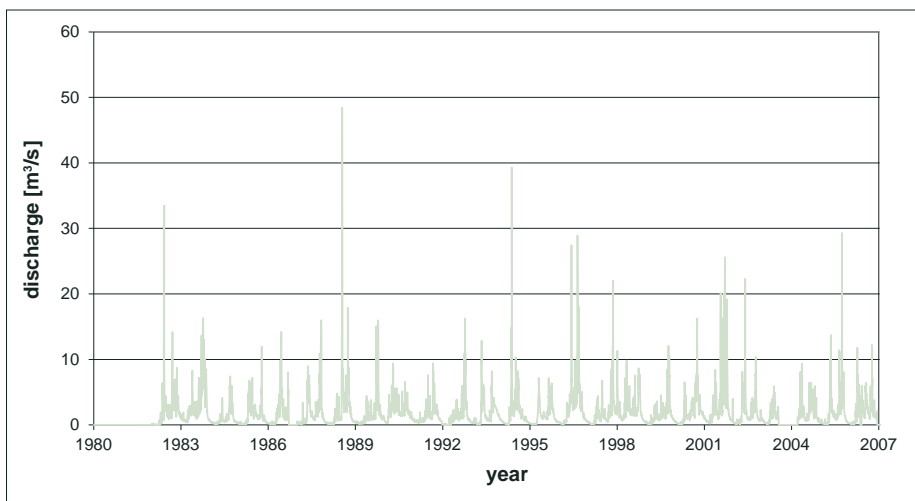
Fig. 2.9 Flow diagram of the Bilate River at the Alaba river gauge

Annual variability of the mean annual flow of the Bilate River at the Alaba river gauge is shown in Fig. 2.10.
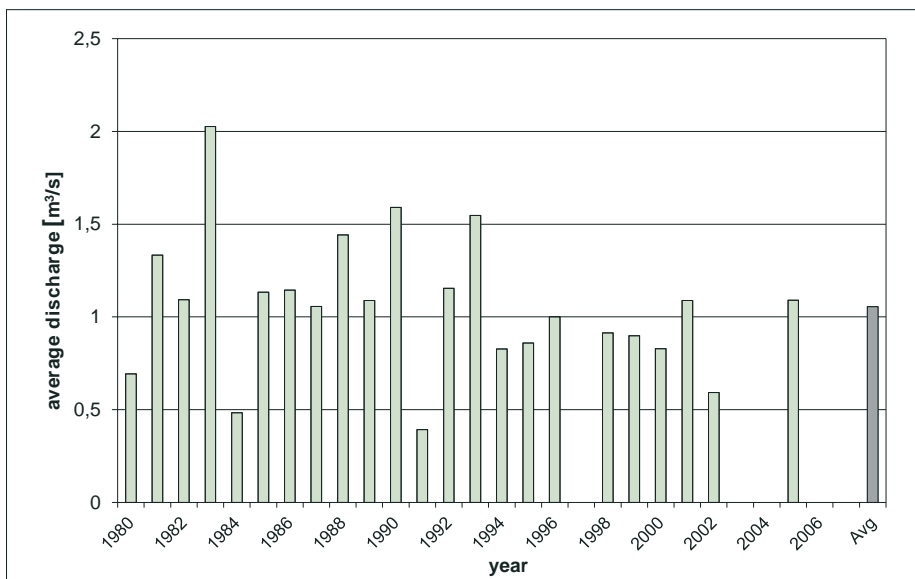
Fig. 2.10 Annual variability of the mean annual flow of the Bilate River at the Alaba river gauge

Measured discharge of the Dedeba River at the Kuyera river gauge in the period from 1980 to 2007 is shown in Fig. 2.11. The figure shows that the flow is relatively regular; however, the total value of annual flow and particularly maximal monthly flow can vary substantially from year to
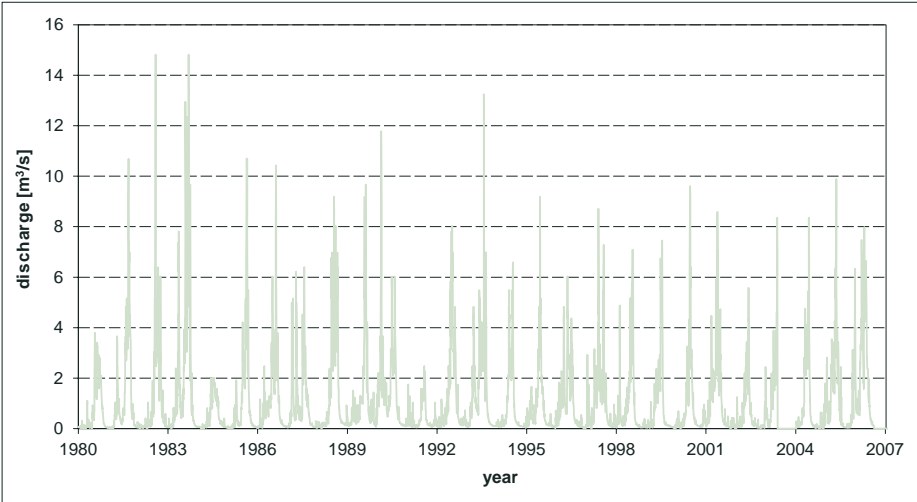
Fig. 2.11 Flow diagram of the Dedeba River at the Kuyera river gauge

year. The lowest daily discharge of 0.007 m³/s (14th and 15th of March, 1984), and the highest daily discharge of 14.82 m³/s (29th of August, 1983) were recorded by the river gauge. The calculated mean annual flow of 1.078 m³/s for the Kuyera station represents flow generated mainly in the eastern highlands where the Deneba River rises (originates) and which receives the highest precipitation within the basin.
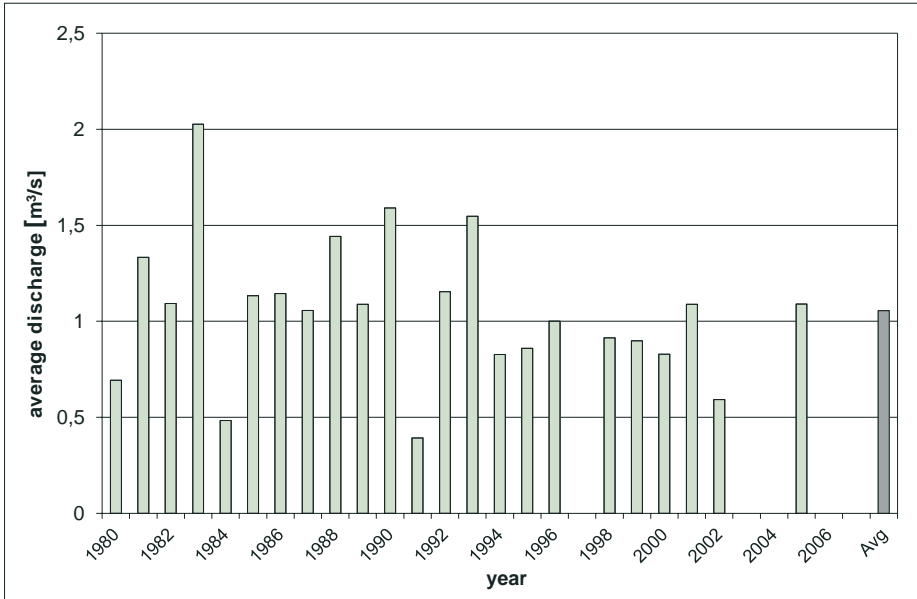
Fig 2.12 Annual variability of the mean annual flow of the Dedeba River at the Kuyera river gauge
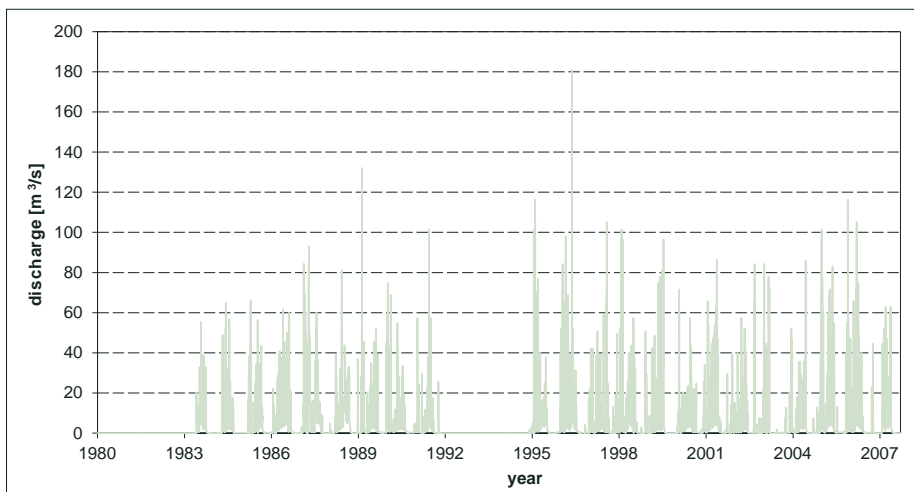
Fig. 2.13 Flow diagram of the Djidu River at the Children village river gauge

Annual variability of the mean annual flow of the Dedeba River at the Kuyera river gauge is shown in Fig. 2.12.

Measured discharge of the Djidu River at the Children village river gauge in the period from 1984 to 2007 is shown in Fig. 2.13. The figure shows that the flow is relatively regular; however, the total value of annual flow and particularly maximal monthly flow can vary substantially from
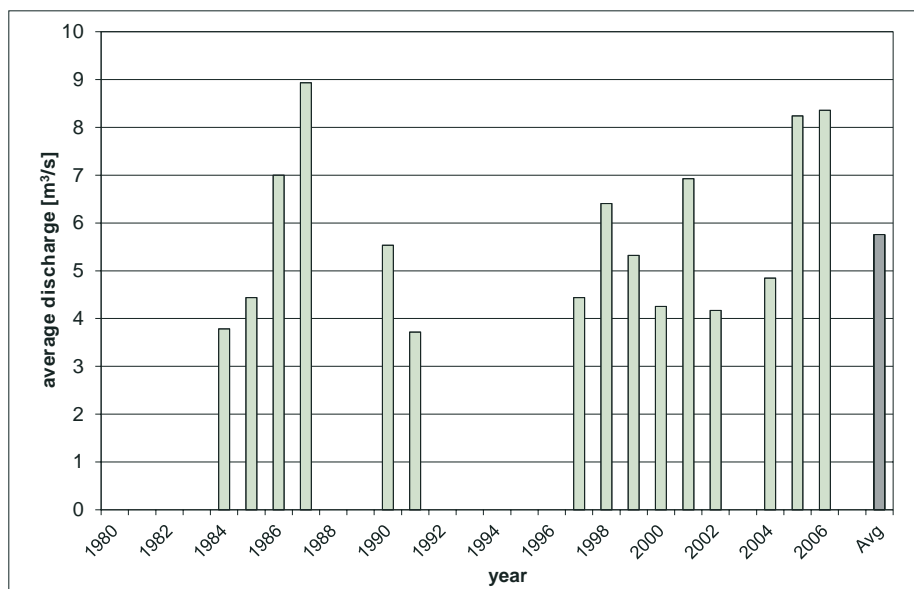
Fig. 2.14 Annual variability of the mean annual flow of the Djidu River at the Children village river gauge
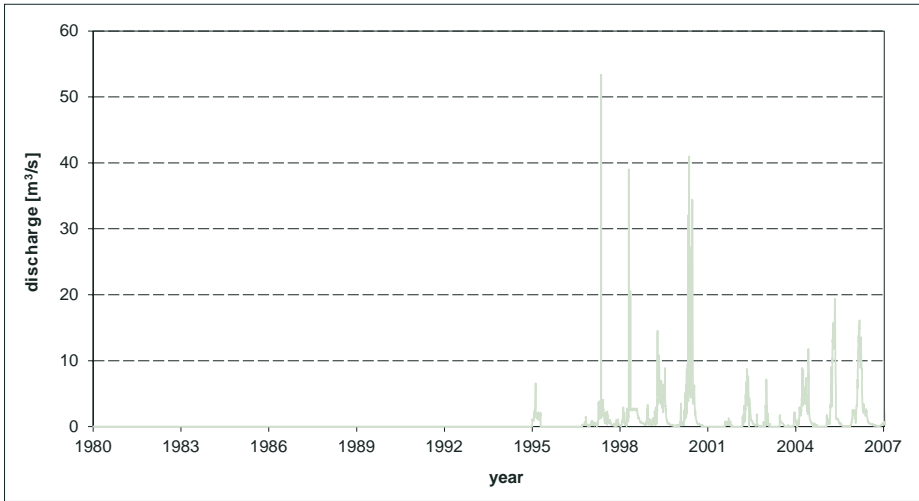
Fig. 2.15 Flow diagram of the Gedemso River near the Langano Lake river gauge

year to year. The river was not flowing in the period from December 1999 to April 2000 and the highest daily discharge of 180.66 m³/s (7th of August, 1996) was recorded at the river gauge. The calculated mean annual flow of 5.846 m³/s for the Children village station represents flow generated mainly in the western highlands where the Djidu River rises (originates) and which receives the highest precipitation within the basin.
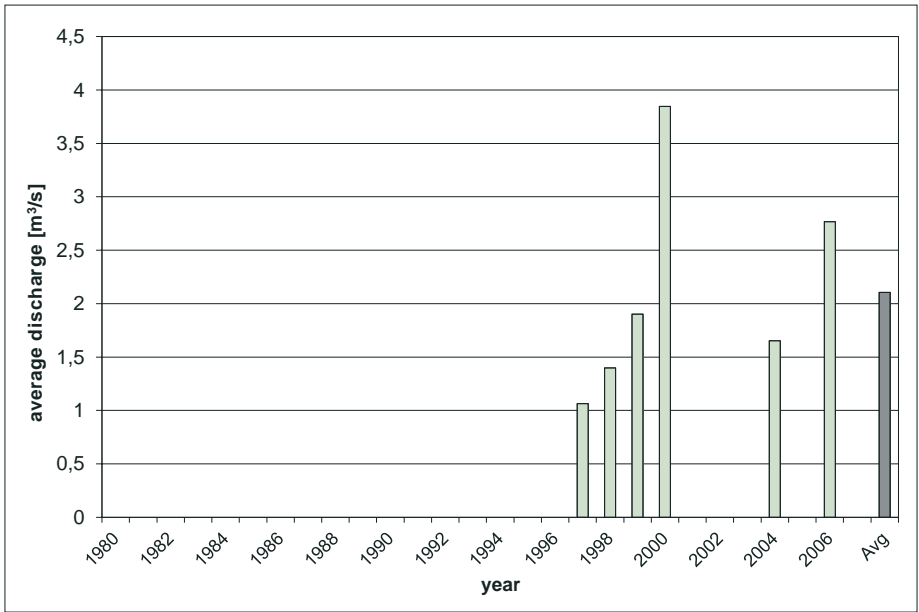
Fig. 2.16 Annual variability of the mean annual flow of the Gedemso River near the Langano Lake river gauge
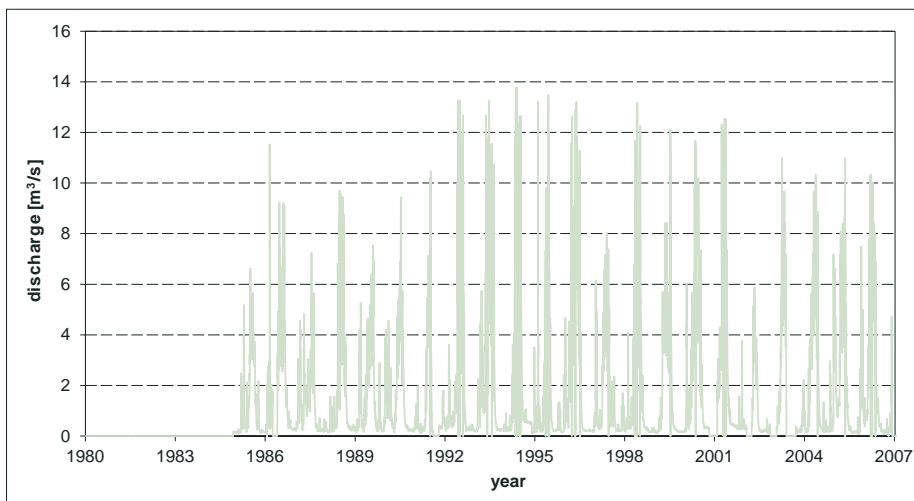
Fig. 2.17 Flow diagram of the Chiufa River at the Arata river gauge

Annual variability of the mean annual flow of the Djidu River at the Children village river gauge is shown in Fig. 2.14.

Measured discharge of the Gedemso River near Langano Lake river gauge in the period from 1998 to 2007 is shown in Fig. 2.15. The figure shows that the flow is relatively regular; however, the total value of annual flow and particularly maximal monthly flow can vary substantially from year to year. The lowest daily discharge of 0.002 m³/s (15th of January, 2004) and the highest daily discharge of 53.365 m³/s (6th of August, 1997) were recorded at the river gauge. The calculated mean annual flow of 2.041 m³/s for the Kuyera station represents flow generated mainly in the eastern highlands where the Gedemso River rises (originates) and which receives the highest precipitation within the basin.

Annual variability of the mean annual flow of the Gedemso River near the Langano Lake river gauge is shown in Fig. 2.16.

Measured discharge of the Chiufa River at the Arata river gauge (Asela sheet) in the period from 1985 to 2007 is shown in Fig. 2.17. The figure shows that the flow is relatively regular; however, the total value of annual flow and particularly maximal monthly flow can vary substantially from year to year. The river did not flow during the period from October to December 1991 and the highest daily discharge of 13.774 m³/s (24th of July, 1994) were recorded at the river gauge. The calculated mean annual flow of 1.809 m³/s for the Arata station represents flow generated mainly in the eastern highlands where the Chiufa River rises (originates) and which receives the highest precipitation within the basin.

Annual variability of the mean annual flow of the Chiufa River near the Arata river gauge is shown in Fig. 2.18.

Measured discharge of the Weira River at the Hosaina river gauge in the period from 1987 to 2007 is shown in Fig. 2.19. The figure shows that the flow is relatively regular; however, the total value of annual flow and particularly maximal monthly flow can vary substantially from year to year. The lowest daily discharge of 0.313 m³/s (October to December 1991) and the highest
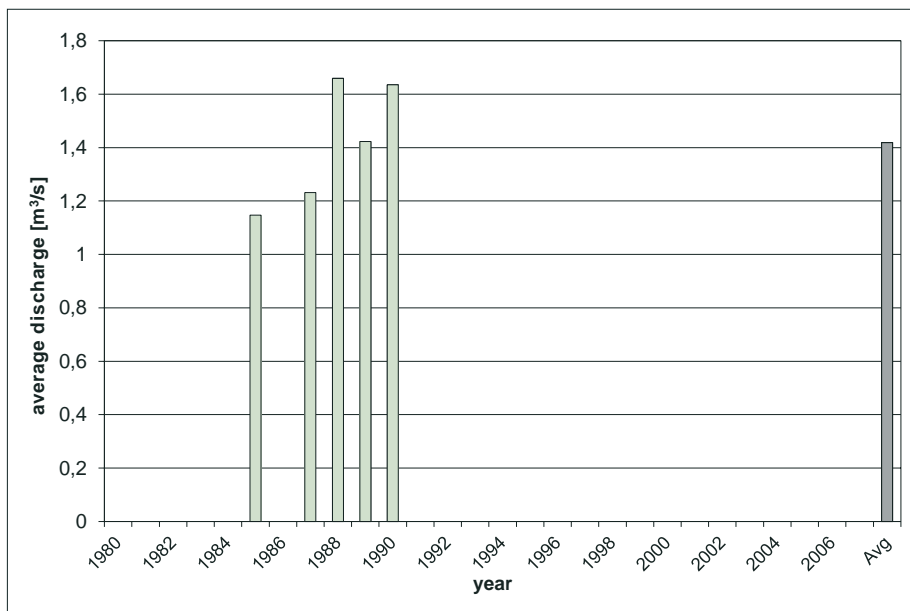
Fig. 2.18 Annual variability of the mean annual flow of the Chiufa River at the Arata river gauge

daily discharge of 239.475 m³/s (4th of October, 1999) were recorded at the river gauge. The calculated mean annual flow of 7.399 m³/s for the Hosaina station represents flow generated mainly in the western highlands where the Weira River rises (originates) and which receives the highest precipitation within the basin.
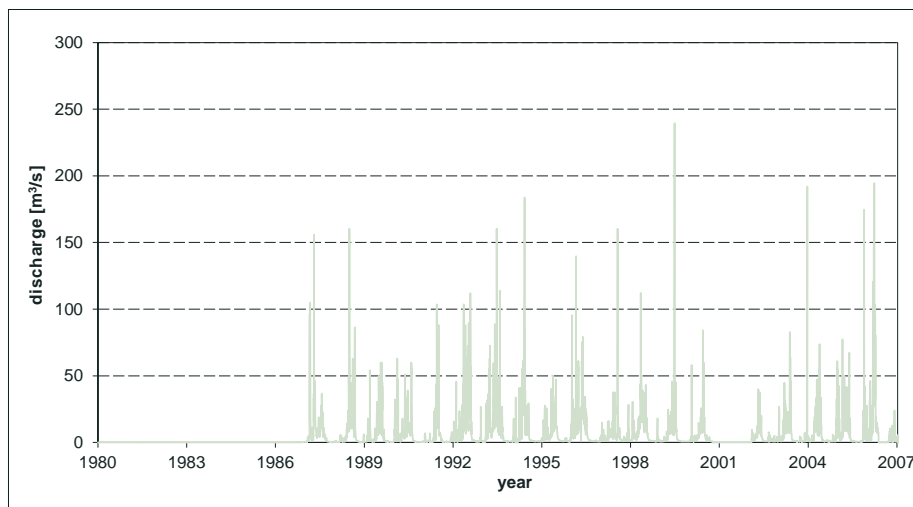
Fig. 2.19 Flow diagram of the Weira River near the Hosaina river gauge
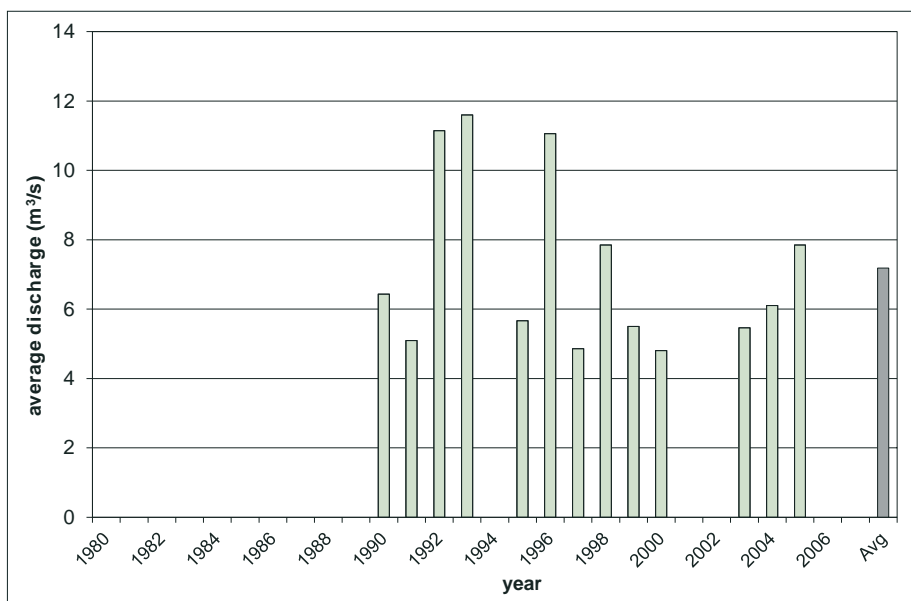
Fig. 2.20 Annual variability of the mean annual flow of the Weira River near the Hosaina river gauge

Annual variability of the mean annual flow of the Weira River at the Hosaina river gauge is shown in Fig. 2.20.

Measured discharge of the Wosha River at the Wondo Genet river gauge in the period from 1980 to 2007 is shown in Fig. 2.21. The figure shows that the flow is relatively regular; however, the total value
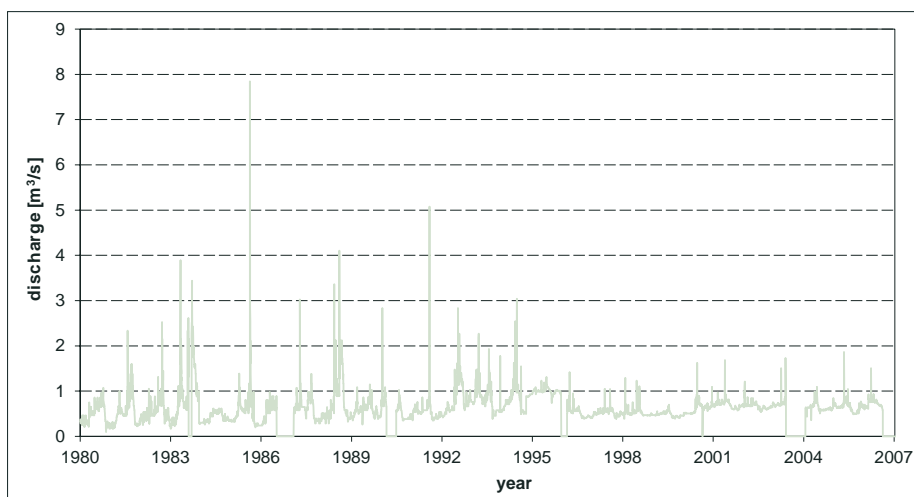
Fig. 2.21 Flow diagram of the Wosha River at the Wendo Genet river gauge

Selected Physical and Geographical Settings
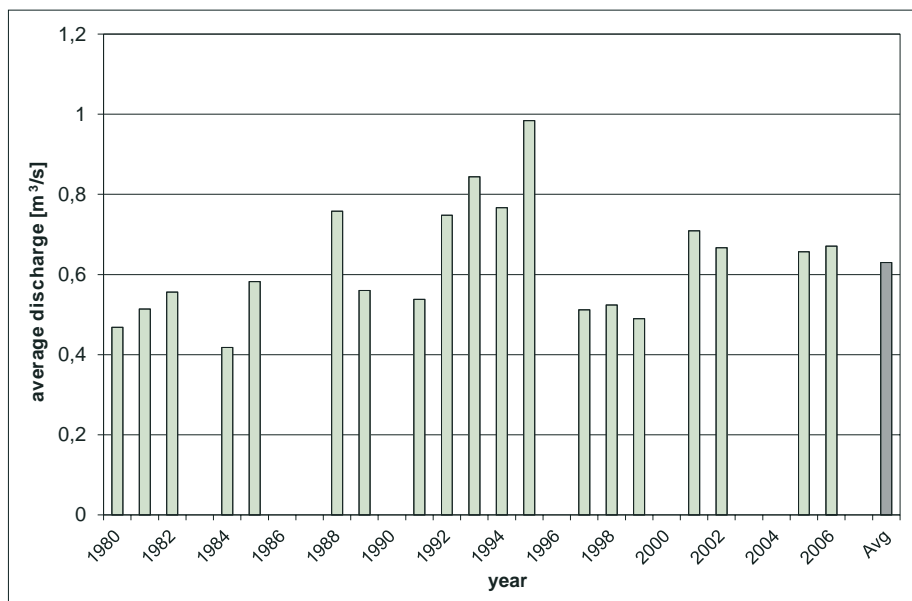
Fig. 2.22 Annual variability of the mean annual flow of the Wosha River at the Wendo Genet river gauge

of annual flow and particularly maximal monthly flow can vary substantially from year to year. The lowest daily discharge of 0.105 m^3/s (14th of November, 1980) and the highest daily discharge of 7.843 m^3/s (4th of October, 1999) were recorded at the river gauge. The calculated mean annual flow of 0.637 m^3/s for the Wondo Genet station represents flow generated mainly in the eastern highlands and escarpment where the Wosha River rises (originates) and which receives the highest precipitation within the basin.
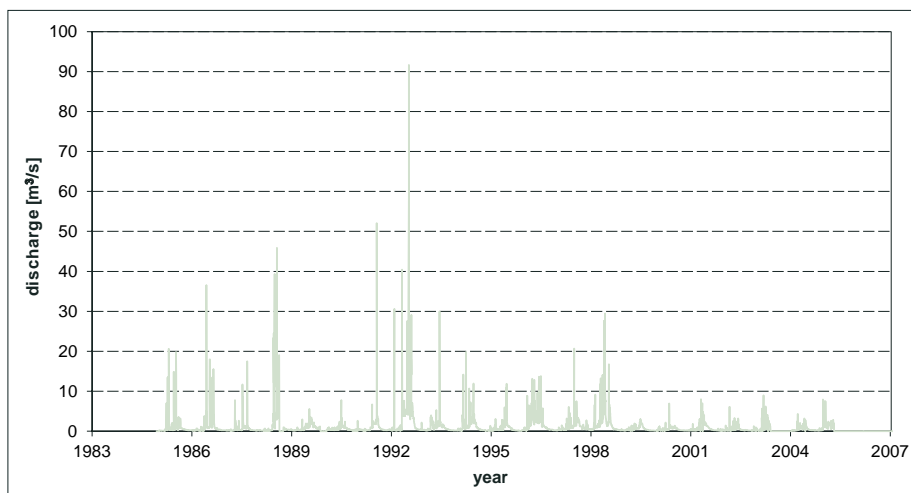
Fig. 2.23 Flow diagram of the Ajancho River at the Areka river gauge
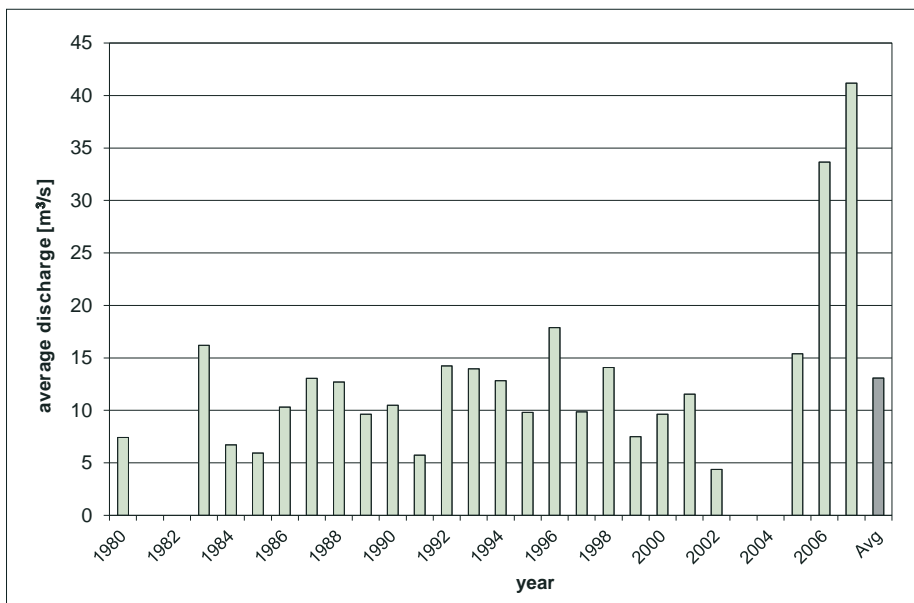
Fig. 2.24 Annual variability of the mean annual flow of the Ajancho River at the Areka river gauge

Tab. 2.6 Estimated average monthly sediment load

Region	Mean monthly flows [m³/s]												Mean annual flow [m³/s]
	Jan	Feb	Mar	Apr	May	Jun	Jul	Aug	Sep	Oct	Nov	Dec	
Meki	0.83	1.88	4.94	6.36	6.66	5.82	18.30	29.67	19.55	8.44	2.99	0.87	8.86
Katar	2.10	2.78	3.89	7.52	7.98	5.81	19.78	50.23	32.44	14.81	4.80	2.40	12.88
Langano WSd	1.43	2.08	2.65	5.28	5.43	4.08	13.45	34.16	22.76	10.07	3.37	1.63	8.86

Region	Mean monthly suspended sediment [tones/month]												Annual	Total sed. load [t]	Sediment yield [t/ km²/y]
	Jan	Feb	Mar	Apr	May	Jun	Jul	Aug	Sep	Oct	Nov	Dec			
Meki	2,917	7,624	29,661	39,869	43,776	35,479	163,284	306,385	172,206	59,594	14,914	3,067	1,142,407	1,485,129	610
Katar	1,415	1,897	3,362	8,171	9,183	5,696	32,690	120,406	63,209	21,813	4,365	1,713	356,097	427,317	128
Langano WSd	825	1,266	1,960	4,983	5,354	3,474	19,059	70,198	38,498	12,717	2,661	999	210,591	252,710	214

Annual variability of the mean annual flow of the Wosha River at the Wendo Genet river gauge is shown in Fig. 2.22.

Measured discharge of the Ajancho River at the Areka river gauge in the period from 1985 to 2006 is shown in Fig. 2.23. The figure shows that the flow is relatively regular; however, the total value of annual flow and particularly maximal monthly flow can vary substantially from year to year. The lowest daily discharge of 0.075 m^3/s (14th of April, 1987) and the highest daily discharge of 91.564 m^3/s (12th of September, 1992) were recorded at the river gauge. The calculated mean annual flow of 1.173 m^3/s for the Areka station represents flow generated mainly in the western highlands where the Ajancho River rises (originates) and which receives the highest precipitation within the basin.

Annual variability of the mean annual flow of the Ajancho River at the Areka river gauge is shown in Fig. 2.24.

The total sediment load estimated by Halcrow (2008) is then calculated as the combined sum of suspended load and bed load and is shown in Tab. 2.6.

2.4.4 Lakes

Monthly measurements of lake levels are conducted at stations of which a list is given in Tab. 2.7. A commentary on recorded lake levels by Halcrow (2008) is given as follows:

- Despite observable variations in record lake levels, over the period of record (1974–2006) there is no apparent trend in the recorded lake levels on Lake Ziway.
- There is a clear decline in the recorded lake levels of Lake Abijata, over the period of record 1976–2005. Two periods of notable decline are identifiable – 1984 to 1988 and 2001 to date. These periods are interrupted by a period of gradual recovery.
- The recorded lake levels on Lake Langano show no clear trend over the period of record 1970–2006. However, the lake appears to be in a period of declining levels that started in 2002.
- Lake Hawasa appears to be experiencing a slight increase in lake levels over the period 1969–2006. This is particularly pronounced from 1969 to 1998, after which time lake levels have been declining towards their earlier levels.

Basic descriptive data about the lakes are given in Tab. 2.8.

Lake Ziway is an open lake, and overflows towards Lake Abijata to the south through the Bulbula River. Lake Ziway is the main feeder, through the Bulbula River, for Lake Abijata. The Katar

Tab. 2.7 Lake level stations

Map_ID	Lake name	Site	X UTM	Y UTM	Altitude [m a.s.l.]	Start date	End date
1	Ziway	at Ziway	472443	873251	1,641.94	May_1974	May_2006
2	Abijata	nr Arore	455210	848479	1,592.36	Feb_1976	Dec_2005
3	Langano	nr Hotel Bekele Molay	465063	834273	1,584.33	Jun_1970	Mar_2006
4	Shalla	Gale	459035	822903	NA	Jan_1976	Apr_2006
5	Hawasa	at Hawasa	439258	779312	1,685.74	Oct_1969	Jul_2006
6	Cheleleka	nr Hawasa	446992	782620	1,686.85	Jan_1980	Mar_2006

Remark: NA – not analyzed

Tab. 2.8 Basic characteristics of lakes

Lake	Elevation [m a.s.l.]	Max. depth [m]	Mean depth [m]	Surface area [km²]	Storage volume [Mm³]	Level fluctuation [m]	Salinity [g/l]
Ziway	1,636–1,642.94	9	2.5	440	1,466	2.07	0.4
Langano	1,584.33–1,590	46	17–22	230–247	3,800–5,555	2.50	1.8
Abijata	1,577–1,592.36	10	6–7.6 ?	133–180	758–954	3.06	18
Shalla	1,558–1,567	256	86–121	302–370	36,472–37,000	NA	19
Hawasa	1,500–1,686.85		10.7	130	1,300	3.49	

Remark: NA – not analyzed

and Meki Rivers originating from the eastern and western highlands are the major influences on Lake Ziway. The water level fluctuation of Lake Ziway has periods of decline; however, it exhibits a roughly flat trend. Beach pebbles and artifacts found on Gedemota ridge (west of Ziway town) suggest that Lake Ziway once stood 210 m above the present day lake level during the late Pleistocene (Lloyd, 1977).

Lake Abijata (Fig. 2.25) is a small closed lake with an average area of 142 km², but has declined over the last 30 years from a maximum of 225 km² in 1970–72 to an area of 166 km² in 2000, declining further more recently to 87 km² (an estimate for 2006). Lake Abijata has highly mineralized (saline-alkaline-sodic) water which is not suitable for irrigation. The direct pumping of water from Lake Abijata for commercial exploitation of soda ash by evaporation of brine has also

Fig. 2.25 The shallow Lake Abijata is surrounded by a wide shore zone

some impacts on lake levels. The official production capacity of the plant is 20,000 tons per year of soda ash, but the most they have produced is about 7,500 tons in 2001 (Halcrow, 2008). For soda ash production of between 4,500 tons and 10,000 tons per year the decrease in lake levels is small ranging from 0.03 m to 0.04 m. This calculation shows that the present large decline in water levels in Lake Abijata is not related to soda ash production but is a result of excessive water use in the Ziway basin and from Lake Ziway.

Lake Langano receives its water through rivers from the highlands on the eastern escarpment. Water from Langano flows towards Lake Abijata to the south through the Horakela River. The present day level of Lake Abijata is only a few meters lower than that of Lake Langano, and the two lakes could unite and overflow to Lake Shalla to the south if they were to rise by a few meters. Lake Langano experiences only small annual water level variations of about 1 m compared to other lakes in the basin. Lake Abijata is less sensitive to reductions in flow in the Horakela River (compared to the Bulbula River) from increased water use in the Lake Langano basin, as this river contributes only about 8 % of the total inflow of Lake Abijata.

Lake Shalla (Fig. 2.26) is the deepest lake, and is separated from Abijata by a volcanic caldera rim. Lake Shalla is a closed lake and is highly alkaline. The alkaline nature of this lake makes direct water abstraction for irrigation impossible.

Lake Hawasa and Lake Cheleleka to the east are situated in the Hawasa caldera and were united as a single lake as recently as the 19th century (Zenaw, T.; Tadesse, D. 2003). The existence of terraced pumiceous lacustrine sediments on both sides of the fresh transverse faulting which limits the present Lake Hawasa basin to the north suggests that in pluvial times this basin was connected to that of Ziway – Shalla. They were separated by post pluvial block faulting and tilting (Mohr, 1960). Lake sediment related to the ancient Hawasa lake level was encountered in a borehole located to the north of the lakeshore at an elevation of 1,700 m a.s.l., which shows a drop of 30 m to the present lake level. If the level of hyaloclastite at 1,725 m is taken, the present day level of Lake Hawasa has dropped by 40 m. The lake is hydrologically separated from the other lakes but includes the former Lake Cheleleka, which is now mainly wetland with grazing and even agriculture production. In 2004, the area of Lake Hawasa was 92 km^2, and from the past three decades had a maximum area of 100 km^2 in 1998 after a significant wet period. The average area of the lake is 93.5 km^2, and has an average depth of 13.6 m and a maximum depth of 32.2 m based on bathymetric survey (WWDSE, 2001). The surface area of Lake Cheleleka was about 12 km^2 in 1972 but has currently transformed into a swamp with practically no open water. Lake Cheleleka is fed by a dense river network from the mountains in the east. The runoff, which is temporarily regulated by the swamp effect, eventually drains via Tikur Woha into Lake Hawasa. Lake Cheleleka acts as a natural regulating reservoir and serves as a transitional impounding reservoir during the rainy season.

The studies performed by WWDSE (2001) and Zenaw (2003) concluded that the gradual increasing trend in the water levels of Lake Hawasa is mainly caused by the gradual depletion of the physical capacity of Lake Cheleleka, whereas the abrupt rise in lake levels in 1977, 1983, 1986 and 1996 is mainly the effect of the cyclic wet years and low evaporation. The rise in the level of Lake Hawasa in recent years is perceived to be a major threat to the town of Hawasa. Periodic oscillation and trend of Hawasa lake levels observed from 1969 to 1999 were analyzed by Zenaw (2003). The lake achieves a maximum level in November whereas the minimum level is observed in April. Regardless of the seasonal fluctuations, the lake has been rising at an average rate of 76 mm per year.

The increase in levels of Lake Hawasa inundates vast areas around the lakeshore leading to many buildings, properties and infrastructure being ruined and also people living around the lake being displaced. Moreover, the rise in the level of the lake has created an environment conducive

for mosquito breeding and the number of malaria patients in the vicinity has increased. The total physical damage caused by the expansion of Lake Hawasa to Hawasa town and the rural areas was estimated by Zenaw (2003) as being Birr 43,490,524.

The main remedial measure suggested in the 2001 study is the abstraction of water directly from Lake Hawasa, and the detention of some of the inflow of the Tikur Woha River in Lake Cheleleka, to draw down lake levels. The study suggests that the abstracted water could be used for irrigation purposes by transferring water from Lake Hawasa to Lake Shalla through an open canal 18.75 km long to a stream that flows to Lake Shalla. The open canal could follow the natural gradient along Shallo farmland via Bura village and finally to Lake Shalla.

Fig. 2.26 Steep scarps of extinct caldera occupied by Lake Shalla

The hydrological and hydrogeological conditions of the studied area have recently been comprehensively summarized by Tilahun and Šíma (2013).

3. Geological Settings

The Hosaina sheet (NB 37-2) of the geological map at a scale of 1 : 250,000 is located in the central part of the NNE – SSW to NE – SW trending Main Ethiopian Rift which belongs to the regional East African Rift System (e.g. Hayward and Elbinger 1996; Bonini et al. 2005). The pre-rift Tertiary volcanic succession consisting of basaltic lavas and felsic ignimbrites plateaus is exposed in the escarpment on both sides of the rift. With the formation of the Wonji Fault Belt, tectonic movements and volcanic activity produced en-echelon arranged structures. Basalts with associate scoriae, rhyolitic ignimbrites, obsidians and unwelded pyroclastic rocks represent products of volcanic activity. Locally, the surroundings of lakes Langano, Ziway and Awassa, are covered by polygenetic sediments comprising re-sedimented pyroclastics and subordinate lacustrine sediments of the Late Pleistocene–Holocene age.

3.1 Previous studies

The Main Ethiopian Rift is shown in generalized form on 1:2,000,000 scale maps by Merla et al. (1973), Kazmin (1973) and Mengesha et al. (1996). Compilation of the geological maps of the Ethiopian Rift at a scale of 1:500,000 and the accompanying report was carried out in early 1980s by Kazmin et al. (1981). More detailed maps of the central part of the rift at a scale of 1:250,000 were published for Nazret (Seife Michael, 1978), Akaki Beseka (Ephrem, 2009), and Dodola sheets (Gobena et al. 1996). During the course of the exploration of geothermal resources in the Rift Valley performed by the Geological Survey of Ethiopia, the geothermal project exploration teams produced geological maps (unpublished) of the Lake Ziway area at a scale of 1:500,000 (Berhane et al., 1976).

Two recent detailed maps (1:50,000) cover the area around Hawasa and Shashemene (Rapprich et al. 2013, Žáček et al. 2014).

3.2 Stratigraphy

A general stratigraphy scheme of the area with the age and generalized lithological descriptions of the formations is shown in Tab. 3.1. The thickness of the formation is based on data published

Tab. 3.1 Lithostratigraphy of the mapped area (Part 1)

Era	Age	Formation	Thickness [m]	Lithology
Pleistoce-ne–Holo-cene		Quaternary sediments	200	Re-sedimented pyroclastics, la-custrine silt, clay and diatomite
		Central volcanic com-plexes	850	Rhyolite, trachyte and obsidian lavas, pumices, tuffs, ignimbrites
		Basalts of the rift floor	250	Basaltic lavas, scoriae, phreato-magmatic tuffs

Tab. 3.1 Lithostratigraphy of the mapped area (Part 2)

Era	Age	Formation	Thickness [m]	Lithology
Pleistocene	1.5–0.8	Dino Formation	300	Ignimbrites, pumices
Pliocene– Pleistocene	4.5–1.5	Chilalo volcanics	700	Alkaline basalt
			850	Trachyte, trachybasalt and peralkaline rhyolite, ignimbrites
Upper Miocene– Pliocene	9.2	Nazret Group	30	Bofa basalt: mildly alkaline basalt
			800	Alkaline and peralkaline felsic ignimbrites, pumices, tuffs, ash-flow deposits, rhyolite and trachyte
Oligocene- Miocene	30–15	Alaji Group (pre-rift volcanics)	1,200	Sub- and mildly- alkaline transitional basalt and rhyolite

by various sources. Quaternary sediments and various volcanic rocks of Quaternary to Tertiary age cover the Rift Valley floor, tectonic escarpment and adjacent plateau.

3.3 Lithology

Pre-Rift Volcanic Rocks consist of basalt, trachybasalt, trachyte and rhyolite. These rocks are exposed on all sides of the Gibe Gorge in the northwestern part of the mapped area. The dominating rock type is densely jointed aphanitic basalt that underlays rhyolite. The base of the basalt is obscured by Holocene deposits of the Gibe River. The trachyte is found mostly on the western side of the Gibe river section. It is highly weathered, fractured and cut by frequent basaltic dykes. Aphyric to plagioclase and pyroxene-phyric basalts and trachybasalts intercalated with rhyolite tuffs are exposed in the northwestern corner of the study area. Approximately 300 to 600 m thick plateau basalts are exposed to the immediate west of Butajira town (adjacent to the study area). They are overlain by Pliocene–Pleistocene felsic volcanic rocks (Nazret Group and Dino Formation).

Nazret Group of Late Miocene age is represented by stratified felsic volcanic rocks, i.e. ignimbrites, un-welded tuffs, ash-flow deposits, rhyolites and trachytes and builds up a considerable portion of the rift escarpments especially in the eastern part near Munesa town, while on the floor they are unconformably overlain by younger volcanic rocks of the Dino Formation and Holocene Volcanoes. More than 400 m of Nazret pyroclastic rocks have been encountered in a deep geothermal exploration well at Aluto volcano (Abebe, 1984). In addition, W/Gabriel et al. (1992) reported a thickness of more than 600 m for the Pliocene pyroclastic units on the eastern margin of the rift in the Munesa area. Basaltic rocks in the upper part of the Nazret Group are known as **Bofa basalts**. Bofa basalts (probably also equivalent to Bale basalts known from the area to the east of the mapped sheet) are represented by a unit of fissural flood basalts named after Bofa village located outside the study area. The basalts of this unit are aphyric and generally form several well-defined flows with brecciated and scoriaceous surfaces, separated also by paleosoils in places. The rocks are generally weakly porphyritic, with a holocrystalline ophitic groundmass with olivine, plagioclase and clinopyroxene. A few olivine and pyroxene-phyric lava flows are reported. The basalts are generally quartz-normative tholeiites with a few olivine basalts. The exposed thickness varies up to about 30 m along the fault escarpments.

Fig. 3.1 Pre-Rift Volcanic Rocks exposed in the Gibe Gorge

Fig. 3.2 Columnar-jointed basalt of the Pre-Rift Volcanic Rocks

Geological Settings

Fig. 3.3 Ignimbrites of the Dino Formation exposed in the scarp of the Shala Caldera

   Chilalo Volcanics built several shield volcanoes on the eastern rift shoulder, such as Chilalo, Bada, Kubsa, Kaka, and Enquolo. These extinct volcanoes form the eastern water divide between the Rift Valley lakes basin and the Wabe Shebele and Genale Dawa basins. The two volcanoes found in the study area are Kubsa and Duro. The older lava flows of these volcanoes might be

Fig. 3.4 Fiamme in welded ignimbrite of the Dino Formation north of Lake Abijata

Geological Settings

Fig. 3.5 Non-welded felsic pyroclastic deposits exposed in a small canyon near Kibet

contemporaneous with the younger ignimbrites of the Nazret group, and partly interfinger with them. The lower complex is composed of intercalating peralkaline ignimbrites and trachytes with prominent flow structures in the latter. The upper complex is represented invariably by very fresh alkaline basalts commonly with a porphyritic structure. In the Duro volcano on the eastern shoulder of the rift only the lower complex is present.

Dino Formation represents the oldest formation of the Wonji Group (Quaternary Volcanic Rocks) and covers a considerable portion of the rift floor. The Dino Formation comprises a number of welded ignimbrites with fiamme, locally intercalated with aphyric basalt and non-welded pyroclastic deposits. The non-welded pyroclastic rocks may represent non-welded facies of ignimbrites at the bases and tops of the units. The thickness varies from a few meters to up to 30 m (Kazmin and Seife, 1978; Kazmin et al., 1980). To the northwest of Lake Hawasa, rocks presumably belonging to the Dino Formation are represented by very coarse light colored non-welded pumiceous pyroclastic deposits intercalated with ignimbrites reaching a thickness of 250 m. The eruption of these pyroclastics was possibly related to the formation of calderas such as Hawasa, Shala and Ziway.

Basalts of the rift floor represent one of the latest volcanic manifestations in the Wonji group. These basalts erupted from fissures during the Late Pleistocene and Holocene. Most of the eruptions are concentrated along the Wonji fault belt, but there are also eruptions in the western marginal part of the rift. The eruption fissures are obviously controlled by extensional fractures. The erupted lava generally display fresh aa surfaces. Chains of scoria cones follow the lines of fractures. Late Pleistocene basalts are exposed to the east of Lake Ziway, south of Lake Shalla, south of Alaba-Kulito and around Hawasa. Holocene basalts make a chain known as the Butajira volcanic field in the northwestern part of the map sheet. Recent flows in many cases follow depressions of relief or flow over the fault escarpment. The eruption of basalts usually followed the formation of silicic pantelleritic volcanoes, but some basalt might be contemporaneous with the latest stages of

Fig. 3.6 Holocene basaltic lava filling up the canyon in felsic pyroclastic deposits of the Dino Formation

their development. Effusions of basaltic lavas were associated with Strombolian eruptions forming scoria cones. Occasionally, ascending basaltic magma reached a water saturated layer resulting in a phreatomagmatic eruption forming a maar or tuff ring.

Fig. 3.7 Scoria cone in the East Ziway Volcanic Field

Fig. 3.8 Bedded basaltic phreatomagmatic tuffs of a tuff ring at Adami Tulu

Central volcanic complexes are disposed along the axial zone of the rift, the Wonji fault belt. They are either huge conical mountains or calderas formed in the place of older volcanoes. The main volcanic centers from north to south within the rift include Aluto, Shala/Fike and Corbetti.

Fig. 3.9 Obsidian lava flow from the Chebi Volcano within the Corbetti Volcanic Complex

Geological Settings

Fig. 3.10 Clast-supported pumice fall deposit

The main rock types are rhyolites (obsidians) and trachytes. In some centers alkaline and per-alkaline products are mainly represented by pumice and non-welded tuffs, often associated with obsidian. In some centers northwest of Hosaina early products are fiamme or other ignimbrites. In several volcanoes southwest of Hosaina and elsewhere, where ignimbrites, rhyolites and unwelded tuffs were mapped together, they are shown on the map as undifferentiated peralkaline silicic rocks. Most of the products of the central volcanoes are peralkaline rhyolites and trachytes of pantelleritic or locally of comendetic affinity (Gibson, 1970; Di Paola, 1976; Brotzu et al., 1980).

Quaternary Sediments are intercalated with Pliocene to Pleistocene ignimbrites both on the rift floor and rift shoulders. The older sediments are lacustrine diatomite, tuffaceous clays and silts interbedded with basal ignimbrites of the Nazret group. At the beginning of the Quaternary a huge ancestral lake stretching form the area around Chamo-Abaya lakes in the south up to Awash basin

Fig. 3.11 Re-sedimented pyroclastic deposits interbedding with lacustrine sediments at Bulbula

in the north existed until it was separated into the present lakes by Late Pleistocene tectonic movement. Pleistocene–Holocene lacustrine sediments cover a significant tract of ground and were deposited in a huge lake whose level 3,500 to 2,100 years ago was 100 m higher than today (Kazmin et al., 1980). The lacustrine sediments are intercalated with redeposited volcanic ash and tuffs and are mainly represented by sand and silt. The major components of the sediments, such as pumice and volcanic ash, obsidian, rhyolite and basaltic rock fragments, are volcanic in origin. On the rift floor, interlayering of primary air fall pyroclastic deposits and lacustrine deposits is common. The subaqueous pyroclastic deposits can be identified by reverse graded bedding of pumice layers. Rounded rock fragments indicating abrasion during transportation by rivers and waves of lakes, poor consolidation, and the presence of evaporites distinguish subaqueous pyroclastic materials form reworked sedimentary deposits. Evaporites such as soda or trona ($NaHCO_3$) and micro-organic (diatomite) deposits occur around Lake Ziway and to the north of Lake Abijata, and attain a thickness of 600 m.

3.4 Tectonics

The main Ethiopian rift has accommodated the active extension between the Nubian and Somalian plates since the Late Miocene (e.g. Ebinger 2005). This area recorded a typical evolution of continental rifting, from fault-dominated rift morphology in the early stages of the continental extension (transtension) to magma-dominated extension during break-up (e.g. Agostini et al. 2011; Accocella 2013). The mapped area itself is predominantly built by effusive rocks and volcaniclastic deposits of the Nazret Group, Chilalo and Dino Formations followed by younger rift-floor basalts with associated pyroclastics and rhyolites with cognate pyroclastics of the Central Volcanic Complexes. In addition, limited Holocene re-sedimented pyroclastic deposits with lacustrine sediments intercalations fill the north-northeast – south-southwest trending tectonic depressions. Across the mapped lithologies different sets of primary volcanic and sedimentary fabrics (flow-banding, flow-foliation and bedding) and brittle rift-related structures (for example normal to strike-slip faults and extensional joints) were identified.

3.4.1 Primary structures

The Holocene pyroclastic deposits and lacustrine sediments include bedding mainly in a subhorizontal orientation (Fig. 3.12 - left; Fig. 3.13). The rhyolites of the Central Volcanic
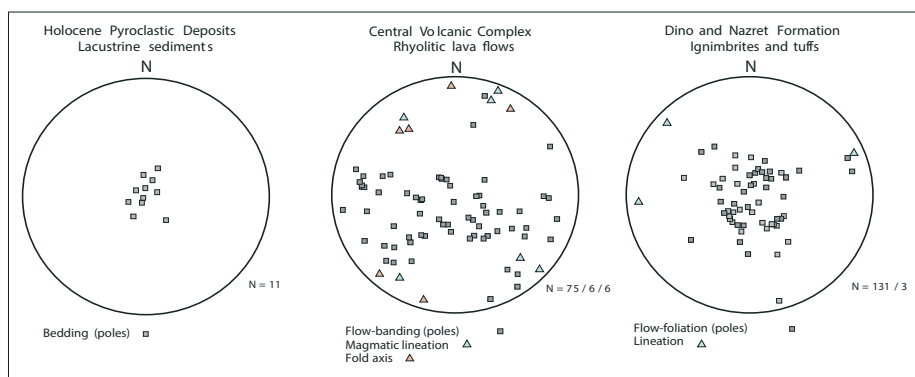
Fig. 3.12 Orientation diagrams of primary and ductile structures: left – Bedding in Holocene deposits (poles); center – Flow-banding, lineation and fold axes in rhyolites of the Central Volcanic Complex; right – Flow-foliation and associated lineation in ignimbrites and tuffs in the Nazret and Dino Formations. Equal projection to a lower hemisphere

Fig. 3.13 Sub-horizontal bedding in Holocene pyroclastic (Alem Tena)

Complexes show flow-banding (Fig. 3.14) defined by a planar preferred orientation of rock-forming minerals or domains with variable amounts of micro-vesicles or micro-crysts. Their orientation is originally sub-horizontal or gently dipping approximately to the north (Fig. 3.12 - centre; maxima in centre of the diagram). Ignimbrites of the Nazret and Dino Formations display flow-foliation

Fig. 3.14 Asymmetric folds of flow-banding (Ebicha)

Fig 3.15 Elongated lithics and pumice fragments in rhyolitic ignimbrite of the Dino Formation (Alekso)

dipping predominantly at low angles to the north-northwest, north or south (Fig. 3.12 - right). The bands of approximately cm-scale often contain elongated mineral grains and lithic fragments or

Fig. 3.16 Large-scale fold of flow-foliation in Dino Formation ignimbrites related to the NNE – SSW trending fault (Alekso)

stretched and welded pumice fragments (Fig. 3.15). Linear preferred orientation of minerals was not observed. The origin of all primary structures in rhyolites and rhyolite ignimbrites was related to the flow-stretching of viscous silicic lava or hot glass (above glass-transition temperature) fragments during flow (either coherent lava or clastic ignimbrite).

3.4.2 Ductile structures

In a number of places the planar fabrics in the Central Volcanic Complex or the Nazret and Dino Formations were folded into asymmetric folds, mainly along the north-northeast – south-southwest trending regional fault zones (Fig. 3.16). The fold limbs dip under various angles to the east-southeast or west-northwest (Fig. 3.12 - centre; maxima in peripheral parts of diagram). Corresponding fold axes plunge under low angles towards the north or south (Fig. 3.12 - centre). Relevant axial planes have mainly a steep to moderate orientation dipping to the east-southeast. In several places the folded magmatic layers contain well developed stretching lineation of deformed minerals and fragments plunging under low angles to the north or north-northwest (Fig. 3.12 - centre).

3.4.3 Brittle structures

Faults and fault zones

Different sets of brittle structures were observed across the mapped area (for example regional normal faults to strike-slip faults and fault zones, and extensional joints). Rare caldera-related faults are associated with the evolution of individual volcanic bodies (e.g., Corbetti Caldera in the southern part of the map sheet) and have a curved asymmetric shape, mostly parallel to the caldera rim. These faults predominantly dip moderately to steeply towards the central parts of the caldera, bearing the evidence of normal kinematics. Regional faults and fault zones related to the East African Rift System significantly affect the geological framework of the area (e.g., Tesfaye et al. 2003) and are mostly parallel to the main axis of the rift and morphological escarpments (Fig. 3.17). These faults dip steeply to the east-southeast (east) or west-northwest (west) bearing well developed steeply plunging slickensides (Fig. 3.18; Fig. 3.19 - upper line of diagrams). The observed slickenside asymmetry reveals normal movement in the direction of the lineation. Subordinate sets of faults predominantly have (a) an approximately west to east trend bearing both normal and dextral strike-slip kinematic indicators (Fig. 3.19, 3.20, 3.21) or (b) a northwest (north-northwest) to southeast (south-southeast) trend including a sinistral and also in some cases a dextral strike-slip component of movement (Fig. 3.19). In several localities across the mapped area the strike-slip faults appear to be older than the normal regional faults. The fault zone followed by River Bilate was also detected by vertical electric sounding near Alaba Kulito (Fig. 3.22).

Fig. 3.17 NNE – SSW trending escarpment parallel to the regional normal faults (Herera)

Fig. 3.18 Regional NNE – SSW trending fault with a normal component of movement (Adami Tulu)

Geological Settings
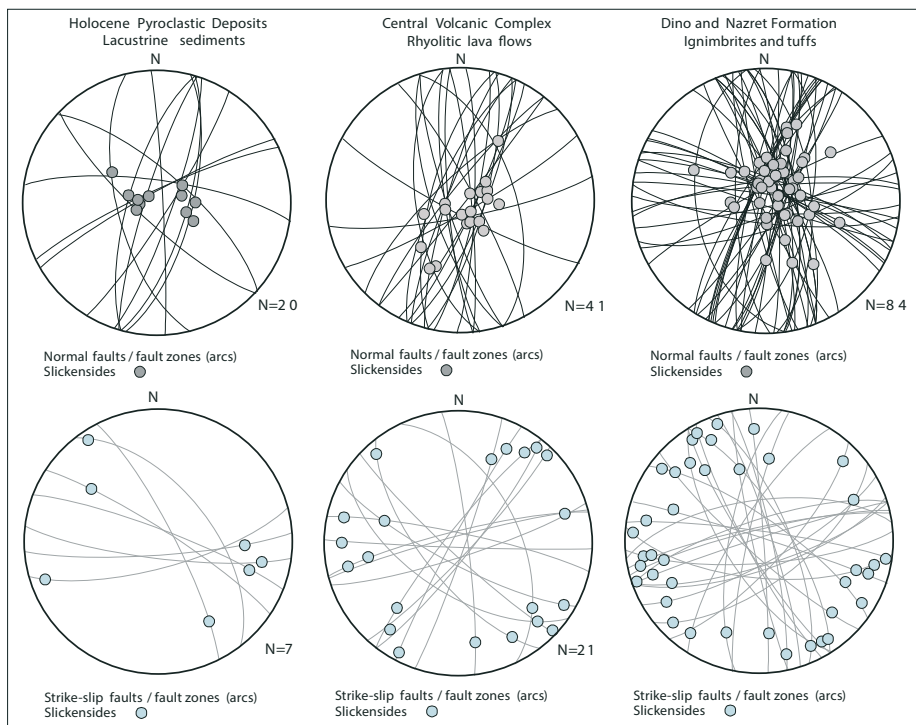
Fig. 3.19 Orientation diagrams of faults and associated slickensides. left – Normal and strike-slip faults in Holocene deposits; center – Normal and strike-slip faults in Central Volcanic Complexes; right – Normal and strike-slip faults in Dino and Nazret Formations. Equal projection to a lower hemisphere

Extensional joints

Extensional joints occur in three distinct sets with similar direction frequencies. Across all of the lithological units on the map sheet extensional joints trending north-northeast – south-southwest,

Fig. 3.20 Regional WNW – ESE trending fault with a strike-slip component of movement (Ebicha)
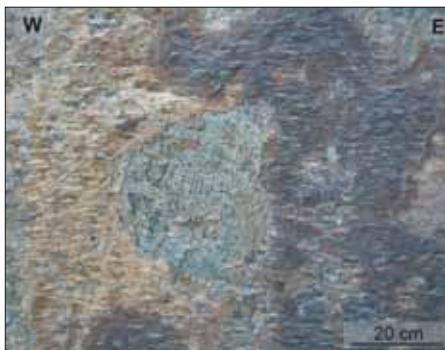
Fig. 3.21 Subhorizontal slickensides associated with a WNW – ESE trending fault (Hawasa)
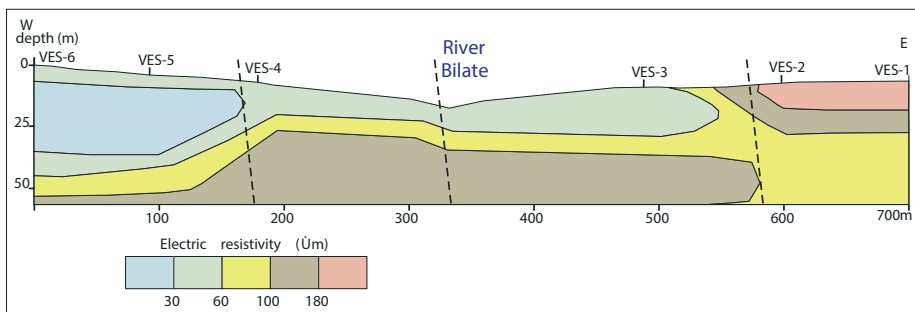
Fig. 3.22 vertical electric sounding profile across fault zone followed by River Bilate near Alaba Kulito
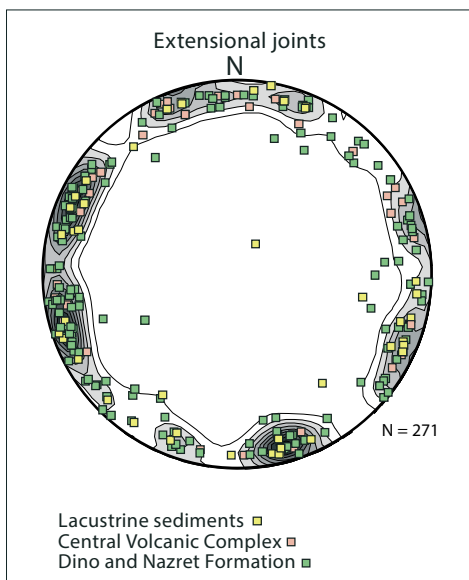
Fig. 3.23 left – Orientation diagram of the extensional joints in different units (poles). Equal projection to a lower hemisphere; center – Rose diagram indicating the dip-direction frequency of extensional joints in all units; right – Rose diagram showing the dip-direction of faults and fault zones in all units

north-northwest – south-southeast and east – west were measured (Fig. 3.22 – left). Their orientation is largely consistent with regional faults (Fig. 3.22 - compare rose diagrams in the centre and right).

3.5 Geochronology

Within the framework of the project, a total of 20 samples of volcanic rocks were dated using the K-Ar method, 12 of which were from the area of the Hosaina map sheet. The geochronological analyses were carried out in the ATOMKI Laboratories (Debrecen, Hungary) by Dr. Zoltán Pécskay. Potassium concentrations were measured using a CORNING 480 digitized flame photometer machine with a Li internal standard. The analyses were controlled by inter-laboratory standards Asia 1/65, LP-6, HD-B1 and GL-O. Argon was extracted from samples by high frequency induction heating. The A 38Ar-spike was introduced to the system from a gas pipette before the degassing started. The isotopic ratios were measured on a 15 cm radius magnetic sector-type mass spectrometer under a static mode, built in Debrecen, Hungary. Balogh (1985) and Odin (1982) described the methods applied in detail. The calculation of ages was based on atomic constants suggested by Steiger and Jäger (1977). The analytical errors are quoted for a 68% confidence level (one standard deviation). The results are listed in Table 3.2 and shown on Fig. 3.24.

The obtained data were compared with previously published data, namely those with precise locations (JICA 2012). The oldest obtained age of 10.3 Ma comes from basaltic rock exposed in the lower part of the scarp in Wendo Genet (Žáček et al. 2014). This age would correspond to basaltic members in the lower part of the Nazret Group. The Dino Formation is represented by

Tab. 3.2 K-Ar data obtained on volcanic rocks from different volcanic fields (2013)

Sample	Rock type	K (%)	$^{40}Ar_{rad}$ (ccSTP/g)	$^{40}Ar_{rad}$ (%)	K-Ar age (Ma)
HSRVR051 – Chefe Jila	scoria	0.671	8.2760×10^{-8}	4.7	3.17±0.87
HSRVR053 – Chefe Jila	basalt	0.605	3.0490×10^{-8}	2.2	1.29±0.86
HSRVR074 – Hawasa	basalt	0.616	No $^{40}Ar_{rad}$	-	-
HSRVR091 – Benkoya	basalt	1.091	2.5503×10^{-8}	2.1	0.60±0.30
HSRVR093 – Dolocha	basalt	0.861	4.1433×10^{-8}	2.0	1.24±0.85
Sd013 – Wendo Genet	rhyolite	3.677	1.6978×10^{-7}	12.7	1.18±0.12
Sd017 – Wendo Genet	rhyolite	3.448	1.3675×10^{-7}	10.4	1.02±0.14
Sd036 – Wendo Genet	ignimbrite	3.715	9.6643×10^{-8}	7.2	0.669±0.129
Sd048 – Wendo Genet	ignimbrite	3.849	2.9929×10^{-8}	2.1	0.20±0.14
Sd042 – Wendo Genet	basalt	0.822	3.3012×10^{-7}	10.3	10.30±1.40
Sd067 – Wendo Genet	ignimbrite	3.568	1.3692×10^{-7}	5.2	0.98±0.26
HSRV136 – Shala	glass from ignimbrite	3.475	1.3839×10^{-7}	1.5	1.02±0.80
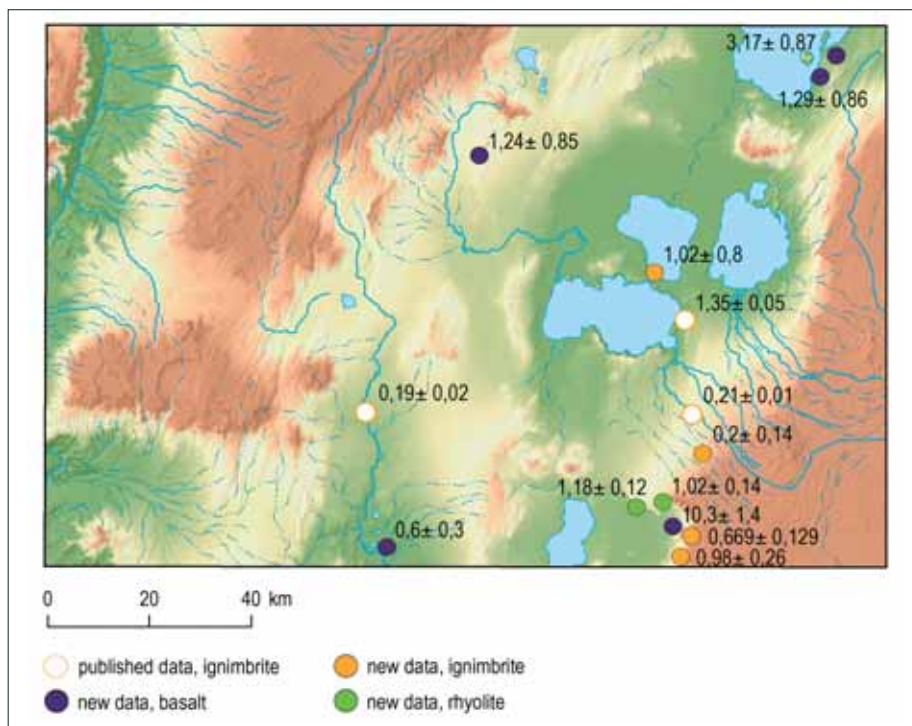
Fig. 3.24 Location of K-Ar geochronological results

"black" ignimbrite from Shalla Caldera (1.02 Ma) and rhyolitic effusions terminating the activity of Hawasa Caldera (1.18 and 1.02 Ma). Subsequent activity leaded to the formation of Corbetti Caldera, which produced several ignimbrites (0.98, 0.669 and 0.2 Ma). We accept the youngest age despite the large error, as this age is in good accordance with data obtained by JICA (2012).

Data from most of the basaltic rocks suggest long lasting activity in monogenetic volcanic fields. The very young ages combined with low potassium content result in large errors. Despite these errors, we are able to state that volcanic activity in the Hawasa-Shalla Volcanic Field lasted longer than supposed and this field should be evaluated as dormant and not extinct. On the other hand, East Ziway and Butajira Volcanic Fields experienced basaltic eruptions as early as 500 ka.

3.6 Geological Evolution

Based on field and structural data and taking into consideration previous regional works the geological history of the Hosaina area can be divided into several episodes. The oldest recorded rocks in the area of interest are grouped into the Alaji Group of Oligocene–Miocene age (pre-rift volcanic succession). Uplift, doming and eventual rupture of the Afro-Arabian region resulted in the formation of the East African Rift system oriented in northeast–southwest and north-northwest–south-southwest directions. The initial sagging of the Main Ethiopian Rift began around 15 to 14 Ma. An important event in the rift development took place around 10 Ma (Kazmin et al., 1980; Davidson, 1983, and others). This development caused faulting of the pre-rift volcanic succession.

The Miocene-Pliocene to Holocene cover of the floor of the Rift Valley (Kazmin et al., 1980 and others) consists of a thick succession of stratified felsic volcanic rocks such as ignimbrites, non-welded tuffs, ash flow deposits, rhyolite and trachyte lavas. These rocks also outcrop on the rift escarpments and adjacent plateau margins and are referred to as the Nazret group (9.5–4 Ma). On the rift floor, the Nazret group is overlain by a sequence of flood basalts of Pliocene age referred to as Bofa basalts (3.5–2 Ma).

With the formation of the Wonji fault belt (Pleistocene to Holocene), tectonic movements produced step-like structures and associated volcanic activity is represented by ignimbrites, basalts and unwedded pyroclastics. The fault zone is straddled by central volcanoes found along the axial zone of the Wonji fault belt. The main products were obsidian, rhyolite and trachyte lavas, pumice and tuffs. The products of the Wonji fault are referred as the Wonji group (Kazmin et al., 1980 and others). Another type of volcanic activity in the Wonji fault belt was the eruption of basalt lava flows from fissures from the Late Pleistocene to the present. The basalts are controlled by extensional fractures and commonly characterized by fresh aa surfaces. Chains of scoria- and spatter-cones, tuff rings and maars follow the lines of fractures. These basalts are mostly found in the rift floor; east and south of Lake Ziway, along the Bilate River, around Dolocha, south of Lake Shalla and around Hawasa. Recent flows in many cases follow pre-existing topographic low relief areas. Although the development of the rift was dominated by volcanic activity, deposition of lacustrine sediments was also common. These sediments cover the rift floor in areas surrounding lakes Ziway, Langano and Abijata. The sediments are mainly represented by re-sedimented pyroclastics, sand and silt.

Geological Settings

4. Rock properties and economic perspectives

4.1 Engineering geology

Engineering geological mapping was carried out by experts from the Geological Survey of Ethiopia (GSE) following their internal standards and methods. Experts from the Czech Geological Survey provided advice in text arrangement and visualization of the results.

In engineering geological mapping, rocks and soil are classified using the principle that the physical or engineering properties of the rocks are a combination of the results of origin, diagenesis, metamorphism, tectonism, alteration, and degree of weathering (IAEG, 1976). Based on the result of the engineering geological investigation using rock strength, genesis, and laboratory tests as crucial criteria, the rocks within the project area are subdivided into five rock mass strength units:

Engineering geological rock units:

- Rock with very high rock mass strength (VHRMS)
- Rock with high rock mass strength (HRMS)
- Rock with medium rock mass strength (MRMS)
- Rock with low rock mass strength (LRMS)
- Rock with very low rock mass strength (VLRMS)

Engineering geological soil unites:

- Alluvial soil
- Residual soil
- Colluvial soil

4.1.1 Engineering classification of rocks

Various lithological units identified and mapped in the study area are further classified into several rock mass strength classes. The main criteria for the classification are rock material strength and discontinuity conditions. Despite the fact that variations in the local engineering attributes are significant, they cannot be displayed on the presented engineering geology map. It must be stated here that the engineering geology mapping was made at a scale of 1:250,000 with the density of documentation corresponding to this scale. Therefore, this engineering geological map is basically useful for regional planning rather than for specific and detailed site characterization. A detailed study of the selected site is required prior to any larger construction work being performed.

Rock properties and economic perspectives

The lithological units mapped in the area of the Hosaina map sheet were tested to determine their geotechnical characteristics. Rock material strength (UCS) was determined in the field using a point load tester and a Schmidt hammer.

Rocks with very high rock mass strength (VHRMS)

Rocks that were classified as VHRMS are dominantly various basalts with minor trachyte. They are exposed on the western, northern and central parts of the study area. These rocks form ridges, hills and hold steep cliffs and scarps. They are characterized by tectonic fractures, mostly steeply dipping, and columnary jointing with variable spacing (Fig. 4.1). The size corrected point load index strength (Is50) values vary in the range of 12.35–19.49 Mpa, and the unconfined compressive strength calculated from point load index strength (Is50) ranges from 132 to 185 Mpa. This implies that the unit belongs to a class of rocks with very high mass strength (VHRMS). The results of laboratory tests of water absorption on representative samples range in values 0.15–9.15 %, porosity in the range of 2.13–18.75 % and bulk density 2.0–2.86 kg/dm^3. Basalts with water absorption values less than 1 % differ significantly from those of trachytes, which can reach up to 9 %. Basalts are hence more suitable for concrete and asphalt mixes than trachytes.

Rocks with high rock mass strength (HRMS)

Rocks that were classified as HRMS are mainly obsidian and rhyolitic lavas. This unit covers the largest part of the study area and it is characterized by a wide range of strength property. The rhyolitic and obsidian lavas are mostly dome-shaped with gentle to moderately steep slopes. These rocks occur in central, southern and northwestern parts of the study area. Black to dark green color is characteristic for rocks of this unit. Rhyolites are fine to medium grained, whereas obsidians are glassy resulting in conchoidal fracturing. Discontinuities are the common structures with systematic as well as non systematic orientation.

The corrected point load index strength (Is50) values of this unit range from 3 to 7 Mpa. The converted calculated unconfined compressive strength of this unit from (Is50) values range from 26 to 165 Mpa, which implies that the unit shows extremely variable strength properties and also that water absorption, porosity and bulk density values vary widely. Hence, this unit requires further investigation and detailed evaluation before major construction work or industrial employment is undertaken.

Fig. 4.1 Trachybasalt jointed into thick columns (Herera, Ziway)

Fig. 4.2 Rhyodacite exposed in an active quarry on the southern edge of Hawasa

Rock properties and economic perspectives

Fig. 4.3 Holocene obsidian exposed on the northern shore of Lake Hawasa

Rocks with medium rock mass strength (MRMS)

This group is composed of rhyolite and ignimbrites exposed in the central part of the study area. It forms gentle to moderately steep, often cliff-forming, topography. Rocks of this group are characterized by light pinkish to yellowish color. Rhyolites are fine to medium grained with a porphyritic texture. Both rock types are moderately weathered and are often columnary jointed. Ignimbrites are locally intercalated with basalt lavas and non-welded pyroclastic deposits. The corrected point load index strength (Is50) ranges from 2 to 3 Mpa, and the calculated unconfined compressive strength of this unit is 27–50 Mpa.

Rocks with low rock mass strength (LRMS)

This group comprises scoriae, poorly welded ignimbrites, and pumiceous pyroclastic deposits exposed in the central to northeastern parts of the study area. These lithologies usually form topographically low relief with elongated ridges and cones. The cinder-cones frequently bound structurally controlled valleys. The slopes are short and moderately steep and less resistant to erosion. Since these loose pyroclastic deposits exhibit weak rock strength, no point load tests or

Fig. 4.4 Rhyolite exposure near Ziway

Fig. 4.5 Columnary jointed slightly weathered ignimbrite exposed near Hosaina

Rock properties and economic perspectives

Fig. 4.6 Scoriae in an exploited scoria cone in Hawasa   *Fig. 4.7 Pumice deposits in Corbetti Caldera*

further physical tests were conducted. They easily disintegrate and fragment under even a light hammer blow.

Rock with very low rock mass strength (VLRMS)

This unit is composed of volcanic ash and tuff deposits and is exposed mainly in the eastern part of the study area. This unit covers most of the floor of the rift. It is light yellowish in color, with an unconsolidated pyroclastic (fragmental) structure, non-welded with a grain size equal to silt or sand. In most places the tuff is covered by brown silty clay soil overlain by sandy gravel.

4.1.2 Engineering classification of soils

Classification of soils is the arrangement of soils into different groups according to their origin and properties. In engineering geology the term "soil" is defined as unconsolidated material composed of solid particles, produced by the disintegration of rocks. Generally, an area with a soil unit thickness exceeding one meter is mapped as a soil unit. If the soil thickness is less than one meter, it is simply mapped as the underlying bedrock. Of the many different soil classification systems, the unified soil classification system (USC) is used in this work. The USC system uses both particle size analysis and the plasticity characteristics of soils.

Fig. 4.8 Bedded to laminated tuffs and lapilli-stones of the phreatomagmatic eruption of Budomeda maar

Rock properties and economic perspectives

The soil type in the study area is classified as alluvial, residual and colluvial. Test pits were dug and representative soil samples were collected for granulometric analysis, atterberg limits and moisture content analysis in the laboratory. The liquid limit and plastic limits are used for soil classification. If the amount of clay minerals present in a particular soil sample is higher, then the soil becomes highly plastic, its shrinkage and swelling values become higher. Consequently, such soil properties mean more problems for construction work.

Alluvial soils

Alluvial soils are found in the flat area of Kulito, Mazoria, Heregdina, Demboya and Neketa, along river channels and in the inter-mountain depressions and flat plains. As observed from soil exposures and test pits, these soils have silt-clayey composition, a brown to reddish brown color, and a rough texture. In general, they show a medium degree of plasticity. The unconfined compressive strength of the alluvial soil ranges from 2 to 10 kg/cm^2 based on in-situ pocket penetrometer measurements.

Residual soils

Residual soils in the study area are found in the Kofle, Kore, Shire and Goffer area. They are developed over ignimbrites, rhyolites and unconsolidated sediments. They are silt-clayey in composition and reddish in color. Ignimbrite is characterized by closely spaced discontinuities, and as a consequence it is affected by weathering, which forms the thick lateritic cover. Leaching of silica has led to the concentration of Fe and Al oxides and formed a thick residual cover over the ignimbrites rock (Fig. 4.9). Red residual soil in the Kofele area is a representative example. The unconfined compressive strength of the residual soil ranges from 4 to 12 kg/cm^2 based on in-situ pocket penetrometer measurements. It is a plastic, fine to medium grained red soil.

Fig. 4.9 Reddish residual soil developed on rhyolitic ignimbrite (Kofele)

Colluvial soils

Colluvial soils are found occupying the foothills of the caldera and fault scarps, particularly around the Wendo Genet recreational area. These soils result from the slow movement of soil developed upon bedrock down-hill due to gravity. The unstratified colluvial soils contain randomly oriented angular blocks of bedrock in a silt-clayey matrix. Granulometric analysis of the sample

Rock properties and economic perspectives

taken at the foothills of the caldera scarp shows a grain size distribution of 12 % fine gravel, 48 % sand, and 40 % silt and clay.

4.2 Economic geology

4.2.1 Construction materials

The rapid growth of the construction sector demands the supply of raw materials. In this regard, the study area is known for its great potential for construction materials suitable for various purposes e.g. dams, bridges, roads, buildings, cement industry, etc.

Basalt

Fresh, fine-grained, jointed and strong basalts are a good source for crushed concrete aggregates, whereas scoriaceous basalts are suitable for road construction. In the study area quarry sites of basaltic rock, which can be mainly used for the construction of road and concrete, were identified and inventoried. The presence of joints makes the basalt easily workable. The basalts have negligible weathering zones, mostly being fresh and strong. There are no intercalations of other soft rocks or soils. The crushed aggregates will not be flaky since the joints are not very closely spaced and have no impurities such as organic matter or clay. Weathered and highly jointed basalts are a good source of materials suitable for use as subbase or as natural gravel. Several active and abandoned quarries of these materials are found in the study area mainly along the main and secondary roads.

Fig. 4.10 Crushing basaltic rock in the quarry for asphalt and concrete mixes

Scoriae

Basaltic scoriae are porous and therefore permeable. On the other hand, they have a relatively high load strength. Therefore, scoriae are used for construction of secondary all-weather gravel roads. Scoria quarries are found where young scoria cones occur e.g. around Ziway and Chefe Jila, in Hawasa, along the road Shashemene – Aje, and around Dolocha.

Rock properties and economic perspectives

Fig. 4.11 Exploitation of a scoria cone near Bura for the construction of secondary roads

Rhyolite

Several rhyolite quarries are inventoried in the study area. Rhyolite is good quality, columnar jointed rock, which is easily workable and can be used for the production of masonry for the construction of buildings, bridges, and other engineering structures.

Ignimbrite

In the study area ignimbrite rocks are extensively used for road construction. Cobble size ignimbrite rocks are shaped into different patterns to make secondary roads which branch out from main roads. Many local people are engaged in cobble stone production.

Fig. 4.12 Quarry producing pavement cobbles from rhyolitic ignimbrite near Hawasa

Fig. 4.13 Cobbles from rhyolitic ignimbrite

Pumice

The rapidly increasing construction industry requires cement for its activities. Different cement factories use pumice as a raw material for cement production. The eastern part of the study area

Rock properties and economic perspectives

has a good potential for pumice rock. The use of pumice in concrete is doubtful due to the high fluorine content in pumice. Acidic reaction of hydrogen-fluoride attacks the concrete and reduces the lifespan of concrete constructions.

4.2.2 Decorative stones

Opal

Southern Ethiopia remains unexplored in terms of decorative stones. Precipitation of silica gels and hydrothermal transformation of obsidian produces placers of opal and other precious varieties of silica, among which many might be of use for jewellery. Opals precipitated from hydrothermal springs were documented on Alutu Volcano. Obsidian transformed to pinkish opal was documented on Macho Hill near Adami Tulu (Fig. 4.14 and 4.15). We recommend further survey and tests in the jewellery use of opals from the Alutu and Macho sites. The increasing number of tourist coming to Southern Ethiopia as well as the growing number of richer Ethiopians represents a potential market for products made from Ethiopian opals.

Fig. 4.14 Macho Hill near Adami Tulu consists of opalized obsidian

Fig. 4.15 Breccia of pinkish opal on Macho Hill

4.3 Geothermal energy

Volcanic activity is usually associated with hydrothermal systems with a great potential for geothermal power production. Reconstruction of the Alutu geothermal power plant inside the caldera of Alutu Volcano (Fig. 4.16) is soon to be completed and the power plant should supply the Ethiopian network with energy. The apex of the entire Alutu Volcano represents an active hydrothermal system (Fig. 4.17) as well as its slopes and foothills.

Fig. 4.16 Steam escaping from one of several wells of the Alutu Geothermal power plant

Fig. 4.17 Steaming hot springs in the apical part of the Alutu Volcano

Rock properties and economic perspectives

A survey performed by the Icelandic company Reykjavik Geothermal focused on the hydrothermal system of the Corbetti Caldera. This volcanic system has less numerous manifestations of hydrothermal activity the than Alutu Volcano. Šíma in Rapprich et al. (2013) interprets this feature as a result of strong subsurface flow of groundwater from Lake Hawasa towards Lake Shalla which also drains the hydrothermal system beneath the Corbetti Volcanic System. Numerous hot springs occur on the southern shores of Lake Shalla. Other groups of hot springs can be found on the northeastern shores of Lake Shalla (Fig. 4.18), in the Shalo area (Fig.4.19) and Wendo Genet east of Hawasa, southeast of Hawasa and along the River Bilate. Most of these hot spring areas have no power production potential but are productive enough for balneological purposes (see e.g. Tilahun and Šíma 2013).

Fig. 4.18 Hot spring on the northeastern banks of Lake Shalla

Fig. 4.19 Shalo hot springs

During the field campaign in 2014, an explosion of an irrigation well at Ashute Buraco (near Butajira) was documented during the night of April 30th to May 1st. Drilling to reach water for irrigation began to produce boiling water at the depth of approximately 200 m. The explosion created a crater 20 m in diameter (Fig. 4.20) and a high discharge rate (50-100 l/s) of hot water flowed like a boiling river into the village of Ashute Buraco. The boiling water injured one woman in the village during the first night. Even though the location of the drilling is to the north of the mapped

Fig. 4.20 Crater of the man-induced geyser in Ashute Buraco (April 1st 2014)

Rock properties and economic perspectives
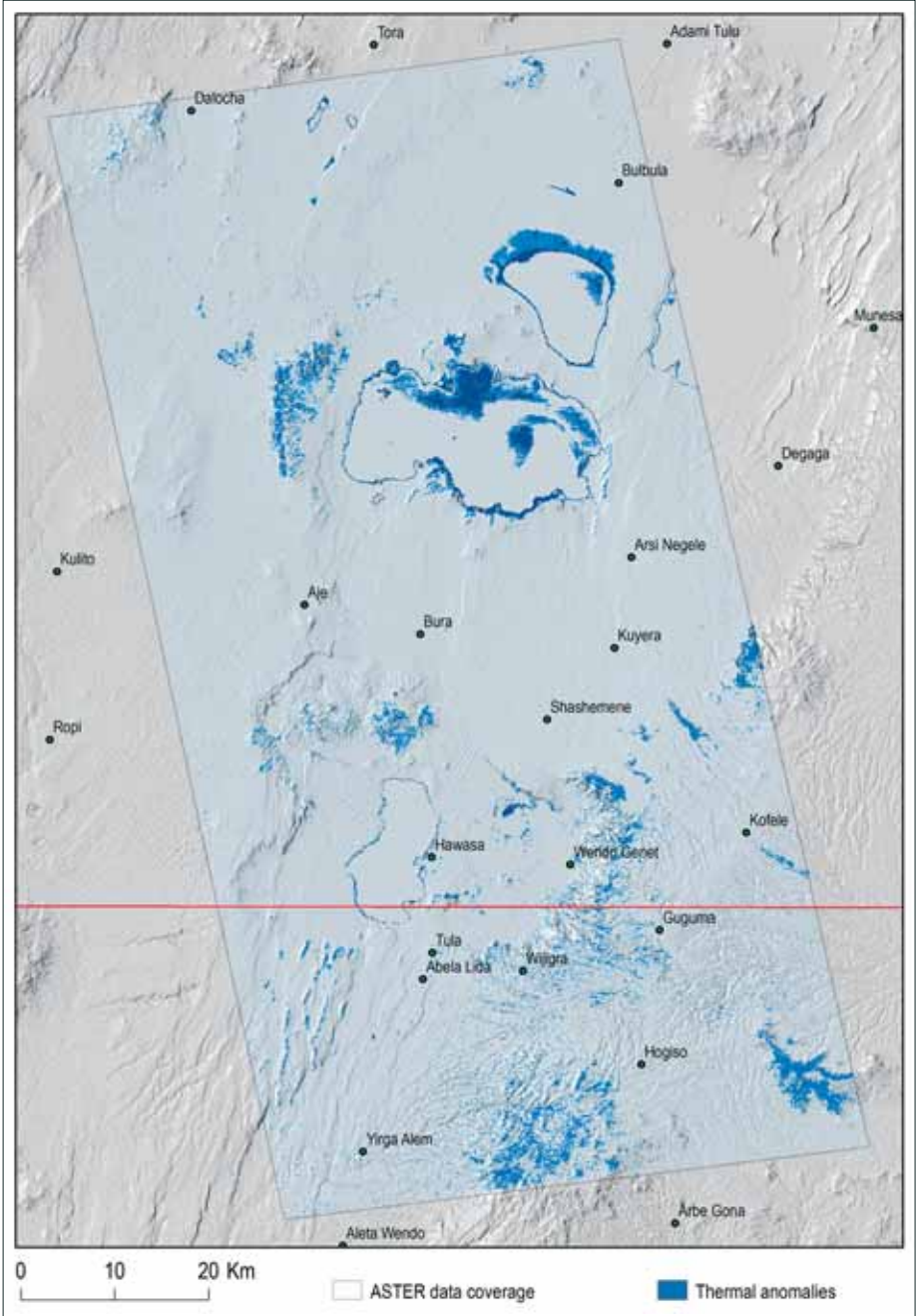
Fig. 4.21 Scheme of thermal anomalies observed from Aster satellite data (night and day images)

Rock properties and economic perspectives

sheet, this incident suggests that the entire Butajira Volcanic Field is volcanically and hydrothermally active and should be the subject of further hydrothermal investigation and exploration.

In parallel to the Butajira Volcanic Field, we may expect the existence of a similar geothermal system in the East Ziway Volcanic Field. This area also requires further geothermal survey and exploration.

To detect potential hotspots, we analyzed night and day thermal Aster images (Fig. 4.21). The resulting image displays known hot spring areas (Lake Shalla, Wendo Genet, southern part of Lake Hawasa), water-saturated areas with dense vegetation (Wendo Genet) and also spots suggesting active (dormant) volcanoes (Corbetti area, scoria cones near Dalocha and Fike Volcano).

4.4 Geotourism potential

Several national parks and reserves have been established in the area of the Hosaina sheet with an aim to protect the remnants of the original wildlife. The Shalla-Abijata National Park (Fig. 4.22) protects various bird species around two large lakes (Shalla and Abijata). On the other hand, East

Fig. 4.22 African ostrich in the Shalla-Abijata National Park

Fig. 4.23 Swayne's hartebeest in the Senkele Hartebeest Sanctuary

Fig. 4.24 Colobus monkey in the Amora Gedel Park

Rock properties and economic perspectives

Langano Natural Reserve focuses on various types of monkeys. The Senkele Hartebeest Sanctuary protects Swayne's hartebeests which are a remnant of the original savanna (Fig. 4.23). Inhabitants of Hawasa may visit Amora Gedel Park which houses many monkeys (Fig. 4.24) near the fish market. Apart from nature protection, these parks also attract tourists. The private sector as well as public budgets therefore benefit from the existence of national parks and reserves.

Compared to other African countries, the wildlife in Ethiopia is relatively poor from a tourism point of view. On the other hand, the geological sites are potentially attractive for visitors. Peaks, volcanoes, lakes and waterfalls commonly represent such geological sites. The area of the Hosaina sheet comprises several geological sites, which could contribute to local (and federal) economy with proper visitor management.

The abandoned quarry in Kubi Kelle (Fig. 4.25) offers a view into a small extinct volcano and its deposits. This locality is close to the Shashemene-Alaba Kulito road and it is also home to a large group of rock hyraxes (Fig. 4.26).

Fig. 4.25 Abandoned quarry in an extinct scoria cone in Kubi Kelle

Fig. 4.26 Rock hyraxes in the abandoned Kubi Kelle quarry

Picturesque landscapes represent attractive tourist destinations. Such landscapes are commonly created by monogenetic volcanism. There are several monogenetic volcanic fields in Southern Ethiopia. Three small lakes filling explosive craters of maar-type volcanoes (Budomeda – Fig. 4.27, Tilio, Machaferra) are arranged along the Bilate River to the south of Alaba Kulito. A picturesque landscape is characteristic also for the Butajira Volcanic Field, where small volcanic cones combine with numerous waterfalls. This is also the area of the proposed Butajira Geopark. With its high peaks attracting climbers, Mount Ambericho (Fig. 4.28) also has a potential for tourism.

Fig. 4.27 Budomeda crater lake in maar

Fig. 4.28 Mount Ambericho

Rock properties and economic perspectives

5. *5. Geological hazards*

5.1 Endogenous geological hazards

5.1.1 Seismic hazards

Seismic hazards in the studied segment of the Main Ethiopian Rift (7° – 8°N) are conditioned by the extensional tectonics in the rift region. From a global point of view, the seismicity connected with rifts (both oceanic and continental) represents about 6% of the seismic energy release. Continental rifts are characterized by a special type of seismicity, including seismic swarms and volcanic earthquakes. The presence of geothermal phenomena is another typical feature of rift regions. Core fluids (magma, CO_2, water, vapor) can decrease mechanical friction in tectonic faults and trigger seismic events. Big earthquakes in rift regions are observed less frequently than at convergent margins of lithospheric plates; however, catastrophic earthquakes are not excluded. The controlling earthquakes have long repeating periods and hence the computation of seismic hazards represents a complex problem, which is an important issue for industrial development.

The East African Rift System (and the Main Ethiopian Rift as its segment in Southern Ethiopia) is not adequately explored. Only a very rough estimation of seismic hazards is available. The rapid growth of urban population, extensive house building, and infrastructure development call for seismological investigation, which is the basis for a more detailed estimation of seismic hazards. A probabilistic approach to seismic hazard estimation is recommended as a standard used in western countries over the last decade. The probabilistic seismic hazard assessment (PSHA) is suitable also for the Rift Valley in Southern Ethiopia. The most important input data is a catalogue of historical earthquakes, seismograms of (small) recent local earthquakes which were instrumentally measured, paleoseismological studies, seismotectonic data and a model of geological media including seismic velocities and attenuation of seismic waves. The computation is performed in four basic steps:

1. Definition of all relevant source zones based on seismological and geological databases and on a seismotectonic model. This step has not been done properly in Southern Ethiopia. Seismological databases are extremely incomplete. This is the main reason for the list of active tectonic faults, which can generate catastrophic earthquakes, being deficient.
2. Definition of magnitude-frequency distribution (Gutenberg-Richter law - GR law) for all source zones. This task has not been performed in Southern Ethiopia yet. Only average parameters of GR-law have been derived for the whole region, while the specific parameters for individual zones are needed. A very important parameter is the maximum regional magnitude. It is unknown but it is clear that it exceeds 7.
3. Definition of the ground motion prediction equation (GMPE). Site-specific GMPEs do not exist for Southern Ethiopia. However, this holds true for many other regions. The average parameters of GMPE could be adopted from global databases. The situation in the Rift Valley is complicated by the fact that it is filled with thick sedimentary layers, which amplify

amplitudes of seismic waves. The shape of the valley significantly affects the propagation of seismic waves. The GMPE has to reflect these facts.

4. Computation of Probabilistic Seismic Hazard Curves (PSHC) The computation involves many scenarios, which can occur in the future. The importance of individual source zones for seismic hazard is also evaluated. The results are presented in the form of curves, which describe the probability that the earthquake exceeds the defined value of Peak Ground Acceleration (PGA).

Historical seismicity

In Southern Ethiopia reliable descriptions of historical earthquakes are sparse. Available data were compiled by Gouin, 1979. In his paper, the territory of Ethiopia is divided to five seismic zones. The region under study belongs to zone C – "Ethiopian Main Rift, Afar, and the Southern Red Sea". Most of earthquakes in this zone are connected to volcanic eruptions. Earthquakes of large magnitudes are located mainly in the northern part of the rift and the Red Sea. However, this is due to the fact that written testimonials were better preserved in northern part of Ethiopia. Certainly, it does not exclude the possibility of large earthquakes in the southern part of the rift. Gouin (1979) states that, "No documents never equates to no earthquakes. This statement is supported by local Galia legends about former locations presumably destroyed by seismic tremors and now covered by lakes. The legends are heard in the Rift Valley from Lake Ziway to Abaya, and on its western escarpment in Gemu-Gofa.

The oldest documented earthquakes inside the rift in Southern Ethiopia are two events from 25.8.1906. They also represent the strongest observed earthquakes in the region. Teleseismic recordings show two important shocks on the 25th of August 1906; the first at U.T. 11:54:48 and the second 2 hours later at U.T.13:47:36. The magnitudes were 6.6 and 6.8 and the number of reporting stations was 30 and 40, respectively. The location of the epicenter is not entirely clear. The most probable epicenter location is N 8.0°, E 38.5°, westward from the town of Adami Tulu. During the 1906 period of seismic activity, a geyser erupted on the island of O'a (N 07.5°, E 38.6°) in the northeastern bay of Lake Langano. At its birth, in 1906, the height of the hot water column was 25-30 m Gouin (1979). This case documents the close connection between earthquakes and geothermal phenomena.

On the 4th of October 1928, a magnitude 6 earthquake was recorded on the scarp of the rift, to the west of Lake Abaya. The most probable location is (N 7.0°, E 38.0°). The reports of a magnitude 6 earthquake on the 6th of September 1944 are disputable (because of war). The location of the epicenter is inaccurate as the error reaches 200 km. The most probable location is (N 7.0°, E 38.5°). It cannot be proven that the epicenter is situated inside the rift. On the 14th of July 1960 at 18:39 UT an earthquake with a magnitude of 6.3 was recorded inside the rift near Chabi volcano. It was felt at a distance of up to 200 km. The average location of epicenter is N 7.1°, E 38.4°. A smaller earthquake with a magnitude below 5 was also detected on the 8th of March 1973 with an approximate location of N 7.7°, E 37.8°.

A global catalogue of earthquakes has been available from United States Geological Survey (USGS) since 1973. However, there are no earthquakes from Southern Ethiopia reported in the catalogue prior to 1983. The events reported in the catalogue are included in Table 5.1. Six earthquakes with a magnitude of more or equal to 4.4 are reported from the mapped area from 1983 to 2013. The recent earthquakes from the 19th of December 2010 and 19th of March 2011 were felt by many people despite the fact that they were relatively small with a magnitude of approximately 5. The epicenters are shown on the map.

Despite the absence of any written chronicles in the Monastery of Tulu Gudo Island (Lake Ziway), which would comprise notes on geological events such as earthquakes or eruptions, the monks

Geological hazards

Date	Time	North (°)	East (°)	Depth (km)	Magnitude
1983-12-02	23:08:39.49	7.030	38.599	10.0	5.1
1991-07-26	15:33:38.46	7.570	37.665	10.0	4.4
1995-01-20	07:14:27.20	7.160	38.441	13.8	5.0
2006-07-04	05:51:58.46	7.917	39.009	10.0	4.5
2010-12-19	12:14:24.51	7.521	37.839	10.0	5.1
2011-10-17	01:03:25.61	7.643	37.868	10.0	4.4

remember "the earth shaking" which caused large blocks to fall from the fault scarps on the island (Fig. 5.1) in 2008.

Conclusions and recommendations: Seismic hazard assessment for the Horn of Africa by probabilistic method was published by Kebede and van Eck (1997). This paper identifes eight source zones. Zone 2 comprises the southernmost rifts of Ethiopia and the Main Ethiopian Rift and also includes the region under this study. The upper magnitude for this zone was estimated to be 7.0 with an error of 0.2. Probabilistic hazard curves were constructed for seven sites in the Horn of Africa but none for Southern Ethiopia. The nearest studied site is Addis Ababa (Central Ethiopia), where a PGA of 150 cm/s^2 was determined for an annual probability of exceedance of 10^{-3}. According to the distribution of historical earthquakes, the seismic hazard in SouthernEthiopia can be expected to be even higher than in Addis Ababa. A better estimation of seismic hazard can be performed only after collecting more reliable input data.

Fig. 5.1 Blocks that fell from the fault scarp on Tulu Gudo Island during a seismic event in 2008

Geological hazards

Intensive urban development has taken place around the lakes inside the rift, which is very worrying considering the seismic hazard. The subsoil in the most populated localities is composed of sediments and loose pyroclastic deposits with extremely low S-wave velocities, which can amplify the amplitude of seismic waves by several times compared to bedrock sites. As previously discussed, the last strong earthquake occurred in 1906, when the population in the region was much sparser and the distribution of urban housing was sporadic. Anti-seismic measures are not satisfactorily applied during house construction and the public is not prepared for a strong earthquake. For these reasons, Southern Ethiopia has to be considered as a region with a high seismic risk.

5.1.2 Ground cracks (fissures)

Ground cracks (fissures) have been documented in various locations in the Ethiopian Rift Valley (Asfaw 1998) and represent a very dangerous geological hazard. Ground fissures parallel to the rift axis were reported to the west of Lake Ziway (north of the mapped area: Asfaw 1998). Well-developed fissure systems of a south-north trend were documented to the south of Lake Shalla (Fig. 5.2). To the west, the fissures around Shala Senbete are developed within lacustrine sediments as well as on the tectonic contact between sedimentary rocks and basalts. On the other hand, further to the east between Lake Shalla and Shashemene, around Habera and Kubsa, the cracks are developed in trachytes and rhyolitic ignimbrites with thin sedimentary cover. The fissures to the south of Shala cross a populated area including the small town of Shala Senbete where one fissure opened in June 2012 destroying the road and several houses (Fig. 5.3). According to reports of local inhabitants, the fissures of the eastern belt around Habera and Kubsa opened repeatedly 20, 8 and 4 years ago (Fig. 5.4). A house with seven inhabitants fell into the crack during one of these events with no survivors.

Another system of ground cracks parallel to the rift axis can be found around Muleti, to the west of Lake Hawasa (Fig. 5.5 and 5.6). Fissures related to a perpendicular W-E to NW-SE fault system were also sometimes observed close to Shamena town, to the west of Hawasa and northwest of Ziway Lake.

Fig. 5.2 Several-kilometer long ground crack between Shala Senbete and Lake Shala

Geological hazards

The mechanism of the formation of the ground cracks is uncertain and the occurrence of fissures is random and unexpected. The conformity of the youngest fault system and fissures indicates

Fig. 5.3 Ground crack open in 2012 crossing the town of Shala Senbete

Fig. 5.4 Four-year old ground crack in Kubsa

a tectonic origin of this phenomenon. Even though local people report opening of fissures mostly after heavy rains, we have witnessed the opening of the fissure in Shalla Senbete during the culmination of the dry season in early June. Generally, the prevailing opening of cracks during the rainy season suggests that exodynamic and hydrogeological factors and processes, in addition to the tectonic trigger, contribute to the final opening of fissure systems. The occurrence of fissures

Fig. 5.5 Ground cracks in the area of Muleti

Fig. 5.6 Grass-house endangered by an opening ground crack in Muleti

Geological hazards

is limited to areas where the volcanic unweathered bedrock is covered by unconsolidated or poorly consolidated sedimentary successions within the rift structure. The association of ground cracks and vertical displacement along normal faults is known elsewhere in the world (e.g., Holzer 1984, Bell et al. 1992, Carpenter 1993). Another hypothesis is aquifer system compaction and horizontal seepage stresses, which are connected to a decline in the groundwater table (Ayalew et al. 2004). The fissure origin could be due to irregular topography (bedrock highs, scarps or buried pediment) at depth such as when compressible deposits overlie bedrocks (Schummann and Poland 1970, Carpenter 1993).

Based on our observations, fissure formations are likely to be related to the tectonic opening of cracks within solid rocks (Fig. 5.7) in the basement of the rift floor and subsequent subsurface erosion of loose material overlying the bedrock. As the soft sediments plastically accommodate the extension in the first phase, the ground cracks may remain unobserved until a devastating collapse of their thin roof (Fig. 5.8). The solid rocks deeper within the cracks are always tectonically fractured with no signs of water erosion. The fissure development is accompanied by surface and shallow subsurface processes such as piping, hydrocompaction and changes in the volume of material. This process causes rapid and unexpected subsidence of the surface and collapses of sidewalls of the fissure. Our hypothesis for the formation and development of ground cracks is summarized in Fig. 5.9.

The occurrence of fissures can be very discreet and in some cases hollows or sinkholes several decimeters deep can develop on the surface (Fig. 5.10). Subsidence accompanied by sinkholes with a width of up to 3 meters is common (Fig. 5.11). Sometimes gravitational collapse of sidewalls and subsidence of blocks or laterally spread erosion enlarge the fissures into several meters to tens of meters (Fig. 5.12). The visible depth is up to approximately 10 meters.

The fissures are frequently developed in highly populated areas and in some causes cross villages or towns (e.g. Muleti in Hawasa area or Shalla Senbete located south of Lake Shalla). Development of these structures and the accompanying processes represent a very dangerous

Fig. 5.7 Solid rocks within the ground cracks are fractured and not eroded (sharp forms)

Fig. 5.8 Partly collapsed thin sedimentary roof of the ground crack

Geological hazards
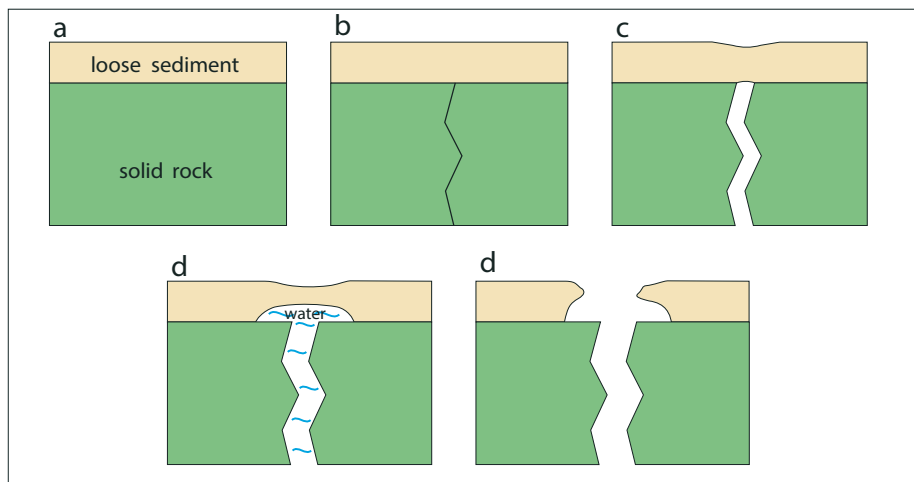
Fig. 5.9 Model of the origin and development of ground cracks: a) loose sediments overlaying solid rock; b) brittle fracturing of the solid rock due to extension; c) opening of the crack associated with stretching of loose plastic sediments; d) ongoing stretching of the sediments combined with subsurface erosion by water flowing through the open crack; e) collapse of the thinned roof over the open crack

Fig. 5.10 Pipe with 20 cm in diameter suggests a new crack is starting to open

Fig. 5.11 Liner arranged sink holes above a new ground crack

Fig. 5.12 Lateral erosion associated with an open crack

Fig. 5.13 Ground crack endangering houses in Muleti near Hawasa

Geological hazards

geological hazard resulting in the loss of buildings, infrastructure and agricultural land. These processes can have an impact on areas with high population density and human activity. The destruction of houses and infrastructure as well as loss of human lives and animals has been documented in connection with ground fissure development (Fig. 5.13).

In extreme cases, the opening of a ground crack may result in the formation of a tectonic cave. Such a tectonic cave has formed near Butajira (Fig. 5.14 and 5.15) just north of the mapped area. The Butajira cave serves as an example of the terminal stage of ground crack opening.

Fig. 5.14 Butajira tectonic cave in coherent fractured basalts

Fig. 5.15 Collapsed roof of Butajira cave

Recommendations: The areas around fissure systems are at permanent risk of the development of new fissures and the accompanying phenomena. Geophysical investigation is recommended for detecting and verifying faults and other discontinuities of rocks where fissures could be
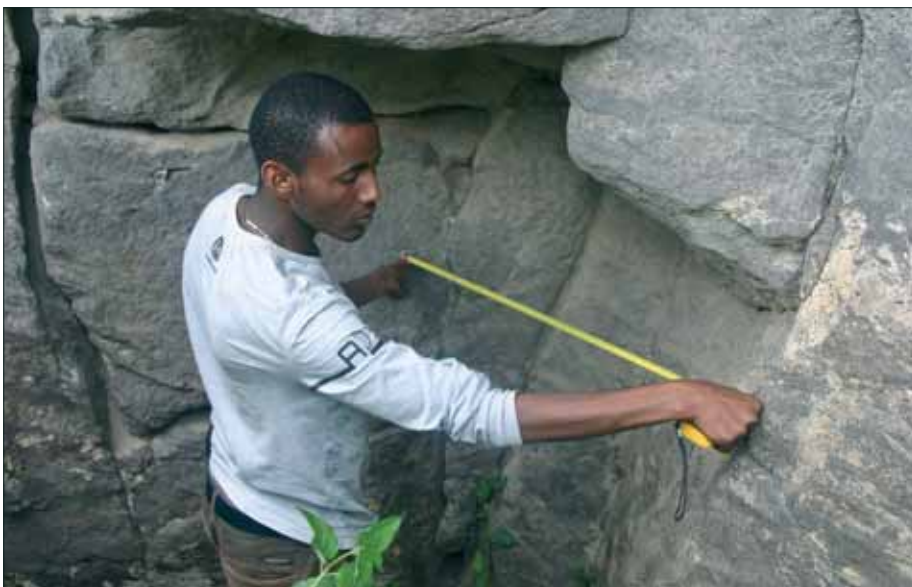
Fig. 5.16 Measuring distance between points in solid rock within the ground crack

Geological hazards

developed. The most dangerous of these are fractures with an intact sedimentary roof; their detection by electrical resistivity profiling is the crucial point of any subsequent survey. The rate of opening of these cracks also remains unclear. To obtain such data, a system of measuring points was located at selected sites (Fig. 5.16). The distance between the points in solid rocks should be repeatedly measured every 6 months to observe the rate of dilatation. In the future, this simple method should be replaced by automatic extensometers.

5.1.3 Volcanic hazards

Continental rifting is associated with intense volcanic activity. As a result, several active or dormant volcanoes and volcanic fields can be found within the rift on the Hosaina map sheet.

Rhyolitic composite (central) volcanoes

During the fieldwork, all known Quaternary volcanoes were briefly visited and investigated in terms of character and distribution of volcanic products and also freshness of the deposits as well as the volcanic edifice suggesting the status of the volcano (dormant/extinct). More detailed conclusions would require a more detailed study as the current research published as a map at the scale of 1:250,000 is only of an inventory nature.

Alutu Volcano

The northernmost active rhyolitic volcano in the investigated area is the Alutu Volcano (Fig. 5.17) located between Lakes Ziway and Langano, less than 20 km to the southeast of the Town Ziway. The complex rhyolitic volcano experienced several explosive eruptions and numerous effusions of obsidian lavas. This volcano does not have a central volcanic cone but volcanic rocks are emitted from various craters and vents. The youngest pumice eruption was dated at about 50 BC (Gianelli and Teklemariam 1993). This relatively thin layer of pumice covers a large area to the south, north and northeast of Alutu. To the south, air-fall pumice overlays re-sedimented pyroclastic deposits (Fig. 5.18). To the north and northeast, the youngest tephra shows two different stages. The eruption started as being phreatomagmatic producing pyroclastic surges and fine ash with accretionary lapilli. Later, the eruption shifted to a Plinian style eruption producing pumice (Fig. 5.19). Before this Plinian style eruption a phreatomagmatic eruption produced a widespread ash layer around 9 ka. We suggest that this phreatomagmatic eruption took place in the Golba crater in the northwestern part of the Alutu Volcano (Fig. 5.20). At least four prominent obsidian lava eruptions have occurred in Alutu since the pumice eruption of 50 BC as these lavas are not covered by the pumice fall. This means that an obsidian lava flow is emitted approximately every 500 years. The exact dates of the obsidian lava eruptions remain unclear. The composition of 3 analyzed obsidian lavas is uniform corresponding to alkaline rhyolite with SiO_2 ranging from 72.9 to 73.1 wt. % and the sum of alkalis ranging from 9 to 9.5 wt. %.

Fig. 5.17 Irregular shape of the Alutu Volcano (Golba phreatomagmatic crater in the center of the photo)

Fig. 5.18 Thin layer of Alutu pumice (40 cm thick whitish layer on top) overlaying re-sedimented pyroclastic deposits on the plain between Alutu and Lake Langano

Geological hazards

Fig. 5.19 Deposits of 50 BC Alutu eruption around Chefe Jila. The first phreatomagmatic stage is represented by pyroclastic surge deposits and fine ash with accretionary lapilli overlain by pumice from the later Plinian stage

   Deposition of pyroclastic material is strongly influenced by the strength and direction of the wind. In the area of Alutu Volcano, the wind blows from the northeast from October to May and from the southwest from June to August. In September the wind direction is bimodal, blowing both from the northeast and the southwest. Therefore, any future explosive eruption occurring between September and May would endanger the town of Bulbula, whereas between June and September the pyroclastic material would blow towards Chefe Jila and Herera.

Fig. 5.20 Golba phreatomagmatic crater of the Alutu Volcanic Complex

Geological hazards

Shalla Volcanic Complex

The caldera of the Shalla (syn. O´a) Volcano is located in the eastern part of Lake Shalla, whereas in the western part of the lake there is a flooded tectonic depression. The distinct character of both parts of the lake can be seen on a bathymetric map of the lake (UNDP 1972).

The caldera erupted several ignimbrite units (Fig. 5.21). According to the on-line Caldera Collapse Database (http://www.bgs.ac.uk/vogripa/searchVOGRIPA.cfc?method=detail&id=244), the latest ignimbrite forming eruption of the Shalla (O´a) caldera occurred 240,000 years ago (K-Ar). On the other hand, JICA (2012) reports the age for the Shalla ignimbrite as being 1.35±0.05 Ma (K-Ar), which is in good accordance with our result of 1.02±0.8 Ma (K-Ar) despite the large error. In order to better understand the evolution of this volcano and determine the correct age of the Shalla ignimbrites more detailed mapping of the distribution of the individual ignimbrite units, detailed volcanostratigraphy of the volcano and more data acquisition are required. The caldera hosts numerous hot springs on its southern and northeastern banks (Fig. 5.22).

Fig. 5.21 ˝Black˝ ignimbrite of the Shalla Caldera dated 1.02±0.8 Ma (K-Ar)

Fig. 5.22 Hot spring on the northeastern banks of Lake Shalla within the Shalla Caldera

The cone of Fike Volcano (Fig. 5.23) emerged to the northwest of the caldera after the ignimbrite-forming caldera eruption. Fike Volcano is horse-shoe shaped with a crater open to the north. It is a source of several phreatomagmatic eruptions producing widespread ash with accretionary lapilli (Fig. 5.24). We assumethe thick deposit of fine ash with accretionary lapilli covering the ignimbrites around Shashemene (Fig. 5.25) to also be associated with the Fike Volcano. Fike Volcano has also produced ignimbrite of a small areal extent and a preserved thickness not exceeding 2 m which spread to the west of Lake Abijata and covers lacustrine sediments (Fig. 5.26).

Fig. 5.23 Horse-shoe shaped silicic Fike volcano with crater open to the north

Fig. 5.24 Phreatomagmatic tuff with huge accretionary lapilli on the Fike cone

Fig. 5.25 Phreatomagmatic tuff with accretionary lapilli exposed to the west of Shashemene

Fig. 5.26 Fike ignimbrite overlaying lacustrine sediments to the northwest of Lake Abijata

There are several basaltic cones around Shalla, described below as the Shalla-Hawasa Volcanic Field.

Corbetti Volcanic Complex

The Corbetti Volcanic Complex is located in the northwestern segment of the older Hawasa Caldera. The eruption of the Hawasa Caldera took place about 1 Ma. The K-Ar age of 1.28 Ma is given by JICA (2012) and between 1.1 and 1.85 Ma by WoldeGabriel et al. (1999). The on-line Caldera Collapse Database (http://www.bgs.ac.uk/vogripa/searchVOGRIPA.cfc?method=detail&id=245) states an age of 1 Ma (method not given). The evolution of the Hawasa Caldera was ended by the growth of the Wendo Koshe rhyolitic volcano on its northeastern edge. This volcano produced obsidian and rhyolitic lavas dated 1.18±0.12 and 1.02±0.14 Ma (Žáček and Rapprich eds. 2014: K-Ar). Subsequently, the Corbetti Volcanic Complex began to develop on the northwestern edge of the Hawasa Caldera. Corbetti Volcano produced several ignimbrite-forming eruptions: 0.98±0.26, 0.669±0.129 and 0.2±0.14 Ma (Žáček and Rapprich eds. 2014: K-Ar). We accept also the youngest age despite the large error, as this value corresponds to the ages obtained by JICA (2012; K-Ar: 0.21±0.01 and 0.19±0.02 Ma).

The active magmatic activity beneath the Corbetti Caldera is revealed by the deformations documented by Biggs et al. (2011). A significant period of deflation was documented between 1997 and 2000, whereas inflation took place in 2010. These processes may represent new magma batches. Two Holocene volcanoes, Chabi and Wendo Koshe, have emerged within the recent Corbetti Caldera (Fig. 5.27). Wendo Koshe (Fig. 5.28) is a stratovolcano with several explosive events. The succession of the pyroclastic deposits that erupted from Wendo Koshe Volcano can be

Fig. 5.27 Wendo Koshe (in front) and Chabi (rear) volcanoes within the Corbetti Caldera

Fig. 5.28 Wendo Koshe Volcano with an asymmetric horse-shoe shaped crater open to the north

Geological hazards

Fig. 5.29 Succession of Wendo Koshe pyroclastic deposits. Bottom to top: 5 m thick surge and ash-fall deposits of phreatomagmatic activity; 1.5 m thick pumice-fall deposit with paleo-weathered surface; 4 m thick young Wendo Koshe pumice

Fig. 5.30 Ill-sorted reverse graded pumice deposited by pyroclastic flow, overlain by a pumice fall deposit (near Bura). Both deposits belong to the latest Wendo Koshe eruption

seen in several gorges cut in loose pyroclastic deposits within the Corbetti Caldera (Fig. 5.29). The dominant unit is young Wendo Koshe pumice overlaying the sequence with a thickness reaching 4 m around the source vent. The young Wendo Koshe pumice is widespread around the volcano.
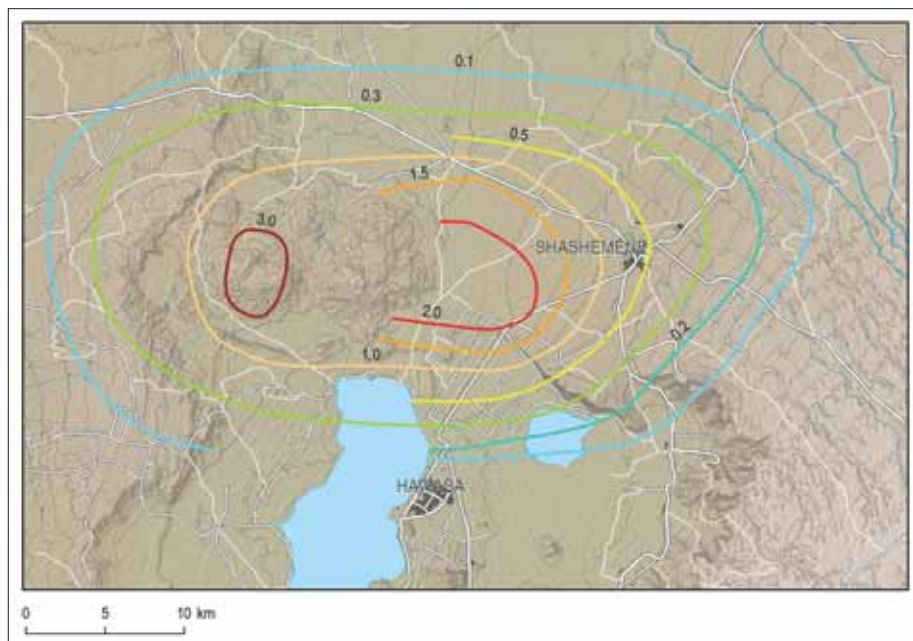
Fig. 5.31 Isopach sketch of a Wendo Koshe young pumice fall deposit

Fig. 5.32 Thickness of the young Wendo Koshe pumice reaches 2 m as far away as along the Shashemene – Hawasa road
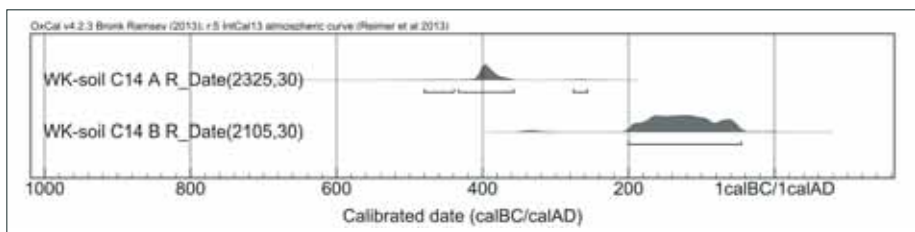
Fig. 5.33 Calibration of radiocarbon data from soils buried by the young Wendo Koshe pumice

Geological hazards

On the other hand, the thinner layer of slightly yellowish pumice beneath can only be observed within the Corbetti Caldera. This older eruption, separated from the young Wendo Koshe pumice by a horizon of fossil weathering, was weaker than the latest pumice event. Below both of these pumice layers, deposits of phreatomagmatic activity comprising surge and ash-fall deposits occur with a thickness exceeding 5 m. The young Wendo Koshe pumice was mostly deposited by fall but local deposits of pumice flows were also documented (Fig. 5.30). An isopach map of the thickness of the pumice fall from the last explosive eruption of the Wendo Koshe Volcano was derived from numerous field measurements and is shown in Fig. 5.31. The deposition of the pumice was strongly influenced by the wind blowing in this area predominantly from west. Therefore, most of the pumice is deposited to the east of the volcano (Fig. 5.31) with a thickness of up to 2 m as far away as along the road from Shashemene to Hawasa (Fig. 5.32).

Two samples of soil buried by the pumice fall were analyzed using the C14 method by Dr. Tomasz Goslar in the Poznań Radiocarbon Laboratory of Adam Mickiewicz University in Poland. The first sample (WK-soil C14-A) was taken from soil buried by 2 m of pumice and gave an age of 2325±30 BP. The second sample (WK-soil C14-B) was taken from soil buried by only 1 m of pumice and gave an age 2105±30 BP. As the first sample (WK-soil C14-A) was better insulated from recent soil and biotic processes, we accept this result as being more reliable. By calibrating the analytical

Fig. 5.34 Chabi rhyolitic shield volcano consists of obsidian lavas

Fig. 5.35 Obsidian lava pre-dating Wendo Koshe pumice (in front) overlain by one of the post-pumice obsidian lavas

Fig. 5.36 Deposits of phreatomagmatic eruptions from the Chopa Crater of the Chabi Volcano exposed by a gorge of an ephemeral stream

Geological hazards

age using OxCal v4.2.3 Bronk Ramsey (2013) with an IntCal13 atmospheric curve (Reimer et al. 2013, Fig. 5.33), we obtain a calendar age suggesting the Wendo Koshe eruption occurred with a 68.2% probability between the years 406 and 381 BC (90% probability between 434 and 358 BC).

According to the geological record, explosive eruptions in the area of the Corbetti Caldera did not happen as frequently as effusive eruptions during the Holocene. The frequency of explosive eruptions is not known. Should a new Plinian style eruption take place on the Wendo Koshe Volcano, even Shashemene would be covered by a 0.5 m thick deposit of pumice preventing cattle from feeding and also covering sources of water.

Chabi Volcano is a rhyolitic shield volcano (Fig. 5.34) with dominantly effusive activity. The Chabi Volcano has emitted four large obsidian lava flows since the last big explosive eruption of Wendo Koshe. The lavas post-dating the voluminous Wendo Koshe pumice eruption can be easily identified due to the absence of pumice cover (Fig. 5.35). Obsidians have a uniform chemical composition (SiO_2 73.7–74.8 wt. % and sum of alkalis 9.3–9.9 wt. %) and no chemical evolution was observed among the obsidian lavas. Even though the Chabi Volcano is dominated by obsidian lavas, it has also experienced several phreatomagmatic explosive episodes in its history, namely from the Chopa Crater (Fig. 5.36). The area of the Chabi Volcano is not inhabited as the blocky and sharp surface of the obsidian lava cannot be used for agriculture. Obsidian lavas could reach the sparsely inhabited zone around Chabi Volcano and destroy grass houses. Due to their high viscosity, obsidian lavas flow relatively slowly and provide enough time for evacuation. No casualties are expected from effusive eruptions.

Fig. 5.37 Monogenetic pumice cone within the Corbetti Caldera

In addition to the two most prominent volcanoes, several smaller pumice cones and pumice rings are found within the Corbetti Caldera (Fig. 5.37).

Basaltic monogenetic volcanic fields
Basaltic volcanism in the studied area forms fields of small monogenetic volcanoes represented by scoria-, spatter- and tuff-cones, tuff rings and maars. These small volcanoes are present in four volcanic fields i.e. East Ziway, Shalla-Hawasa, Bilate and Butajira.

East Ziway Volcanic Field
Numerous basaltic scoria cones are aligned along north-northeast-south-southwest trending fractures to the east of Lake Ziway (Fig. 5.38). The 50 BC Alutu pumice covers most of these

Geological hazards

scoria cones. Even though the peaks are not covered by pumice due to the wind, superposition of pyroclastic events at the foothills remains clear (Fig. 5.39). Only a few exceptions seem not to be overlain by pumice and therefore younger than 50 BC. Among them is an unnamed scoria cone 2.5 km to the southeast of Chefe Jila. A few scattered scoria cones of this volcanic field are also found to the southeast and west of Alutu Volcano.

Fig. 5.38 East Ziway Volcanic Field with numerous monogenetic basaltic scoria cones

Fig. 5.39 Scoria cone at Herera overlain by 50 BC Alutu pumice

The most frequent volcanic landforms of this volcanic field are scoria cones but several tuff cones and tuff rings were also documented on the shores and as islands on Lake Ziway. A representative example of a tuff ring is Golba, located on the northern foothills of the Alutu Volcano and sharing the name with a phreatomagmatic crater within the Alutu Volcano (Fig. 5.40). Tuff cones and their remnants can be found as islands on Lake Ziway (e.g., Gelila Island – Fig. 5.41). These occurrences suggest a more explosive scenario in the case of eruptions within and nearby the lake. No fresh volcanic forms were documented on Tulu Gudo Island. The available geochronological data document the long-lasting activity of the East Ziway Volcanic Field with a relatively low frequency of small volume volcanic eruptions.

Fig. 5.40 Golba tuff ring

Fig. 5.41 Gelila Island tuff cone on Ziway Lake

Shalla-Hawasa Volcanic Field

No fresh-looking scoria cone morphology can be found around Hawasa or to the south of Lake Shalla. It seems that this is not as much due to erosion since the volcanic activity ceased as human activity having a much more significant effect on these small cones. Previous reports suggest the scoria cones around Hawasa and to the south of Lake Shalla are not associated with any fumarolic activity. Our geochronological data (below the detection limit) suggest this volcanic activity is younger than previously supposed. On the other hand, all of the basaltic monogenetic volcanoes in this area are older than 400 BC (Wendo Koshe pumice – Fig. 5.42).

Geological hazards

Fig. 5.42 Wendo Koshe (400 BC) pumice overlaying scoria cones to the south of Lake Shalla

Bilate Volcanic Field

Several monogenetic volcanoes are located along the River Bilate to the south of Ropi. This volcanic field can be subdivided into two parts. Volcanic edifices represented by scoria cones and tuff rings on the right bank of the River Bilate (southern part) have fresh morphology, but this area is difficult to access and was not reached during this project. From aerial photos, these east-west aligned cones are not affected by erosion and are most probably of Holocene age. Three maars and several small, eroded scoria cones (Fig. 5.43) are located on the left bank of the River Bilate (northern part). The single K-Ar age suggests activity about half million years ago (Fig. 3.23). Despite the maars having perfect morphology on satellite and aerial images, the field survey discovered significant erosion of the craters (Fig. 5.44 and 5.45). We do not expect these eruptions to have occurred during the Holocene. Hot springs present in two of the three maars are most probably associated with a fault zone followed by the River Bilate as several hot springs can also be found along the river to the north and south of the volcanic field. The exact age of termination of volcanic activity in this area remains unclear.

Fig. 5.43 Small, eroded scoria cones to the south of Ropi

Fig. 5.44 Crater of Tilio maar

Geological hazards

Fig. 5.45 Scoria cone forming an island within the Machaferra maar

Butajira Volcanic Field

Butajira Volcanic Field is a row of scoria cones, spatter cones and maars following the western margin of the Main Ethiopian Rift for a length of approximately 80 km. It also exceeds the north of the studied area. Our geochronological data suggest the activity of this volcanic field could have started 1 Ma (Fig. 5.46). On the other hand, Debes Quoto Volcano (or Gisila – Fig. 5.47) has very fresh morphology and unvegetated lava. This volcano is probably of a very young age and represents the youngest activity of the Butajira Volcanic Field.

Fig. 5.46 About 1 Ma scoria cone near Dolocha

Fig. 5.47 Debes Quoto (Gisila) – most probably the youngest scoria cone of the Butajira Volcanic Field

Recommendations: There is currently no monitoring apparatus installed on any of the volcanic systems in Southern Ethiopia. We also lack the historical and geochronological data on the potentially hazardous volcanic systems to understand the evolution of these volcanoes, the frequency of eruptions and time since the last eruption. An explosive eruption of the large central

Geological hazards

rhyolitic volcanoes would endanger a large area (hundreds of km2). On the other hand, the area impacted by an eruption of a basaltic monogenetic volcano would not exceed 10 km^2, but a new vent may appear anywhere within the volcanic field. Construction of a local seismological network in Southern Ethiopia monitoring the activity of the volcanoes is highly recommended with further monitoring systems to follow. The large rhyolitic volcanoes also need more detailed studies and mapping showing eruptive styles and their past evolution.

5.2 Exogenous geological hazards

5.2.1 Erosion hazards

Erosion is one of the most important exodynamic processes in the area of the Hosaina sheet and represents a major cause of land devastation. Wind erosion is sometimes observed; however, water is the most important agent of erosion. As a natural exogenous process of the landscape, it is frequently accelerated by human activities in the form of intense agriculture associated with deforestation. Also climatic characteristics with stormy rains producing rapid runoff promote favorable conditions for erosion. Areas with weakly compacted alluvial and lacustrine deposits, re-sedimented volcaniclastics and weathered ignimbrites producing light sandy residual soils are the most prone to erosion (Fig. 5.48). The highest intensity of erosion is generally on fault- and
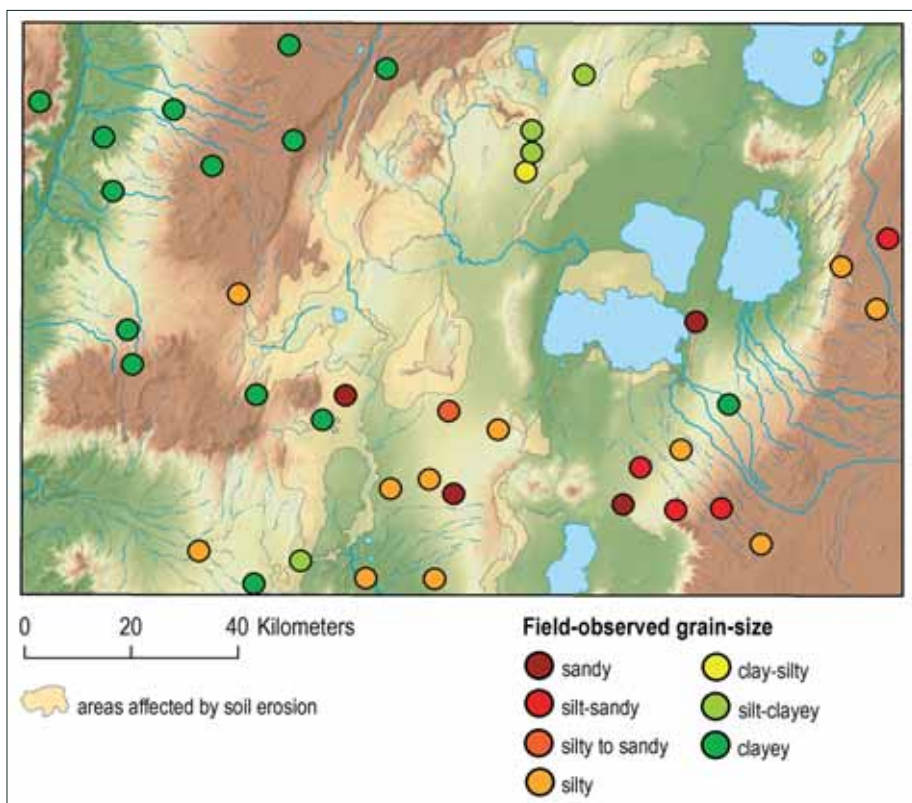
Fig. 5.48 Scheme comparing the extent of the areas affected by soil erosion and distribution of light (sandy and silty) soils

Geological hazards

Fig. 5.49 Sheet erosion around Alaba Kulito

Fig. 5.50 Soil erosion around Alaba Kulito from Google Earth View

erosional scarps; however, erosional rills and gullies are also locally developed in less inclined areas. Rapid surface flow and channeling of runoff water are the most common mechanisms of the creation of erosional rills and gullies. However, piping as a result of subsurface erosion can also result in gully growth (e.g., Morgan 1996, Bryan and Jones 1997). The creation of erosional structures is accompanied by subsequent processes as well as gravitational collapse of the sidewalls of gullies, mass flow movement and rapid accumulation of material at the foot of slopes. Locally, the landscape of scarps is characterized by badland morphology (an unvegetated surface dissected by a high density of rills and gullies, Fig. 5.49). In areas with thin layers of uncompacted and weathered rocks or residual soils deep gully structures are unlikely to develop and sheet erosion becomes predominant (Fig. 5.50).

Fig. 5.51 Deep gully near Alaba Kulito

Geological hazards

The areas most affected by erosion are the Bilate river catchment, fault scarps located to the west of Hawasa Lake, Shala Lake and Ziway Lake, all within the rift. Erosion also occurs on the highlands to a lesser extent.

Badlands with well-developed gully systems were located along the right banks of ephemeral streams of the Bilate River to the southwest of Alaba Kulito or on the western scarps of the Hawasa Lake catchment. The gullies are only a few meters deep but can range locally up to 20 m (Fig. 5.51) and the documented width is up to 25 m; however, Moges and Holden (2008) reported gullies and pipes in the Hawasa area being up to 33 m wide. The length of the gullies ranges from tens of meters to several kilometers.

In the area along the Bilate River (e.g. around Alaba Kulito) the residual soils and weathered horizons are only a few meters thick and sheet erosion is predominant.

Erosion, gully formation and badland development represent a serious problem as they cause degradation and loss of soil and strongly affect the livelihoods of farmers. The loss of human lives and serious injuries are also known. Erosional processes strongly affect the infrastructure as gullies can cut across roads and reduce accessibility to the area.

Recommendation: Reforestation is necessary to decrease the rates of erosion and planting of trees in the margin of badlands can help slow down badlands extension. To decelerate the runoff of surface water it is recommended to plant rows of trees and construct small dams in the gullies (trapped sediment in the damps could be later used as a fertilizer for arable land). Trees and deep-rooted bushes should also be planted on the boundaries of land-plots to prevent soil-erosion. Fortunately, the presence of paleosoils and the climatic conditions can aid the possible recovery of soil if the erosion is stopped.

Fig. 5.52 Debris flows with accumulation fans near Golbo from Google Earth View

Geological hazards

5.2.2 Accumulation of sediment

The risk of high rates of accumulation of sedimentary material is greatest in areas with an abrupt decrease in slope gradient, where the water flow velocity and competency of current decrease. This could result in rapid sedimentation of material eroded and transported from upper parts of the scarps and catchments during heavy rains. The processes lead to the creation of alluvial fans in the mouths of gullies as well as erosional and stream valleys. Rapid sedimentation of a large volume of material and the formation of alluvial fans in the foothills are also associated with earth flow processes (Fig. 5.52). A high rate of sedimentation in combination with floods can also be expected in endorheic depressions, e.g. in Cheleleka Lake to the east of Hawasa (described in more detail below). The high rates of sedimentation mainly associated with earth flows could have catastrophic impacts on settlements.

Recommendation: The accumulation is related with floods. These places are not suitable for settlement and they are more convenient for agriculture.

5.2.3 Slope deformation hazards

All forms of slope deformation were documented on the Hosaina map sheet. The extent of the landslide areas in the Gibe River valley, two devastated debris flows on slopes along the Weyra River near Gomoro village and the rock falls on Weransa Ridge were mapped. Furthermore, other areas vulnerable to slope movements were identified. The most risky area is considered to be along the Weyra River, which has a high susceptibility to debris flow. Slope deformation was mapped from remote sensing data and fieldwork. Published studies from the area were also used for recognition of zones prone to slope deformation hazards.

Landslides

The large extent of ancient landslides became clear from the results of the fieldwork along the Gibe River (Fig. 5.53). The landslide occurrence in the study area is closely related to the geological and hydro geological conditions. The main landslide area extends on the eastern slopes of Gibe Gorge where suitable geological and geomorfological conditions prevail. Geological composition is particularly pertinent to landslides due to the alternation of hard and soft rock. Hard rigid blocks of basalt slide over soft and more plastic tuffs layers. The presence of loose unconsolidated deposits overlaying the highly weathered basalt is one of the factors influencing landslides. Highly weathered bedrock provides a potential risk as increased groundwater levels due to the infiltration of rainwater can induce landslides. Moreover, the inclination of layers on the eastern part of Gibe Gorge is "down the slope" which facilitates sliding. The total distance of sliding slopes along the Gibe River is at least 50 km. The slides damage settlements and infrastructure such as houses, farmlands, and roads.

The Ameca landslide has been the subject of a detailed case study (see below).

Ameca landslide – case study

The documented dimensions of this compound slope deformation are 4.5×2.5 km with slid blocks measuring 900 m wide and 200 m long (Fig. 5.54). The main scarp of the landslide is more than 150 m high (Fig. 5.54 and 5.55) and has a curved "horseshoe" shape. The shape of surface has a typical "blocky stairs structure" in combination with hilly relief (Fig. 5.56). These events are probably caused by tectonic settings and erosion of the Ameka River under suitable geological and geomorfological conditions. Geological settings consist of basalt and tuffs in the base covered by rhyolitic ignimbrites, trachyte and tuffs. The vertical distance between the crown and the toe of the landslide is 450 m. Waterfalls formed from the main scarp (Bischo Falls, Ameka Falls).
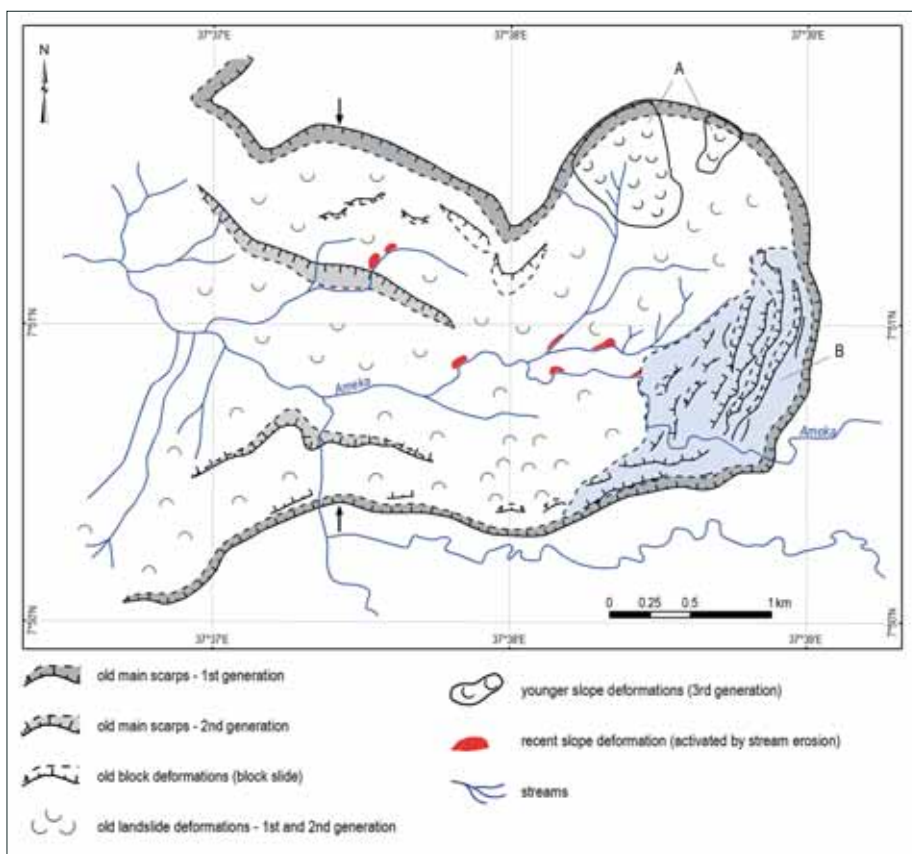
Fig. 5.53 Map of Ameca landslide

Fig. 5.54 Main scarp with stepped surface shapes and a blocky structure

Fig. 5.55 Main scarp with the landslide block and an undrained depression below
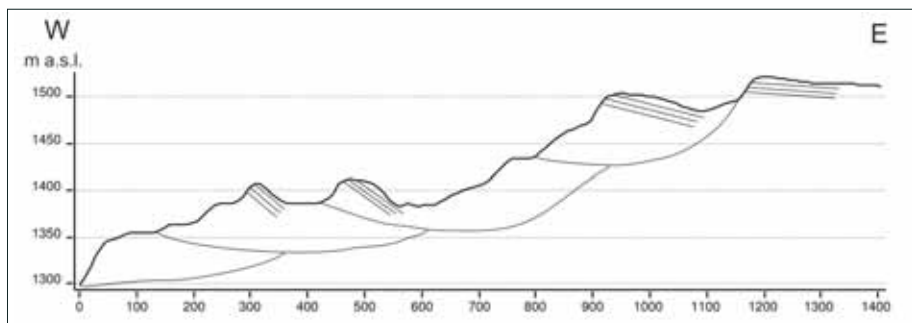
Fig. 5.56 Hypothetical cross section of the Ameca landslide

Other smaller landslides can be found in the area (Fig. 5.57). Rotational movements of the large blocks within the landslide can be demonstrated on the tilted dip of tuff bedding (Fig. 5.58).

Fig. 5.57 Active small landslide on the toe of a compound slope deformation due to erosion from the Ameca River

Fig. 5.58 Rotation of tuff layers on the foot of a landslide shows rotational movement of the sliding

Recommendations: The whole Ameca landslide area is potentially susceptible to further landslides. Therefore, this area should be indicated as a risk zone with restricted construction of houses in area of landslide and near its scarp.

Rock fall and toppling

Vertical slopes, especially on tectonic scarps, are prone to rock fall and toppling. These processes do not occur over large areas. The risk of rock fall is concentrated to small isolated areas. One of the largest is Weransa Ridge. The main rock-fall triggering factors are heavy rains and seismic events. Measures to protect constructions against rock falls are only implemented in one area. A dynamic barrier and nets were installed in the area of a turbine house of the Gilgel Gibe II Power Station.

Weransa ridge – case study

Areas endangered by rock fall and toppling are located especially on the southern slopes of Weransa Ridge. The scarp is 100–300 m high and about 4 km long. The rockwalls rise nearly vertically, with a talus of debris cones and old rock-fall deposits on the foothills (Fig. 5.59 and 5.60).

Geological hazards

Fig. 5.59 Rock-fall deposits on the foothill of the Weransa Ridge slope, some collapsed blocks have volumes exceeding 20 m³

Fig. 5.60 Columnar jointing of rhyolite with the collapsed part of the massif

The thickness of deposits could exceed 50 m. Large blocks (Fig. 5.59) and debris deposits from extensive rock falls are documented over the entire length of Weransa Ridge. The slopes are formed by Hawasa crystal-rich rhyolite and in the western part by blocky Corbetti rhyolitic ignimbrite. Both lithologies are characterized by columnar jointing which predisposes the decomposition of the rocks and slope movement. The slope is of tectonic origin and the columnar jointing results from cooling contraction of volcanic rocks and welded pyroclastic deposits (ignimbrites).

Recommendation: The dirt road along the foothill is at permanent risk of rock falls. Therefore, we recommend shifting the road away from the slope. If any buildings were constructed with the

Fig. 5.61 Dynamic barrier – ring panel. Source: Maccaferri

Geological hazards

aim of balneological use of the Shalo thermal spring, technical protection of the site would be necessary. Remediation of the site is possible using dynamic barrier systems on the foothill of the slope (Geobrugg AG, Maccaferri S.p.a., Fig. 5.61). More detailed site investigation is necessary before any work is performed.

Debris flow

Vulnerability of the landscape to debris flow is greatest on the tectonic slopes of the Main Ethiopian Rift (MER) which is approximately 80 km to the north of Hosaina town. Two large and one smaller debris flow were documented in the area along Weyra (Bilate) River (Fig. 5.52; 5.62). Debris flow could occur on steep slopes with highly weathered rocks and represents a high risk phenomenon. The velocity of movement in the case of a huge flow can reach 100 km per hour and in some cases the velocity can be over 300 km per hour.
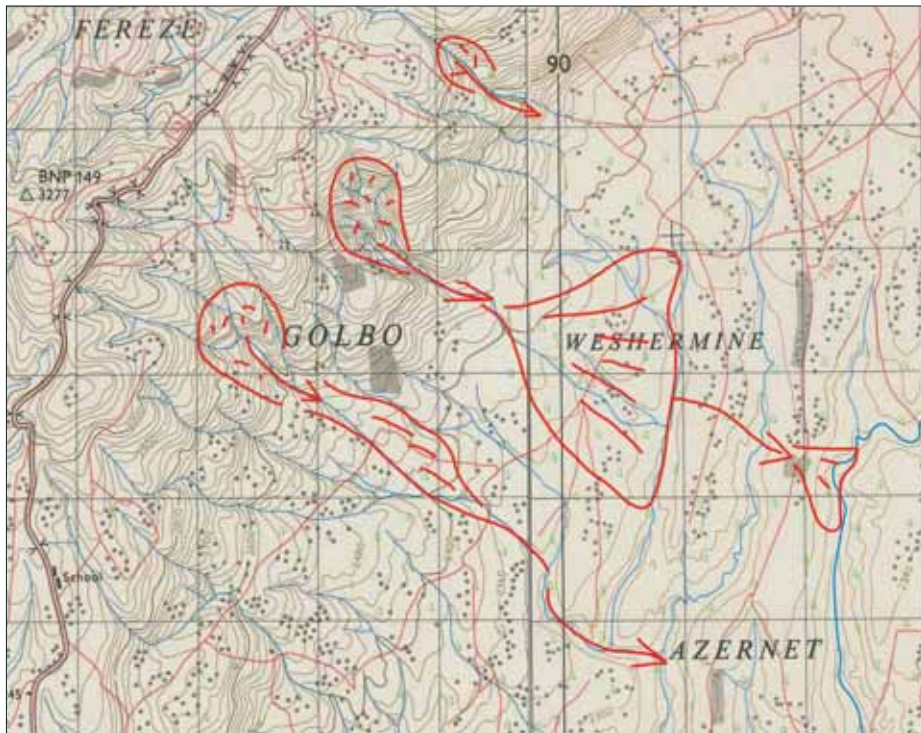
Fig. 5.62 Golbo debris flow on the topographic map

Golbo debris flow – case study

This feature has documented dimensions of about 3.6 km in length and 1 km of width. The debris flow was probably enabled by the tectonic settings and weathering and triggered by heavy rains. The geological settings consist of highly weathered ignimbrites. A profile of the debris flow is shown in Fig. 5.63. Information from the locals is not reliable so the extent of damage is uncertain but some locals say that 50 people died. The date of origin is unclear but the process is probably a recurring phenomenon. The last event may have occurred in the 1980s.
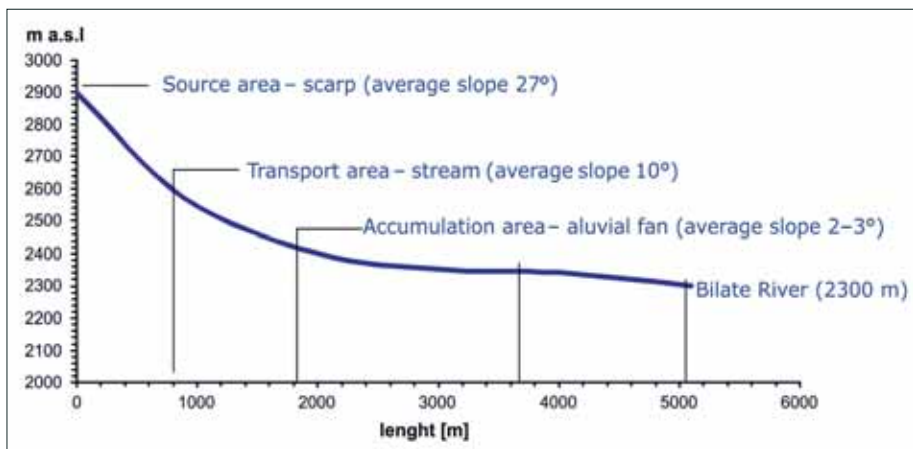
Fig. 5.63 Profile of the Gobo debris flow. Vertical distance is 600 m (2900 - 2300 m a.s.l.)

Recommendations: The whole area of the slopes of the MER is potentially susceptible to such a phenomenon (flow). Therefore, tectonic scarps should be indicated as a high risk zone. Debris flows are a very rapid and dangerous phenomenon. Land use planning is lacking on the slopes of the MER. For the future, construction of houses and roads should be limited, especially near erosion gullies and on the foot of the slopes (Fig. 5.64 and 5.65).

Fig. 5.64 Accumulation area – alluvial fan of debris flow – the most risky area

Fig. 5.65 Transport area – stream channel of debris flow

5.3 Hydrological and hydrogeological hazards

5.3.1 Inundation

A fluvial system with well-developed flood plains is rare, thus inundations and floods are related mainly to ephemeral river systems and erosion valleys on the Hosaina sheet. Newly formed tectonic endorheic depressions with the creation of temporal lakes or the shoreline around permanent lakes could be also inundated.

Fig. 5.66 Tectonically predisposed endorheic depressions to the east of Lake Ziway from Google Earth View

The principal fluvial systems are represented by the River Gibe in the western part of the sheet, the River Bulbula connecting Lake Ziway with Lake Abijata and the River Bilate, which forms an axial drainage system in this part of the MER. The flood plains are inundated during high discharge from river channels. However, the drainage systems of the area have a character of bedrock rivers with a very limited occurrence of flood plains. Flood events are related to deep erosion; lateral erosion of banks could occur especially on the outer banks. Ephemeral streams must also be including in the inundation risk due to flooding during rainy seasons. Flash floods caused by torrential rains also frequently occur in the drainage systems of small catchments.

Avulsion (rapid change of river channel trajectory) can also occur in alluvial fans during floods. Due to the aggradation of sediment within an active channel the capacity of the channel is degreased and in the case of higher discharge the streams could reoccupy older abandoned channels or brake levees (rivers banks) and new river channels can be formed.

Endorheic depressions are dry during dry seasons; however, during rainy seasons they could also be inundated (e.g. a small depression to the northwest and southwest of Wanchikota Bonosha in the Bilate river catchment or tectonically predisposed depressions to the east of Lake Ziway, Fig. 5.66).

Geological hazards

Water level fluctuation of lakes may represent a serious natural hazard, mainly in the case of Lake Hawasa. The level of Lake Hawasa has risen since 1970. The cause and whether it is related to tectonic processes, climatic factors or anthropogenic factors are not clearly established. Ayenew (2009) adds the role of tectonic processes to the rise in the lake level, which is demonstrated by the disappearance of Lake Debra in the Muleti sub-basin (west of Hawasa), after the formation of fissures generated by an earthquake in the late 1980s. The role of tectonic processes would be demonstrated by a change of lake morphology, and unequal changes in the shoreline (landward progradation of the shore, as well as retreat on the opposite side of the lake). However, only minor changes in the shape of the lake have been observed during the last 26 years. Zenaw (2003) states that the rise in the lake level is a result of siltation of Lake Cheleleka (east of the sub-sheet), which is connected with Lake Hawasa. The surface area of Lake Cheleleka was about 12 km2 in 1972, but it is currently completely filled with sediment transported from the eastern highlands due to deforestation of this area. Sediment now flows directly to Lake Hawasa (Gebreegziabher 2004). Change in the lake level could also be caused by climatic factors. The rise was caused by high rainfall intensity during 1996, 1997 and 1998, which is 16%, 7% and 12% above average values, respectively (Gebreegziabher 2004). The total damage caused by the expansion of Lake Hawasa was estimated by Zenaw (2003) to be Birr 43,490,524 for the scarce population scattered in the swamps around the lake. The rise in the water level of Lake Cheleleka is caused by sediment aggradation in the basin. Siltation of Lake Cheleleka was documented by Tadesse and Zenaw (2003). The surface area of Lake Cheleleka was about 12 km2 in 1972, but currently it is completely filled with sediment transported from the eastern highlands due to deforestation in this area (Fig. 5.67).

Fig. 5.67 Lake Cheleleka to the east of Hawasa from Google Earth View

Geological hazards

Recommendation: Eliminate human activity in inundation areas, i.e. settlements due to the potential loss of life during floods and industry as a source of contamination). For a reduction of loss during floods it is recommended to remove the accumulated material from active channels.

These geological hazards significantly increase the poverty and morbidity in the region. More detailed geomorphological and geological analysis (based on DEM of high resolutions and detailed topographic data) is necessary in order to predict natural hazards and eliminate their impacts. These studies and geological hazards maps represent a basic dataset for effective mitigation projects, spatial planning and development of the region.

5.3.2 Fluoride

The problem with the high fluoride content in the water of the Hawasa and Shashemene area is very well known and is described in many studies. The fluoride concentration frequently exceeds 3 mg/l which can cause mild fluorosis (mottling of teeth). Higher fluoride concentrations in drinking water cause both dental and skeletal fluorosis resulting in serious public health problems. The treatment of fluoride in groundwater, if viable, could resolve a number of pressing water supply problems in the area.

Fluoride concentrations are particularly high in areas with an occurrence of thermal waters or near areas of recent volcanism within the MER (Fig. 5.68). There is a direct correlation between silicic
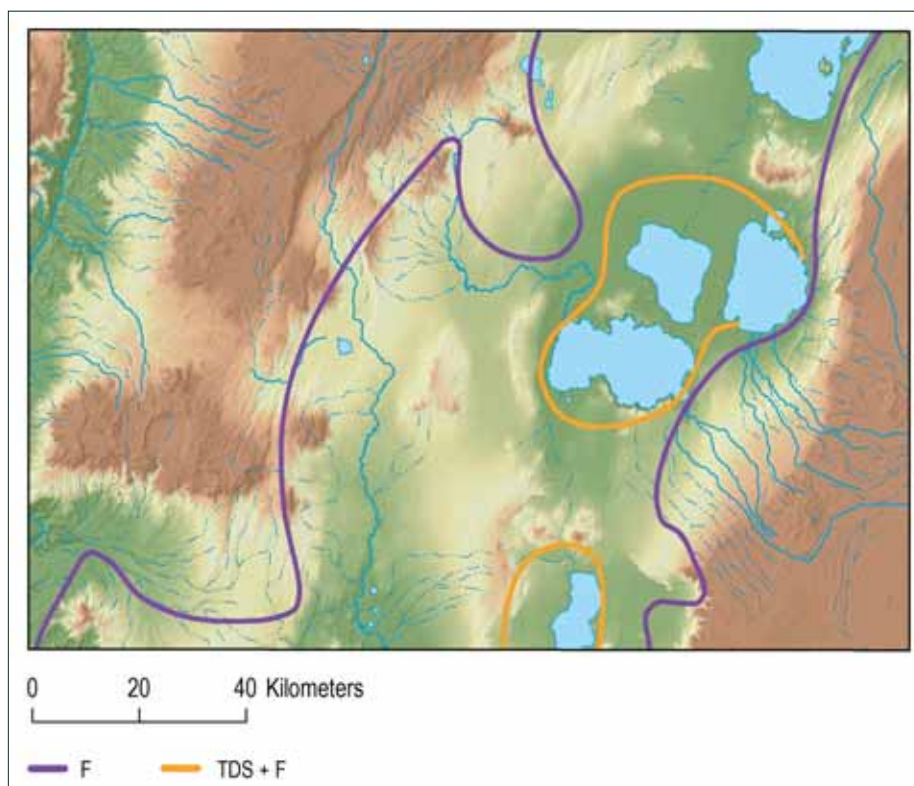
Fig. 5.68 Scheme of the area affected by high fluorine concentrations in the Hosaina map sheet area

Geological hazards

volcanic rocks such as obsidian and pumice and high concentrations of fluoride in groundwater. It is considered that leaching of water soluble Na-fluorides coating pyroclasts is the most likely source of fluoride. The rhyolitic rocks are extremely poor in phosphorus which would lead to fixing of the fluorine in apatite and they lack calcium which would react with fluorine producing non-leachable calcium fluoride. The interaction of the rhyolitic pyroclastic rocks with a large effective surface and percolating groundwater and carbon dioxide at high pH causes the release of fluoride into the groundwater. It is suggested (Rango et al. 2009) that the fluoride concentration in groundwater is inversely related to the concentration of Ca. This permits free mobility of the fluoride ion into groundwater at lower Ca content. This effect (Ca deficiency) is magnified where cation exchange takes place within the sediments (fluvio-lacustrine, volcano-lacustrine) causing the removal of ions from the solution (mainly Ca^{2+}) and replacement with Na^+ ions from the clay. Such hydrogeochemical processes are responsible for the evolution of Ca (Mg)–HCO_3 types of water of the highlands and the escarpment area to Na–HCO_3 types of groundwater (including the thermal water of the rift floor).
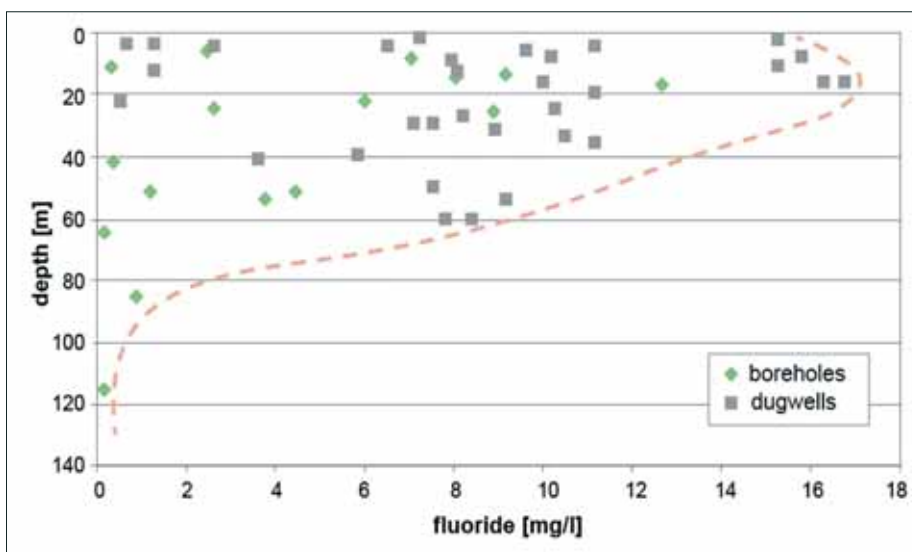
Fig. 5.69 High content of fluoride is caused by its leaching from silicic pyroclastic deposits. A decrease in fluoride content in groundwater with increasing depth is most likely the effect of depletion of older pyroclastic deposits and lacustrine sediments due to greater age and longer leaching of fluoride in the past.
After Tadesse and Zenaw (2003).

Thermal water tends to have a higher fluoride content than cold water as the water temperatures allow greater dissolution of fluoride. This probably explains the preponderance of high fluoride in waters around Hawasa town. It was also mentioned that closed terminal lakes attain high fluoride, salinity and alkalinity as a result of evaporation and the groundwater flux that comes through the acidic rocks. High concentrations can also be observed in the northeastern area of the Bilate River, the surroundings of Lake Hawasa as well as in the lake itself.

It was shown by Tadesse and Zenaw (2003) and by JICA (2012) that fluoride content decreases with increasing depth of the water source (testing wells). This confirms that the main source of fluoride is related to infiltration of rain water through young deposits of silicic volcanic activity. The concentration of course can be enhanced in geothermal systems. The same is also valid

Geological hazards

for the concentration of chlorides as well as nitrates. Tadesse and Zenaw (2003) noted that the decrease of fluoride with depth in the area indicates that the shallower lacustrine aquifer has a high concentration of fluoride (Fig. 5.69).

UNDP (1971) stated that the content of fluoride in Chabi obsidian is 2,500 ppm, pumice 440 ppm, obsidian 400 ppm, rhyolite 300 ppm, and ignimbrite 410 ppm. Samples of rocks were collected from the tuff and pumice of the Shashemene area during the field trip of 2012. Partial results of the chemical composition of samples analyzed in the laboratory of CGS are shown in Table 5.2 as well as the composition of leachate analyzed in the laboratory of AQUATEST.

Tab. 5.2 Chemical composition of rock samples in wt. % and chemical composition of leachate from these rocks in mg/l. See Annex 1 for details of sample locations and complete geochemistry.

Sample	Rock sample composition				Leachate composition			
	CaO	Na$_2$O	K$_2$O	F	Ca	Na	K	F
HSRV009	1.18	3.52	4.76	0.209	2.5	32.8	5.28	4.16
HSRVR069D	0.58	4.13	4.19	0.199	4.2	6.42	0.74	1.37
Sd007	0.28	4.96	4.39	0.218	5.4	4.25	< 0.5	0.74

A number of fluoride removal methods are practiced in basic water treatment plant design. The method of adding gypsum to the artificial sand-pack filter of a borehole and mixing of hot water with cold water was successfully tested in fluoride rich groundwater in Mexico (Carrillo-Rivera, 2002).

5.3.3 Unexpected discharge of thermal water

Active volcanic zones are associated with hydrothermal systems. The thermal waters can be used for power production or balneological purposes. On the other hand, an unexpected discharge

Fig. 5.70 River of boiling water flowing from the geyser to the village (April 1st 2014)

Geological hazards

of hot water also represents a serious hazard in the studied area. In the night of April 30th, an irrigation-well exploded and hot water started to discharge in a form of a geyser to the east of Lake Shetan near Butajira. The hot water flowing into the village Ashute Buraco (Fig. 5.70) injured a woman. Attention should be paid to potential sources of thermal water when drilling irrigation wells within active volcanic systems and fields.

Geological hazards

References

Abebe (1984): Geological and Petrochemical Study of Tulu Moye and Gedemsa Geothermal Project, Pisa, Italy.

Acocella V. (2010): Coupling volcanism and tectonics along divergent plate boundaries: Collapsed rifts from central Afar, Ethiopia. Geological Society of America Bulletin 9-10: 1717–1728.

Agostini, A., Bonini, M., Corti, G., Sani, F., Manetti, P. (2011): Distribution of Quaternary deformation in the central Main Ethiopian Rift, East Africa. Tectonics 30.

Asfaw, L. M. (1998): Environmental hazard from fissure in the Main Ethiopian Rift. Journal of African Earth Sciences. 27, 481-490.

Ayalew, L.; Yamagishi, H.; Reik, G. (2004): Ground cracks in Ethiopian Rift Valley: facts and uncertainties. Engineering Geology, 75, 309-324.

Ayenew, T. (2009): Natural Lakes of Ethiopia, Addis Ababa University press, ISBN 978-99944-52-21-7, pp. 197

Balogh, K. (1985): K/Ar Dating of Neogene Volcanic Activity in Hungary: Experimental Technique, Experiences and Methods of Chronologic Studies. ATOMKI Rep., D/1: 277–288.

Bell, J.W.; Price, J.G.; Mifflin, M.D. (1992): Subsidence induced fissuring along preexisting faults in Las Vegas Valley, Nevada. In: Engineering Geology into the 21st Century, Proceedings of the 35th Annual Meeting of the Association of Engineering Geologists, Los Angeles, CA, 66–75.

Berhane et al. (1976): Geological map of Lake Ziway area, 1:500,000 scale. Unpublished report.

Biggs, J.; Bastow, I.D.; Keir, D.; Lewi, E. (2011): Pulses of deformation reveal frequently recurring shallow magmatic activity beneath the Main Ethiopian Rift. Geochemistry, Geophysics, Geosystems 12: Q0AB10.

Bonini, M.; Corti, G.; Innocenti, F.; Manetti, P.; Mazzarini, F.; Abebe, T.; Pécskay, Z. (2005): Evolution of the Main Ethiopian Rift in the frame of Afar and Kenya rifts propagation. Tectonics 24.

Bronk Ramsey, C. (2013): OxCal Program, version 4.2 (http://c14. arch. ox. ac. uk/oxcal. html), Radiocarbon Accelerator Unit. University of Oxford.

Brotzu, P.; Morbidelli, L.; Piccirillo, E.M.; Traversa, G. (1980): Volcanological and magmatological evidence of the Boseti Volcanic Complex (Main Ethiopian Rift). Accad. Naz. Lincei, Rome, 47, 317–362.

Bryan, R.B.; Jones, J.A.A. (1997): The significance of soil piping processes: Inventory and prospect. Geomorphology 20, 209–218.

Carpenter, M.C. (1993) Earth fissure movements associated with fluctuations in groundwater levels near the Picacho Mountains, South-central Arizona, 1980–84. US Geological Survey Professional Paper 497-H, Washington, 40 pp.

Carrillo-Rivera, J.J. (ed. 2002): Use of abstraction regime and knowledge of hydrogeological condition to control high-flouride concentration in abstracted groundwater: San Luis Potosí basin, Mexico, Jurnal of Hydrogeology 261, 24–47.

Davidson (1983): The Omo River Project, Reconnaissance Geology and Geochemistry of Parts of Ilubabor, Kefa, Gemu Kefa and Sidams, Ethiopia.

Di Paola, G.M. (1976): Geological, Geothermal Report on Central Part of the Main Ethiopian Rift Valley. Geological Survey of Ethiopia, Addis Ababa, Ethiopia.

Ebinger, C. (2005): Continental breakup: The East African perspective: Astronomy and Geophysics, 46: 216–221.

Ephrem (2009): Geology of the Akaki-Beseka area. Basic Geoscience Mapping Core process, Geological Survey of Ethiopia, Addis Ababa.

FAO -UNESCO (1978): FAO-UNESCO, Soil map of the World, 1:5,000,000 (download for ArcGis) - http://www.lib.berkeley.edu/EART/fao.html

Gamatchu D. (1977): Aspects and Water budget in Ethiopia, AA University Press, Addis Ababa.

Gebreegzeibher, Y. (2004): Assesment of water balance of Lake Hawasa Catchment, Ethiopia. PhD. Thesis. International Institute for Geo-Information Science And Earth Observation. Enschede, The Netherlands.

Gianelli, G., Teklemariam, M. (1993). Water-rock interaction processes in the Aluto-Langano geothermal field (Ethiopia). Journal of volcanology and geothermal research, 56(4), 429-445.

Gibson, I.L. (1970). A pantelleritic welded ash-flow tuff from the Ethiopian Rift Valley. Contributions to Mineralogy and Petrology, 28(2), 89-111.

Gobena, H.; Belayneh, M.; Kebede, T.; Tesfaye, S.; Abraham, A. (1996): Geology of the Dodola area. Geological Survey of Ethiopia, Addis Ababa.

Gouin, P. (1979): Earthquake history of Ethiopia and the Horn of Africa. Ottawa, Ont., IDRC, 259 p.

Gozalbez, J.; Cebrian, D. (2006): Touching Ethiopia 2nd English edition, 2006, Shama Publisher.

Halcrow (2008): Rift Valley Lakes Basin Integrated Resources Development Master Plan Study Project, Draft Phase 2 Report Part II Prefeasibility Studies, Halcrow Group Limited and Generation Integrated Rural Development (GIRD) consultants. Unpublished report. Addis Ababa.

Hayward, N.J., Ebinger, C.J. (1996): Variations in the along-axis segmentation of the Afar Rift system. Tectonics 15: 244–257.

Holzer, L.T. (1984): Ground failure induced by groundwater withdrawal from unconsolidated sediment. – In: Holzer, L.T. (ed.): Man Induced Land Subsidence, Reviews in Engineering Geology vol. 6. The Geological Society of America, Boulder, Colorado, pp. 67–105.

IAEG (1976): Engineering geological map: a guide to their preparation. UNESCO Press, Paris, 79 pp.

JICA (2012): The Study on Groundwater Resources Assessment in the Rift Valley Lakes Basin in the Federal Democratic Republic of Ethiopia, Japan International Cooperation Agency (JICA), Kokusai Kogyo Co., Ltd., Ministry of Water and Energy (MoWE), The Federal Democratic Republic of Ethiopia. Final Report (Main Report).

Kazmin, V. (1973): Geological Map of Ethiopia. Geological Survey of Ethiopia: Addis Ababa, Ethiopia.

Kazmin, V.; Seife, M.B. (1978): Geological map of Nazreth Sheet, Scale 1:250,000, Geological Survey of Ethiopia, Addis Ababa.

Kazmin, V.; Seife, M.B.; Nicoletti, M.; Petrucciani, C. (1980): Evolution of the northern part of the Ethiopian Rift. Accad. Naz. Lincei, Rome 47, 275-291. Italy.

Kazmin, V.; Berhe, S.M.; Wondm-Agennehu, B. (1981): Geological Map of the Ethiopian Rift. The Ethiopian Government – Ministry of Mines, Energy and Water Resources, Addis Ababa.

Kebede, F.; Van Eck, T. (1997): Probabilistic seismic hazard assessment for the Horn of Africa based on seismotectonic regionalisation. Tectonophysics, 270, 221-237.

Koeppen in NMSA (1989): Climatic and Agroclimatic Resources of Ethiopia, NMSA, AA, August 1989.

Lloyd, E.F. (1977): Geological Factors Influencing Geothermal Exploration in the Langano Region, Ethiopia, NZ Geological Survey, Rotorua, New Zealand.

Mengesha, T.; Tadiwos, C.; Workneh, H. (1996): The geological map of Ethiopia, 1:2,000,000 scale, (2nd editon), EIGS, Addis Ababa.

Merla, G.; Abbate, E.; Canuti, P.; Sagri, M.; Tacconi, P. (1973): Geological map of Ethiopia and Somalia, 1:2,000,000. Consiglio Nazionale delle Ricerche Italy, Stabilimento Poligrafico Fiorentino, Firenze.

Moges, A.; Holden, M.N. (2008): Estimating the rate consequences of gully development, a case study of Umbulo catchment in southern Ethiopia. Land Degrad. Develop.19

Mohr (1960): The geology of Ethiopia, Asmara, Poligrafia.

Morgan, R.P.C. (1996): Soil erosion and conservation, 2nd edition. Longman: Harlow.

NMA (2006): Annual Climatic Bulletin 2006, Federal Democratic Republic of Ethiopia, Ministry of Water Resources, National Meteorological Agency (NMA) Climatolocical Service Team.

NMSA (1996): Assessment of Drought in Ethiopia, Meteorological Research Reports Series No. 2, Addis Ababa, Ethiopia.

Odin, G.S. (1982): Numerical Dating in Stratigraphy. John Wiley and Sons, New York, pp 1–1040.

Rango, T.; Bianchini, G.; Beccaluva, L.; Ayenew, T.; Colombani, N. (2009): Hydro-geochemical study in the Main Ethiopian Rift: new insights to the source and enrichment mechanism of fluoride. Environmental Geol. 58: 109–118.

Rapprich V., Čížek D., Daniel K., Firdawok L., Habtamu B., Hroch T., Kopačková V., Málek J., Malík J., Mišurec J., Orgoň A., Šebesta J., Šíma J., Tsigehana T., Verner K., Yewubinesh B. (2013): Explanation Booklet to the Set of Geoscience maps of Ethiopia at scale 1 : 50,000, subsheet 0738-C4 Hawasa. Czech Geological Survey/ Aquatest/Geological Survey of Ethiopia, Praha/Addis Ababa, Czech Republic/Ethiopia.

Reimer, P. J.; Bard, E.; Bayliss, A.; Beck, J. W.; Blackwell, P. G.; Ramsey, C. B.; van der Plicht, J. (2013): IntCal13 and Marine13 radiocarbon age calibration curves 0–50,000 years cal BP. Radiocarbon, 55, 1869-1887.

Schumann, H.H.; Poland, J.F. (1970): Land subsidence, earth fissures and groundwater withdrawal in south-central Arizona, USA. – In: TISON L.J. (ed.), Land Subsidence. International Association of Hydrological Sciences, Tokyo, Japan, pp. 295– 302.

Seife Michael, B. (1978): Geological map (1:250,000) of the Nazret area. Ethiopian Inst. Geol. Surv., Addis Ababa, sheet NC37-15.

Setegn, S.G. (2010): Modeling Hydrological and Hydrodynamic Processes in Lake Tana Basin, Ethiopia, KTH. TRITA-LWR PhD Thesis 1057.

Steiger, R.H.; Jäger, E. (1977): Subcommission on Geochronology: convention on the use of decay constants in geo- and cosmochronology. Earth and Planetary Science Letters, 36: 359–362.

Tadesse, D.; Zenaw, T. (2003): Hydrology and Engineering Geology of Awasa Lake Catchment, Geological survey of Ethiopia, 1–67 + 2 maps.

Tesfaye, Ch. (1993): Hydrogeology of Ethiopia and Water Resources Development – MS EIGS, Ministry of Mines and energy, Addis Ababa.

Tesfaye, S., Harding D.J., Kusky, T.M. (2003): Early continental breakup boundary and migration of the Afar triple junction, Ethiopia Geological Society of America Bulletin 115/9: 1053–1067.

Tilahun, K.; Šíma, J. (2013): Hydrogeological and hydrochemical maps of Asela NB 37-3. Explanatory notes. Aquatest a.s., Praha, Czech Republic.

UN – UNDP (1971): Ethiopia: Investigation of Geothermal Resources for Power Development (ETH 26). Geology, Geochemistry and Hydrology of Hot Springs of the Eastern African Rift System in Ethiopia.

WoldeGabriel G., Aronson J.C., Walter R.C., Hart W.K. (1992) : Geochronology and Distribution of Silicic Volcanic Rocks of Plio-Pleistocene Age from the Central Sector of the Main Ethiopian Rift. Quaternary International 13–14: 69–76.

WoldeGabriel, G.; Walter, R.C.; Hart, W.K.; Mertzman, S.A.; Aronson, J.L. (1999): Temporal relations and geochemical feature of felsic volcanism in the central sector of the Main Ethiopian Rift. Acta Vulcanol. 11: 53–67.

WHO (2006): World Health Statistics, http://www.who.int/countries/eth/eth/en/

WWDSE (2001) The study of Lake Awassa level rise (Main Report, Vol II). Unpublished report of the Water Works Design and Supervision Enterprise, Addis Ababa, Ethiopia, pp 291.

Žáček, V.; Rapprich, V.; Aman, Y.; Berhanu, B.; Čížek, D.; Dereje, K.; Erban, V.; Ezra, T.; Firdawok, L.; Habtamu, M.; Hroch, T.; Kopačková, V.; Kycl, P.; Málek, J.; Mišurec, J.; Orgoň, A.; Pécskay, Z.; Šíma, J.; Tarekegu, D.; Verner, K. (2014): Explanation Booklet to the Set of Geoscience maps of Ethiopia at scale 1 : 50,000, subsheet 0738-C4 Hawasa. Czech Geological Survey/Aquatest/Geological Survey of Ethiopia, Praha/Addis Ababa, Czech Republic/Ethiopia.

Zenaw, T.; Tadesse, D. (2003): Hydrology and Engineering Geology of Awasa Lake Cahtchment, Geological survey of Ethiopia.

Annex No. 1

Sample	locality	rock	Coordinates (Adindan)		LAB	SiO$_2$	TiO$_2$	Al$_2$O$_3$	Fe$_2$O$_3$	FeO
			X	Y						
HSRVR009	Shashemene	tuff	450718	798466	CGS	68.79	0.46	9.62	3.14	1.65
HSRVR010	Corbetti	ignimbrite	431316	801037	CGS	74.51	0.34	10.13	1.62	2.70
HSRVR030	Debes Qoto	basalt	422483	878215	CGS	47.02	2.66	14.39	3.47	7.81
HSRVR035	Hawasa	basalt	444587	780361	CGS	44.82	4.14	13.98	6.78	9.15
HSRVR036	Algerima	obsidian	438840	790088	CGS	74.79	0.26	9.42	2.06	2.70
HSRVR037	Algerima	pumice	438453	789644	CGS	72.61	0.26	9.14	2.36	2.25
HSRVR038	Algerima	obsidian	438634	789103	CGS	74.58	0.25	9.30	2.47	2.43
HSRVR039	Algerima	pumice	438455	788919	CGS	72.42	0.25	9.17	2.28	2.37
HSRVR041	Bura	pumice	442565	801686	CGS	72.07	0.24	9.23	3.52	1.30
HSRVR042	Shalla Sodi	scoria	437006	809417	CGS	47.02	3.44	13.53	9.15	4.70
HSRVR051	Herera	basalt	490174	878138	CGS	47.75	2.05	14.73	4.75	6.30
HSRVR053	Lalo	basalt	487023	873793	CGS	48.86	1.93	17.07	4.95	5.95
HSRVR056	Butajira	basalt	436801	901980	CGS	47.12	2.37	15.54	2.52	8.26
HSRVR067	Kambolcha	obsidian	439352	799415	CGS	73.79	0.28	9.46	2.13	2.63
HSRVR068	Kambolcha	obsidian	439826	800806	CGS	74.75	0.34	10.23	1.68	2.35
HSRVR069C	Korbeti	pumice	432244	798033	CGS	70.39	0.26	9.24	2.45	2.30
HSRVR069D	Korbeti	pumice	432244	798033	CGS	69.67	0.26	9.44	2.56	2.20
HSRVR071	Wendo Koshe	obsidian	431377	795833	CGS	74.00	0.27	9.56	2.18	2.67
HSRVR074	Kubi Kelle	basalt	437700	804862	CGS	46.79	4.29	12.66	5.91	9.25
HSRVR087	Hawasa	obsidian	442599	793206	CGS	73.68	0.28	9.53	2.23	2.62
HSRVR091	Alem Tena	basalt	401771	777883	CGS	46.52	4.13	13.86	4.02	10.13
HSRVR092	Koshame	basalt	418016	844428	CGS	45.65	4.06	14.54	12.26	1.85
HSRVR093	Dolocha	basalt	419903	857754	CGS	46.76	3.43	16.80	9.84	2.23
HSRVR102	Alutu	obsidian	472267	864707	CGS	73.05	0.22	8.83	2.24	3.63
HSRVR105	Ziway	scoria	470034	866433	GSE	59.7	1.67	15.8	8.62	
HSRVR112	Alutu	ignimbrite	478134	865075	CGS	73.19	0.23	9.23	4.99	0.70
HSRVR115	Alutu	obsidian	478830	859057	CGS	73.16	0.33	9.45	1.92	3.25
HSRVR135	Shalla	ignimbrite	455321	831698	GSE	65.82	0.34	10.02	5	
HSRVR136	Shalla	ignimbrite	454473	833808	GSE	73.22	0.32	8.59	6.92	
HSRVR137	Shalla	basalt	449687	833872	GSE	48.38	2.87	16.68	12.26	
HSRVR140	Alutu	obsidian	473655	862856	CGS	72.74	0.27	8.77	2.31	3.67
HSRVR146B	Mito	ignimbrite	443042	852251	GSE	78.98	0.27	6.13	3	
HSRVR177	Hawasa	basalt	445342	777919	CGS	43.46	3.48	14.53	4.88	9.62
HSRVR182	Langano	obsidian	491642	832440	GSE	73.92	0.25	12.38	2.2	
HSRVR195	Ambericho	obsidian	377635	804072	CGS	70.00	0.28	12.97	1.76	1.99
HSRVR196	Angacha	ignimbrite	382186	807327	CGS	74.06	0.30	10.80	2.61	1.09
Sd007	Shashemene	tuff	448112	791717	CGS	71.28	0.28	9.23	2.27	2.41
Sd013	Shashemene	trachyte	450850	786089	CGS	75.16	0.22	10.46	1.82	1.70
Sd017	Shashemene	rhyolite	456028	787109	CGS	74.45	0.17	12.20	2.20	0.21
Sd036	Shashemene	ignimbrite	461719	780190	CGS	73.51	0.29	11.49	2.52	0.90
Sd042	Shashemene	basalt	458284	781715	CGS	49.71	2.73	17.89	11.07	1.38
Sd048	Shashemene	ignimbrite	463925	797042	CGS	72.11	0.40	10.30	5.07	0.49
Sd061	Shashemene	basalt	453471	773156	CGS	48.63	2.17	16.87	3.13	7.66
Sd067	Shashemene	trachyte	468772	772822	CGS	73.00	0.40	10.07	4.57	1.03

	MgO	MnO	CaO	Li$_2$O	Na$_2$O	K$_2$O	P$_2$O$_5$	F	CO$_2$	C(ost.)	S(tot.)
HSRVR009	0.50	0.171	1.18	0.007	3.52	4.76	0.084	0.209	0.61		0.023
HSRVR010	0.11	0.198	0.45	0.004	4.37	4.68	0.017	0.094	0.06	0.031	< 0.010
HSRVR030	8.48	0.149	10.53	< 0.001	3.05	1.17	0.630	0.101	< 0.01	0.024	< 0.010
HSRVR035	5.03	0.230	10.01	0.003	3.08	0.71	0.606	0.109	0.23		< 0.010
HSRVR036	< 0.01	0.184	0.24	0.007	5.22	4.37	0.013	0.221	< 0.01	0.005	< 0.010
HSRVR037	0.02	0.177	0.24	0.007	5.11	4.25	0.013	0.251	< 0.01	0.077	< 0.010
HSRVR038	< 0.01	0.196	0.22	0.009	5.25	4.39	0.012	0.264	< 0.01	0.017	< 0.010
HSRVR039	0.01	0.185	0.22	0.007	5.04	4.35	0.013	0.246	< 0.01	0.044	< 0.010
HSRVR041	0.03	0.198	0.25	0.007	4.81	4.30	0.013	0.248	0.01	0.039	< 0.010
HSRVR042	6.66	0.211	9.98	< 0.001	2.71	0.65	0.536	0.087	< 0.01	0.010	< 0.010
HSRVR051	8.67	0.193	9.74	< 0.001	2.42	0.79	0.322	0.069	0.11		0.016
HSRVR053	5.94	0.188	9.36	0.001	3.36	0.83	0.306	0.086	0.05		< 0.010
HSRVR056	8.92	0.184	9.73	0.001	3.14	0.99	0.547	0.081	0.01		< 0.010
HSRVR067	0.01	0.210	0.18	0.007	5.27	4.47	0.021	0.291	< 0.01		< 0.010
HSRVR068	0.03	0.208	0.26	0.004	4.71	4.62	0.025	0.143	0.01		< 0.010
HSRVR069C	0.05	0.199	0.30	0.007	4.05	4.17	0.023	0.192	< 0.01		< 0.010
HSRVR069D	0.11	0.200	0.58	0.006	4.13	4.19	0.030	0.199	0.07		0.011
HSRVR071	0.02	0.209	0.18	0.007	5.30	4.47	0.028	0.254	< 0.01		0.011
HSRVR074	5.78	0.231	9.62	0.001	2.82	0.71	0.661	0.117	0.02		< 0.010
HSRVR087	0.03	0.207	0.21	0.007	5.36	4.50	0.022	0.228	< 0.01		< 0.010
HSRVR091	5.70	0.236	8.64	0.001	3.15	1.19	1.027	0.141	< 0.01		< 0.010
HSRVR092	5.90	0.221	8.58	< 0.001	3.25	1.20	0.957	0.231	0.04		0.022
HSRVR093	5.02	0.177	9.42	< 0.001	3.54	1.04	0.733	0.107	< 0.01		0.015
HSRVR102	0.02	0.239	0.23	0.006	6.02	4.52	0.022	0.261	< 0.01		< 0.010
HSRVR105	2.56	0.16	4.58		4.2	2.32	0.23				
HSRVR112	0.04	0.216	0.21	0.005	5.33	4.53	0.025	0.229	< 0.01		0.028
HSRVR115	0.02	0.215	0.29	0.004	5.58	4.63	0.024	0.201	< 0.01		0.019
HSRVR135	0.26	0.14	0.08		4	2.44	0.07				
HSRVR136	0.08	0.38	0.16		5.26	4	0.03				
HSRVR137	5	0.22	8.96		2.98	0.44	0.57				
HSRVR140	0.02	0.259	0.29	0.005	5.86	4.61	0.024	0.229	< 0.01		< 0.010
HSRVR146B	0.34	0.12	0.44		2.08	2.02	0.04				
HSRVR177	8.44	0.208	10.25	0.002	3.04	0.60	0.414	0.076	0.10		< 0.010
HSRVR182	0.14	0.06	0.38		4.28	4.22	0.13				
HSRVR195	0.16	0.202	0.31	0.005	5.98	4.80	0.025	0.239	< 0.01		< 0.010
HSRVR196	0.11	0.122	0.26	0.005	4.74	4.32	0.025	0.124	< 0.01		< 0.010
Sd007	0.05	0.196	0.28	0.007	4.96	4.39	0.025	0.218	0.05		< 0.010
Sd013	0.03	0.082	0.14	0.007	4.46	4.57	0.035	0.140	< 0.01		< 0.010
Sd017	0.02	0.089	0.16	0.002	4.85	4.38	0.021	0.048	< 0.01		< 0.010
Sd036	0.11	0.094	0.12	0.005	4.17	4.43	0.041	0.094	< 0.01		0.054
Sd042	1.35	0.122	6.66	< 0.001	4.22	1.27	0.477	0.065	< 0.01		< 0.010
Sd048	0.16	0.240	0.29	0.004	4.65	4.55	0.034	0.118	< 0.01		0.014
Sd061	5.50	0.174	9.21	0.001	3.47	1.00	0.395	0.073	0.16		< 0.010
Sd067	0.14	0.242	0.31	0.004	4.50	4.52	0.027	0.169	< 0.01		< 0.010

	H$_2$O(+)	H2O(-)	LOI	F(ekv)	S(ekv)	Total	Co_XRF	Cu_XRF	Cr	Cr_XRF
HSRVR009	4.33	0.53		-0.088	-0.006	99.57		6		< 2
HSRVR010	0.59	0.09		-0.040	0.000	99.99		4	4.0	< 2
HSRVR030	0.27	< 0.05		-0.043	-0.001	99.79		53	371.0	295
HSRVR035	0.43	0.18		-0.046	-0.002	99.49		22	29.0	30
HSRVR036	0.43	< 0.05		-0.093	-0.001	99.93		3	7.0	< 2
HSRVR037	2.84	0.32		-0.106	-0.001	99.93		4	4.1	< 2
HSRVR038	0.50	< 0.05		-0.111	nest.	99.92		< 2	5.9	< 2
HSRVR039	2.54	0.73		-0.104	-0.002	99.89		6	4.1	< 2
HSRVR041	2.60	0.26		-0.104	-0.001	99.12		4	5.4	< 2
HSRVR042	0.59	0.06		-0.037	0.000	99.36		35	149.4	109
HSRVR051	1.33	0.20		-0.029	-0.004	99.43		35	217.6	212
HSRVR053	0.40	< 0.05		-0.036	-0.002	99.32		27	217.6	38
HSRVR056	0.26	< 0.05		-0.034	-0.001	99.68		67	313.0	313
HSRVR067	0.44	0.08		-0.123	-0.002	99.26		7	3.7	3
HSRVR068	0.43	0.05		-0.060	0.000	99.84		4	1.9	< 2
HSRVR069C	5.17	0.55		-0.081	-0.002	99.37		5	2.1	< 2
HSRVR069D	4.96	0.60		-0.084	-0.003	99.22		6	2.1	< 2
HSRVR071	0.42	< 0.05		-0.107	-0.003	99.58		5	2.2	< 2
HSRVR074	0.36	< 0.05		-0.049	0.000	99.24		29	37.3	35
HSRVR087	0.52	< 0.05		-0.096	-0.001	99.46		5	2.2	< 2
HSRVR091	0.53	0.07		-0.059	-0.002	99.35		17	21.9	23
HSRVR092	0.46	0.09		-0.097	-0.005	99.31		21	14.2	19
HSRVR093	0.33	< 0.05		-0.045	-0.004	99.45		26	23.3	20
HSRVR102	0.45	0.11		-0.110	nest.	99.85				
HSRVR105	0.21		0.79			100.84	30.4	13.2		
HSRVR112	0.55	0.16		-0.096	-0.007	99.68				
HSRVR115	0.51	0.09		-0.085	-0.005	99.70				
HSRVR135	4.94		6.15			99.26	14	0.6		
HSRVR136	0.07		0.49			99.52	21.6	1.2		
HSRVR137	0.44		0.14			98.94	39.4	13.8		
HSRVR140	0.47	0.06		-0.096	0.000	99.60				
HSRVR146B	1.58		3.57			98.57	21.2	1.2		
HSRVR177	0.35	0.18		-0.032	-0.001	99.62		33	8.1	36
HSRVR182	0.18		0.4			98.54	22	1.8		
HSRVR195	0.60	0.05		-0.101	-0.001	99.39			1.3	
HSRVR196	0.69	0.18		-0.052	0.000	99.43			1.7	
Sd007	3.11	0.36		-0.092	-0.001	99.11			4.2	
Sd013	0.35	0.07		-0.059	0.000	99.26			5.4	
Sd017	0.20	< 0.05		-0.020	nest.	99.04			4.9	
Sd036	0.81	0.10		-0.040	-0.013	98.74			3.9	
Sd042	1.45	1.41		-0.027	-0.001	99.79			1.1	
Sd048	0.69	0.10		-0.050	-0.004	99.23			5.1	
Sd061	0.69	0.19		-0.031	-0.002	99.33			34.1	
Sd067	0.67	0.24		-0.071	0.000	99.90			2.5	

	Ga	Hf	Mo_XRF	Nb	Nb_XRF	Ni	Ni_XRF	Pb	Pb_XRF
HSRVR009			3		159		15		19
HSRVR010	33.4	9.5	< 1	62.2	103	10.1	4	14.4	10
HSRVR030	18.2	2.2	< 1	32.0	34	105.8	92	4.0	< 2
HSRVR035	20.1	4.1		21.6	25	26.6	25	1.8	3
HSRVR036	38.7	20.4	7	114.5	198	32.3	15	25.5	23
HSRVR037	36.6	19.7	5	117.7	195	9.7	18	25.4	23
HSRVR038	39.3	23.0	5	137.3	226	29.2	17	94.7	26
HSRVR039	35.5	19.3	5	114.0	194	11.1	16	27.3	23
HSRVR041	37.5	19.8	6	127.5	197	11.0	14	25.5	20
HSRVR042	20.7	2.4	< 1	38.1	23	60.5	46	6.2	< 2
HSRVR051	20.2	4.4	< 1	28.1	24	42.9	48	4.1	4
HSRVR053	21.0	4.8	2	28.3	21	21.6	19	2.0	< 2
HSRVR056	17.4	4.1	< 1	35.1	28	102.3	108	2.0	< 2
HSRVR067	38.5	36.6	6	182.3	197	14.4	16	20.6	26
HSRVR068	27.8	14.9	4	98.8	107	6.6	7	8.9	11
HSRVR069C	38.4	37.3	5	182.3	191	12.4	15	22.7	25
HSRVR069D	37.6	37.6	5	173.6	188	14.5	17	20.4	24
HSRVR071	40.6	38.7	6	174.2	200	13.5	18	22.6	25
HSRVR074	20.8	4.8	< 1	29.1	23	22.5	20	2.1	< 2
HSRVR087	39.4	37.7	5	189.7	197	14.9	17	21.5	24
HSRVR091	21.9	5.3	< 1	39.8	34	19.3	15	4.1	5
HSRVR092	20.7	4.7	< 1	36.5	33	15.3	17	2.1	< 2
HSRVR093	21.2	3.7	2	30.0	23	21.1	17	2.5	3
HSRVR102									
HSRVR105							3.2		< 0.2
HSRVR112									
HSRVR115									
HSRVR135							< 0.2		24
HSRVR136							< 0.2		6.8
HSRVR137							20.4		< 0.2
HSRVR140									
HSRVR146B							2		3.8
HSRVR177	18.3	2.8		8.8	17	33.7	23	0.9	< 2
HSRVR182							1		4.6
HSRVR195	25.8	16.3		44.3		1.1		59.3	
HSRVR196	27.3	23.1		37.1		0.9		15.1	
Sd007	31.6	30.1		107.6		10.6		26.0	
Sd013	32.8	33.0		98.8		11.6		26.4	
Sd017	22.7	15.5		49.7		11.9		14.3	
Sd036	26.7	21.4		64.1		10.0		19.9	
Sd042	22.6	6.2		19.9		3.1		1.6	
Sd048	36.6	22.6		89.8		12.3		17.4	
Sd061	18.8	4.0		24.0		20.3		2.2	
Sd067	35.2	22.9		56.5		3.9		13.4	

	Rb	Rb_XRF	Ta	Th	U	U_XRF	V	Zn_XRF	Zr	Zr_XRF	Sn_XRF
HSRVR009		102				5		288		1298	8
HSRVR010	40.1	76	10.2	14.2	1.2	7	3.9	178	503.5	629	10
HSRVR030	10.6	19	7.3	3.4	0.9	< 2	270.3	81	128.0	125	< 2
HSRVR035	7.9	8	8.0	2.6	0.3	< 2	407.5	102	157.9	158	< 2
HSRVR036	68.5	108	13.8	14.0	5.7	6	1.6	331	1313.0	1514	7
HSRVR037	75.1	107	18.2	14.0	5.5	5	2.1	361	1319.0	1491	8
HSRVR038	69.6	118	29.5	17.6	6.6	4	2.1	397	1508.5	1699	10
HSRVR039	59.9	106	17.0	13.6	5.3	7	2.2	368	1325.5	1498	6
HSRVR041	80.2	105	17.1	14.3	5.7	5	3.5	367	1355.5	1474	10
HSRVR042	6.7	8	13.5	2.8	0.6	< 2	372.5	90	133.1	129	< 2
HSRVR051	12.3	14	6.9	< 0.1	0.7	< 2	277.2	93	139.1	145	< 2
HSRVR053	13.7	13	11.4	< 0.1	0.6	< 2	235.9	86	125.6	131	< 2
HSRVR056	16.1	15	8.6	< 0.1	0.6	< 2	243.5	77	126.6	132	< 2
HSRVR067	108.2	111	15.0	15.7	5.0	5	4.0	366	1462.0	1542	6
HSRVR068	61.7	67	7.7	< 0.1	2.1	3	3.8	208	795.4	813	7
HSRVR069C	110.2	106	14.0	15.3	5.1	7	5.3	371	1488.5	1521	10
HSRVR069D	113.0	98	14.5	14.9	4.6	4	6.6	363	1493.5	1482	13
HSRVR071	101.6	112	17.1	18.9	5.4	5	3.0	364	1580.0	1554	8
HSRVR074	7.9	8	10.8	< 0.1	0.5	< 2	638.5	106	149.4	160	< 2
HSRVR087	112.0	109	15.2	17.0	5.2	5	6.3	365	1497.5	1523	< 2
HSRVR091	12.7	16	10.5	< 0.1	0.5	< 2	390.8	109	157.7	165	< 2
HSRVR092	17.1	15	9.4	< 0.1	0.7	< 2	314.6	111	141.8	158	< 2
HSRVR093	15.8	13	7.7	< 0.1	0.5	< 2	310.3	90	108.3	112	< 2
HSRVR102											
HSRVR105								68.4			
HSRVR112											
HSRVR115											
HSRVR135								198.2			
HSRVR136								159.2			
HSRVR137								85			
HSRVR140											
HSRVR146B								70.8			
HSRVR177	3.8	6	< 5.0	1.0	0.1	< 2	98.9	93	106.9	117	< 2
HSRVR182								38.6			
HSRVR195	106.2			18.9	3.4		2.2		479.3		
HSRVR196	90.7			15.4	2.2		13.6		1014.0		
Sd007	69.2		13.7	17.2	3.6		1.8		1350.0		
Sd013	142.8		15.2	21.3	2.1		1.9		1452.0		
Sd017	65.4		7.9	12.0	1.1		1.4		878.0		
Sd036	57.0		9.6	13.1	0.6		6.2		935.0		
Sd042	20.9			4.1	0.6		170.1		234.7		
Sd048	62.0		12.4	17.0	1.9		4.9		974.0		
Sd061	11.2			4.3	0.4		249.1		150.0		
Sd067	88.1			20.3	2.9		8.9		937.6		

	Sr	Sr_XRF	Sc	Ba	Y	Y_XRF	La	Ce	Pr	Nd
HSRVR009		62				147				
HSRVR010	11.5	5	17.8	32.9	32.73	46	73.0	156.7	18.26	72.0
HSRVR030	726.5	670	34.3	459.9	22.67	30	32.6	62.6	7.94	35.3
HSRVR035	445.6	545	3.7	330.1	25.85	34	22.1	52.0	6.69	31.6
HSRVR036	7.7	< 1	20.3	94.4	175.00	177	204.6	397.7	48.40	200.7
HSRVR037	8.7	2	13.0	109.4	168.95	176	199.0	384.3	46.98	193.8
HSRVR038	618.0	2	15.0	183.	189.60	198	241.3	441.0	53.20	218.4
HSRVR039	8.2	< 1	14.0	92.2	158.30	175	185.4	360.7	44.37	181.4
HSRVR041	8.7	3	21.6	86.9	168.90	178	196.8	381.1	46.80	193.2
HSRVR042	500.0	473	39.6	294.9	25.56	33	22.0	45.8	6.09	29.5
HSRVR051	458.1	429	31.1	259.0	24.4	33	24.6	48.4	6.07	26.0
HSRVR053	553.5	544	25.9	286.1	25.1	32	21.7	41.8	5.40	23.4
HSRVR056	616.0	604	27.3	356.1	23.5	32	25.0	49.6	6.35	27.7
HSRVR067	4.1	2	7.1	73.2	171.1	181	158.3	405.3	42.35	170.0
HSRVR068	4.2	4	3.6	86.9	73.2	97	81.6	158.3	19.13	78.4
HSRVR069C	5.4	4	7.6	76.7	177.9	180	151.2	421.3	43.89	176.1
HSRVR069D	7.7	8	8.3	95.2	166.3	172	153.9	405.7	40.92	165.8
HSRVR071	4.9	1	8.4	75.3	184.1	182	153.0	440.8	44.96	182.8
HSRVR074	443.3	468	32.9	296.4	29.5	40	22.8	48.0	6.40	30.0
HSRVR087	5.1	4	8.4	80.9	175.2	179	160.8	410.1	42.67	172.8
HSRVR091	549.0	558	29.0	621.9	34.5	41	38.2	71.5	9.45	42.4
HSRVR092	753.3	772	25.9	518.8	26.1	35	31.1	63.5	8.25	37.0
HSRVR093	957.6	909	24.5	482.9	21.2	28	25.9	52.1	6.80	30.9
HSRVR102										
HSRVR105										
HSRVR112										
HSRVR115										
HSRVR135										
HSRVR136										
HSRVR137										
HSRVR140										
HSRVR146B										
HSRVR177	329.6	445	< 1.0	230.1	19.53	30	16.3	38.0	4.89	22.5
HSRVR182										
HSRVR195	6.6		< 1.0	12.4	62.95		102.6	197.5	23.20	81.8
HSRVR196	21.0		< 1.0	178.1	105.10		113.5	249.9	28.70	113.6
Sd007	9.9		< 1.0	69.6	159.10		169.2	311.6	44.90	174.9
Sd013	4.2		< 1.0	22.9	160.75		153.0	297.6	36.35	135.9
Sd017	6.6		< 1.0	1042.0	56.45		80.3	184.9	22.00	83.9
Sd036	9.1		< 1.0	273.3	79.05		111.6	249.8	31.96	118.1
Sd042	998.5		6.1	485.5	30.59		34.6	69.5	9.13	39.5
Sd048	18.9		< 1.0	46.7	97.05		140.1	300.9	35.50	134.4
Sd061	950.0		< 1.0	370.9	19.66		20.3	43.1	5.70	23.8
Sd067	13.6		< 1.0	44.2	42.01		93.3	211.9	25.42	90.1

	Sm	Eu	Gd	Tb	Dy	Ho	Er	Tm	Yb	Lu
HSRVR009										
HSRVR010	13.54	1.83	10.08	1.60	9.05	1.60	4.14	0.62	4.41	0.71
HSRVR030	7.16	2.75	5.80	0.89	5.03	0.96	2.32	0.32	2.03	0.32
HSRVR035	6.74	2.34	6.14	0.98	5.41	1.00	2.63	0.38	2.31	0.32
HSRVR036	39.37	6.37	32.66	5.81	37.13	7.38	19.50	2.90	18.93	2.95
HSRVR037	38.91	6.23	32.05	5.68	35.85	7.09	18.92	2.79	18.13	2.88
HSRVR038	42.83	9.36	36.04	6.33	40.28	8.03	21.49	3.23	20.63	3.26
HSRVR039	36.21	5.74	30.05	5.26	33.73	6.64	17.68	2.69	17.04	2.79
HSRVR041	38.53	6.24	32.35	5.63	36.06	7.17	18.86	2.80	17.91	2.94
HSRVR042	6.52	2.76	5.65	0.97	5.97	1.08	2.79	0.36	2.35	0.34
HSRVR051	5.53	1.78	5.08	0.85	4.87	0.94	2.49	0.36	2.24	0.37
HSRVR053	5.07	1.79	4.56	0.82	4.72	0.94	2.46	0.35	2.29	0.37
HSRVR056	5.91	2.07	5.28	0.86	4.69	0.89	2.34	0.33	2.06	0.32
HSRVR067	35.02	4.80	33.23	5.59	32.92	6.62	17.86	2.69	16.77	2.69
HSRVR068	15.71	2.27	15.16	2.47	14.26	2.83	7.74	1.18	7.32	1.18
HSRVR069C	36.49	5.00	34.48	5.71	33.78	6.73	18.28	2.81	17.27	2.76
HSRVR069D	34.22	4.68	32.76	5.38	31.92	6.43	17.14	2.67	16.56	2.60
HSRVR071	37.30	5.10	35.43	5.98	35.94	7.19	19.27	2.96	18.40	2.92
HSRVR074	6.97	2.55	5.62	1.06	6.11	1.17	2.92	0.42	2.55	0.40
HSRVR087	35.64	4.81	34.08	5.67	33.46	6.74	18.20	2.74	17.12	2.73
HSRVR091	9.00	3.23	7.68	1.30	7.01	1.34	3.40	0.46	2.85	0.44
HSRVR092	7.87	2.89	6.71	1.07	5.58	1.03	2.71	0.35	2.25	0.34
HSRVR093	6.61	2.54	5.52	0.87	4.55	0.83	2.16	0.28	1.76	0.27
HSRVR102										
HSRVR105										
HSRVR112										
HSRVR115										
HSRVR135										
HSRVR136										
HSRVR137										
HSRVR140										
HSRVR146B										
HSRVR177	4.86	1.77	4.55	0.73	3.98	0.77	2.10	0.25	1.63	0.25
HSRVR182										
HSRVR195	14.15	0.86	13.42	2.10	11.94	2.32	7.19	1.01	6.72	1.07
HSRVR196	22.01	2.65	19.44	3.00	18.16	3.66	10.85	1.55	10.16	1.58
Sd007	35.09	5.32	30.36	5.15	32.51	6.78	18.03	2.72	18.42	2.79
Sd013	28.35	0.95	25.90	4.61	29.40	6.39	16.85	2.49	16.94	2.55
Sd017	16.24	2.62	13.02	2.13	12.83	2.60	6.91	1.04	7.39	1.13
Sd036	23.05	3.29	17.51	3.00	18.16	3.75	10.23	1.58	11.69	1.73
Sd042	7.69	2.61	7.22	1.05	5.80	1.11	3.13	0.41	2.63	0.36
Sd048	25.92	3.38	21.70	3.67	22.06	4.47	11.85	1.77	12.27	1.81
Sd061	4.63	1.70	4.88	0.75	4.01	0.78	2.09	0.28	1.83	0.28
Sd067	16.20	1.94	13.76	2.06	10.70	1.98	5.91	0.93	6.78	1.09

ID	Coordinates (Adindan)		elevation	land-use and cover
	X	Y		
HSWL 1	452514	785359	1690	grazing / grassland
HkWL 1	479873	787767	2674	grazing / grassland
HZWL 1	471592	840000	1639	grazing / grassland
HKUWL 1	396217	825798	1888	grazing / grassland
HBWL 1	468149	852149	1600	grazing / grassland
HHWL 1	375249	831074	2200	grazing / grassland
HHWL 2	375285	831879	2209	grazing / grassland
HTWL 1	433257	881178	1819	grazing / grassland
HHWL 3	373967	836715	2309	grazing / grassland
HDOWL 1	397184	877995	2876	grazing / grassland
HGIWL 2	345464	812692	2617	grazing / grassland
HHOWL 1	350680	835279	1986	grazing / grassland
HGIWL 1	355836	825529	2110	grazing / grassland

Annex No. 3

ID	Coordinates (Adindan)		elevation	lithology	Point Load test		Schmidt hammer	weathering	joints		water absorption (%)	porosity (%)	bulk density (g/cm³)
	X	Y			IS 50 (MPa)	UCS (MPa)	compressive strength (MPa)		spacing (m)	opening (m)			
HSR-1	457012	775972	1775	ignimbrite	1.17	27	22.8	SW			40.4	45.8	1.1
HSR-2	459880	781752	2107	ignimbrite	2.98	69	29.1	SW			70.9	29.7	1.4
HSR-3	447480	789892	1747	rhyolite	2.45	56	48.1	SW			4.4	10.3	2.3
HSR-4	452561	785371	1697	trachyte	9.17	211	54.6	SW			1.4	3.4	2.6
HSR-5	455279	784038	1716	trachyte	9.55	220	60	SW	1.5	0.13	1.1	2.8	2.6
HSR-6	462470	793380	2161	ignimbrite	2.91	67	20.3	S-MW			14.2	25.8	1.8
HSR-7	445249	775046	1725	trachyte	9.09	209	57	SW					
HSR-8	445002	774961	1726	basalt	7.16	165	16.2	HW					
HSR-9	438756	799715	1772	obsidian	4.11	94	60	S-MW					
HSR-10	478074	790284	2609	ignimbrite	2.31	53	19.1	SW					
HSR-11	437794	804945	1722	basalt	5.75	132	21.4	S-MW			20.8	33.9	1.6
HSR-12	437489	805880	1686	basalt	9.79	225	24.3	S-MW					
HSR-13	437234	816434	1623	trachyte	2.44	56	27.4	MW					
HSR-14	429280	807200	1842	trachyte	7.22	166	43.9	SW					
HSR-15	436561	812855	1657	obsidian	3.66	84	13.5	SW			5.8	13.3	2.3
HSR-16	461769	804562	1960	ignimbrite	6.59	152	48.1	SW	3.5	0.06	0.2	0.4	2.4
HSR-17	462318	826870	1685	ignimbrite	3.43	79	25.9	S-MW					
HZR-1	460953	877391	1766	trachyte	17.01	391	60	S-MW	5.5	0.15			
HZQ-2A	463859	877253	1672	rhyolite	5.15	119	21.4	SW	1	0.05	0.8	1.9	2.6
HZR-2B	463859	877253	1672	trachyte	12.35	284	30.7	S-MW			11.5	23.1	2
HZR-3	463965	866376	1670	trachyte	8.03	185	14.9	MW			0.7	1.8	2.6
HZR-4	470178	868806	1641	trachyte	1.74	40	25.9	SW					
HDR-1	479402	809589	2125	trachyte	2.59	60	25.9	S-MW					
HDR-2	482407	813328	2129	trachyte	3.69	85	43.9	S-MW					
HDR-3	480682	820631	2015	trachyte	2.42	56	24.3	S-MW			10.7	21	2

ID	Coordinates (Adindan)		elevation	lithology	Point Load test		Schmidt hammer	weathering	joints		water absorpti-on (%)	porosity (%)	bulk density (g/cm³)
	X	Y			IS 50 (MPa)	UCS (MPa)	compressive strength (MPa)		spacing (m)	opening (m)			
HDR-4	472423	826124	1688	rhyolite	3.89	90	21.4	S-MW			9.8	20.1	2.1
HDR-5	483423	829888	1865	rhyolite	0.69	16	41.6	SW			8	17.1	2.1
HDR-6	484937	825124	2090	rhyolite	1.72	40	24.9	SW					
HDR-7	492967	823396	2736	rhyolite	2.37	55	29.1	SW					
HDR-8	492543	819940	2751	rhyolite	3.11	72	17.4	S-MW					
HDR-9	491992	818092	2739	rhyolite	0.97	22	41.8	SW					
HDQ-10	494224	814067	2796	rhyolite	9.07	209	29.1	S-MW					
HDR-12	497955	805678	2877	rhyolite	2.78	64	36.1	SW					
HMR-1	443054	852304	1618	ignimbrite	3.52	81	24.3	S-MW			24.2	38.4	1.6
HMR-2	435915	842844	1596	ignimbrite	3.03	70	20	S-MW			3.3	7.8	2.3
HMR-4	428036	842394	1733	ignimbrite	2.52	58	25.9	S-MW					
HKER-1	484445	832018	1877	rhyolite	8.91	205	50.2	S-MW	0.5	0.04	3.4	7.6	2.2
HKER-4A	494299	849266	2417	ignimbrite	2.1	48	36.1	S-MW					
HTR-1	421309	862049	1982	trachyte	19.49	448	25.9	S-MW					
HTR-2	423934	861440	1946	ignimbrite	6.76	155	32.5	S-MW					
HTR-3	435972	871331	1930	ignimbrite	1.49	34	17.4	MW					
HKUQ-1	396908	803684	1712	ignimbrite	3.1	71	45.9	S-MW	0.3	0.06	19.4	32.4	1.7
HKUR-2	396908	803684	1712	rhyolite	0	0	24.5	S-MW					
HKUR-3	398067	808828	1759	rhyolite	1.7	39	25.9	S-MW					
HKUQ-4	396616	809165	1775	ignimbrite	4.42	102	52.5	S-MW			16.6	30.3	1.8
HKUR-5	393027	816172	1917	ignimbrite	2.27	52	21.5	S-MW			6.5	13.5	2.1
HKUR-6	399074	827917	1900	ignimbrite	2.46	57	30.9	MW			17.1	31.2	1.8
HHQ-2	380108	838135	2174	ignimbrite	3.14	72	20.3	SW			12.7	23.7	1.9
HHQ-3	380432	836788	2155	ignimbrite	2.61	60	13.7	S-MW	1.5				
HHR-5	369867	836569	2200	ignimbrite	1.8	41	16	S-MW					

Annex No. 3 Rock property data (Part 2)

ID	Coordinates (Adindan) X	Y	elevation	lithology	Point Load test IS 50 (MPa)	UCS (MPa)	Schmidt hammer compressive strength (MPa)	weathering	joints spacing (m)	opening (m)	water absorption (%)	porosity (%)	bulk density (g/cm³)
HHR-6	366704	837857	2188	rhyolite	5.92	136	23.3	S-MW					
HHR-8	344792	793128	1338	basalt	5.17	119	60	SW					
HWR-1	389664	847673	2073	ignimbrite	3.47	80	30.7	S-MW					
HWR-4	445002	774961	1726	ignimbrite	2.68	62	13.7	S-MW					
HHOR-4	352251	836115	1943	basalt	7.38	170	39.9	S-MW					
HHOR-1	351537	850411	1870	rhyolite	1.26	29	44.1	S-MW					
HAWR-9	437229	789998	1713	obsidian	5.61	129	60	S-MW					
HFOR-1	360361	870873	1956	rhyolite	2.08	48	30	S-MW					
HFoR-2	356455	867915	1795	rhyolite	5.27	121	33.6	S-MW					
HFOR-4	337941	863355	1648	trachyte	3.26	75	39.9	S-MW					
HFOR-5	337123	862499	1471	trachyte	12.72	292	52.7	S-MW					
HFOR-6	338046	861019	1508	trachyte	7.35	169	43.9	S-MW					
HFOR-7	340404	860222	1370	ignimbrite	12.2	281	33.6	S-MW					
HARR-2	359434	800024	1987	rhyolite	2.68	62	37.5	S-MW	0.5	0.02			
HARR-4	342127	786449	1443	basalt	8.27	190	39.5	S-MW	0.3				
HTR-1	421309	862049	1982	basalt	12.9	297	25.9	S-MW					
HGIR-1	349350	825201	2010	basalt	12.02	276	24.9	S-MW	0.7				
HGIR-2	348591	824037	1997	ignimbrite	3.93	90	30	S-MW					
HGIR-3	358245	822028	2121	ignimbrite	6.28	144	60	S-MW					
HGIO-5	355955	828097	2022	basalt	6.14	141	41.8	S-MW	0.4				
HHR-7	388886	850382	2039	rhyolite	1.35	31	27.4	SW		0.07			
HGJR-1	363245	875734	2015	rhyolite	11.18	257	59.5	S-MW					
HGJR-2	386188	864255	3115	rhyolite	3.93	90	32.5	S-MW					
HSHR-1	373426	799844	2021	ignimbrite	5.34	123	20	S-MW					
HSHQ-2	372491	797523	2054	ignimbrite	3.15	72	30	S-MW		0.03			

ID	Coordinates (Adindan)		elevation	lithology	Point Load test		Schmidt hammer	weathering	joints		water absorpti-on (%)	porosity (%)	bulk density (g/cm³)
	X	Y			IS 50 (MPa)	UCS (MPa)	compressive strength (MPa)		spacing (m)	opening (m)			
HSHR-3	365811	794429	1845	rhyolite	1.83	42	25.9	S-MW					
HDOR-1	479402	809589	2125	ignimbrite	2.6	60	43.9	S-MW					
HDOR-2	482407	813328	2129	ignimbrite	2.92	67	33.6	S-MW					
HDOR-4	472423	826124	1688	ignimbrite	2.44	56	13.7	S-MW					
HAGQ-1	374487	814007	2168	ignimbrite	3.24	75	17.4	HW	0.4				
HAGQ-2	382175	807364	2071	ignimbrite	3.61	83	32.5	HW					
HCR-2	493816	874730	1717	ignimbrite	0.84	19	20	MW					
HCR-3	493182	875801	1726	basalt	5.55	128	29.1	S-MW	2				
HCR-4	496955	870651	1914	ignimbrite	5.16	119	24.3	S-MW					
HCR-5	433938	869303	1688	ignimbrite	6.85	158	23.3	S-MW	1.5				
HCR-6	492916	866718	1895	ignimbrite	4.18	96	21.5	MW					
HCR-7	473743	868635	1715	obsidian	3.69	85	48.1	S-MW			15.1	26.7	1.8
HCR-8	474460	869085	1729	ignimbrite	4.06	93	14.9	S-MW			0.4	0.9	2.3
HCR-9	484286	866577	1657	basalt	6.58	151	41.6	S-MW			8.4	15	1.8
HCR-10	487734	868197	1778	basalt	15.74	362	30.7	S-MW					
HCR-11	490082	868848	1994	ignimbrite	2.03	47	20	S-MW			1.5	4.1	2.8
HCR-12	472350	868929	1968	obsidian	2.65	61	60	SW			36	46.3	1.3
HKER-6	477816	850809	1683	rhyolite	6.38	147	35.5	S-MW			0.2	0.5	2.4
HKER-7	479311	851280	1657	ignimbrite	3.74	86	26.5	S-MW					
HZR-5	467974	869211	1660	ignimbrite	4.97	114	18	MW					
HBR-1	447875	833797	1683	ignimbrite	5.25	121	26.5	S-MW					
HNR-4	461192	826605	1634	ignimbrite	1.7	39	18.6	S-MW					
HNR-5	459454	826767	1570	ignimbrite	1.41	32	36.1	M-HW					
HKUR-8	410522	817767	2039	trachyte	9.2	212	39.9	S-MW					
HHQ-4	376864	846546	2391	ignimbrite				HW					

Annex No. 3 Rock property data (Part 4)

ID	Coordinates (Adindan)		elevation	lithology	Point Load test		Schmidt hammer	weathering	joints		water absorption (%)	porosity (%)	bulk density (g/cm³)
	X	Y			IS 50 (MPa)	UCS (MPa)	compressive strength (MPa)		spacing (m)	opening (m)			
HAGQ-5	363677	805821	2556	ignimbrite				S-MW					
HARQ-1	360166	795889	1758	ignimbrite				HW					
HARQ-2	359434	800024	1987	ignimbrite				HW					
HwQ-1	399342	840516	2032	ignimbrite				SW					
HTQ-3	428651	883986	1838	basalt				SW					
HDOQ-1	407002	865192	2138	ignimbrite				SW					
HTQ-2	425772	884585	2103	ignimbrite			45.9	SW		0.05			
HDOQ-2	408493	869594	2160	ignimbrite				S-MW					
HDOQ-3	404784	871255	2494	rhyolite			24.3	S-MW	0.5	0.03			
HDOQ-4	392350	864237	2383	ignimbrite				S-MW					
HFOQ-1	360360	870873	1956	basalt				S-MW					
HFOQ-2	356455	867915	1795	ignimbrite				S-MW					
HGIQ-1	349350	825201	2010	rhyolite				S-MW	0.3	0.02			
HHQ-6	369867	836569	2200	rhyolite				S-MW					
HHQ-7	366704	837857	2188	ignimbrite				S-MW					
HHOQ-1	356258	835965	2012	rhyolite				S-MW	0.4	0.03			
HGIQ-2	348591	824037	1997	rhyolite				S-MW					
HGJQ-2	382117	881997	2583	rhyolite				S-MW					
HGJQ-3	385135	878985	2712	basalt				S-MW					
HGJQ-1	386188	864255	3115	basalt				S-MW					
HHQ-8	372279	833418	2301					HW					
HCQ-1	491231	878196	1714	scoria				SW	0.5	0.04			
HAWQ-1	441555	773969	1727	rhyolite			29.1	S-MW					
HKUQ-2	397590	805825	1722	ignimbrite				S-MW					
HKUQ-4	399500	828489	1923	ignimbrite				S-MW	0.5	0.04			

ID	Coordinates (Adindan)		elevation	lithology	Point Load test		Schmidt hammer	weathering	joints		water absorpti-on (%)	porosity (%)	bulk density (g/cm³)
	X	Y			IS 50 (MPa)	UCS (MPa)	compressive strength (MPa)		spacing (m)	opening (m)			
HKUQ-5	403248	825322	1871	ignimbrite				M-HW					
HSQ-2	456992	776682	1734					S-MW					
HSQ-3	457023	775968	1775					HW	0.4	0.01			
HSQ-4	468752	787348	2446					MW					
HAGQ-2	372618	820932	2131	pyroclastic deposit				HW					
HAGQ-1	372633	821483	2143	ignimbrite				MW					
HHQ-3	375205	840242	2298	ignimbrite				HW					
HNQ-1	481769	804562	1960	ignimbrite				SW					
HNQ-2	460902	806665	1891	ignimbrite				SW		0.01	5.7	12.9	2.3
HNQ-3	464027	820355	1849	ignimbrite				mw					
HKQ-6	494689	775297	2581	scoria				SW			10.5	20.9	2
HZQ-1	461513	877400	1756	trachyte				SW					
HAWQ-3	445375	777967	1749	basalt			39.5	SW					
HAWQ-4	445467	779559	1720	scoria and ignimbrite				SW					
HAWQ-5	444348	780530	1713	scoria				SW					
HSQ-1	455572	787566	1886	pyroclastic deposit				S-MW					
HSQ-2	456992	776682	1734	ignimbrite				S-MW					
HSQ-3	457023	775968	1775	ignimbrite				S-MW	0.5	0.02			
HSQ-4	468752	787348	2446	ignimbrite				S-MW					
HSQ-6	450713	798441	1815	ignimbrite				S-MW					
HSQ-7	446366	800938	1791	scoria				MW					
HAQ-1	437022	809418	1699	scoria				MW					
HAQ-2	429534	806824	1838	rhyolite				S-MW			3	8.4	2.8
HAQ-3	432660	805800	1679					S-MW					

ID	Coordinates (Adindan) X	Y	elevation	lithology	Point Load test IS 50 (MPa)	UCS (MPa)	Schmidt hammer compressive strength (MPa)	weathering	joints spacing (m)	opening (m)	water absorption (%)	porosity (%)	bulk density (g/cm³)
HGJR-5	385739	862974	3025	rhyolite			17.4	S-MW		0.06			
HGJR-4	387981	867854	2911	rhyolite			30.9	S-MW	0.7	0.01			
HFOR-3	339261	864668	2058	ignimbrite			30	MW					
HAQ-8	437691	804895	1705	scoria			20.3	S-MW					
HDR-11	497591	807898	2866	rhyolite			20	MW					
HWR-3	401088	853697	2054	rhyolite			24.5	S-MW					
HAQR-8	340404	804000	1370	trachyte			33.6	S-MW					
HFOR-8	341136	858699	1157	trachyte			30	S-MW					
HDOR-1	405008	859438	2023	ignimbrite			43.9	S-MW					
HDOR-2	410757	868635	2057	ignimbrite			33.6	S-MW	0.5	0.02			
HDOR-3	404784	871255	2494	ignimbrite			24.3	S-MW					
HGIR-1	349350	825201	2050	basalt			24.9	SW					
HGIR-2	348591	824037	1997	ignimbrite			30	S-MW					
HGRI-3	358245	822028	2121	ignimbrite			60	S-MW					
HGIR-4	359602	828554	2039	rhyolite			59.5	S-MW					
HGIR-5	355955	828097	2022	basalt			41.8	S-MW					
HGIR-6	348222	822683	2042	basalt			21.8	S-MW					
HARR-2	359434	800024	1987	rhyolite			37.5	S-MW					
HARR-3	340056	786063	1433	rhyolite			20.3	MW			2.7	7.8	2.8
HARR-4	342127	786449	1443	basalt			39.5	S-MW					
HRR-1	405774	783578	1679	ignimbrite			14.9	S-MW			5.9	13.2	2.2
HHR-1	375625	835436	2248	ignimbrite			54.8	M-HW					
HHR-2	380108	838135	2174	ignimbrite			20.3	S-MW					
HHR-3	380432	836788	2155	ignimbrite			13.7	SW					
HHR-5	369867	836569	2200	ignimbrite			16	S-MW					

ID	Coordinates (Adindan) X	Y	elevation	lithology	Point Load test IS 50 (MPa)	UCS (MPa)	Schmidt hammer compressive strength (MPa)	weathering	joints spacing (m)	opening (m)	water absorption (%)	porosity (%)	bulk density (g/cm³)
HHR-6	366704	837857	2188	rhyolite			23.3	S-MW					
HHR-7	388886	850382	2039	rhyolite			27.4	S-MW					
HWR-1	389664	847673	2073	ignimbrite			37.9	S-MW					
HWR-2	399342	840516	2032	ignimbrite			21.8	S-MW	0.8	0.04			
HWR-3	401088	853697	2054	rhyolite			24.5	S-MW					
HSHR-1	373426	799844	2021	ignimbrite			20	S-MW					
HSHR-2	372491	797523	2054	ignimbrite			30	S-MW					
HSHR-3	365811	794429	1845	rhyolite			25.9	S-MW					
HHOR-1	351537	850411	1870	rhyolite			44.1	S-MW					
HHOR-2	354771	847612	1892	ignimbrite			48.1	S-MW					
HHOR-3	356318	835944	1999	rhyolite			24.5	S-MW					
HHOR-4	352251	836115	1943	basalt			39.9	SW					
HAGR-1	374487	814007	2168	ignimbrite			17.4	S-MW	1.5				
HAGR-2	382175	807364	2071	ignimbrite			32.5	S-MW	0.4				
HBR-1	447875	833797	1683	ignimbrite			26.5	S-MW					
HFOR-9	356455	867915	1795	ignimbrite			33.6	S-MW		0.08			
HHR-8	344792	793128	1338	basalt			60	FRESH					
HHR-9	344818	792068	1470	ignimbrite			60	SW					
HHR-10	344775	793097	1387	basalt			57.5	SW					
HHR-11	369921	836663	2202	ignimbrite			31.8	SW					
HNR-2	461050	806721	1887	ignimbrite			24.3	S-MW					
HCR-1	476111	869515	1613	ignimbrite			16	S-MW					
HSR-1	459739	782263	1964	ignimbrite			23.3	S-MW		0.03			
HZR-2	461731	877994	1869	rhyolite			21.4	S-MW					
HKUR-9	408480	804625	1947	ignimbrite			36.1	S-MW					

ID	Coordinates (Adindan) X	Y	elevation	lithology	Point Load test IS 50 (MPa)	UCS (MPa)	Schmidt hammer compressive strength (MPa)	weathering	joints spacing (m)	opening (m)	water absorption (%)	porosity (%)	bulk density (g/cm³)
HAWR-8	431754	774267	1723	ignimbrite			17.4	MW					
HKER-3	492881	838921	2554	ignimbrite			18.2	MW					
HKER-2	491624	837039	2538	rhyolite			18.6	S-MW					
HKER-5	453844	856218	1852	basalt			23.3	S-MW					
HAJR-7	436561	812855	1657	basalt			32.5	S-MW					
HMR-3	841213	433921	1626	ignimbrite			25.9	S-MW					
HAR-5	818345	436666	1605	basalt			16	S-MW					
HAR-3	814200	436580	1654	basalt				MW					
CHCSS-3	493182	875501	1726	basalt				SW	2	0.25			
HAWR-10	438898	787633	1684	obsidian				S-MW					
HSF- 1	453034	785260	1699	trachyte				MW					
HKEF -1	477848	850512	1673	trachyba-salt				S-MW					
HCF- 1	496054	873019	1799	ignimbrite				SW					
HFOF- 1	359431	871544	1953	ignimbrite				MW					
HFOF- 3	337123	862499	1471	ignimbrite				S-MW					
HFOF- 2	346425	858775	1441	ignimbrite				MW					

ID	Coordinates (Adindan)		elevation	depth (m)	UCS (MPa)	specific soil density (g/cm³)	plastic limit of soil (%)	liquid limit of soil (%)	plasticity index (%)	Description
	X	Y								
HRTP 1A	415617	793343	1936	0.5						dark grey, stiff, massive, dry, coarse, low plasticity, high diletancy, has planty root on the top of sandy soil, well sorted, poorly graded
HRTP 2A	411097	796198	1871	0.5	3.25					light grey, less stiff, massive, dry, fine to medium, low plasticity, high diletancy, have concretion, silty
HRTP 2B	411097	796198	1871	1		1.9				yellowish gray, less stiff, massive, less moist, fine to medium, low plasticity, high diletancy, silty sand
HRTP 3A	403791	794337	1761	0.5	2	1.9				light grey, stiff, massive, dry, fine to medium, low plasticity, high diletancy, have concretion, silty soil, road cut
HRTP 5	399114	777108	1544	2		2.1				yellowish grey, stiff, massive, dry, fine, low plasticity, high diletancy, some concretions, silty alluvial soil along River Bilate
HR TP 4	412046	776956	1733	1		1.9				light grey, silty, massive, dry, fine, low plasticity, high diletancy, have concretion, sility,
HS TP 1	457353	790235	2062	1.1	2.5	2				brown grey, moderately stiff, heterogenous, dry, fine to medium grain size, moderately plastic, medium diletaancy, some concretion, well-sorted, finer up ward, 15cm thick pyroclastic deposit
HSTP 2	447419	791333	1774	4		2				light brown, stiff, fissured, blocky, prismatic, dry, fine to medium, low plasticity, high diletancy, some concretion, well sorted, poorly graded, gully erosion, the soil sandwiched by pumice and tuff
HSTP 3	465918	790535	2333	1.3	2.75					brown, less stiff, fissured, prismatic, dry, medium to coarse grained, low plasticity, high diletancy, shows concretion, heterogenous structure, residual soil silty sandy soil
HSTP 6A	450713	798441	1815	0.8						yellowish grey, moderately stiff, fissured, medium plasticity and diletancy, road cut
HSTP 6B	450713	798441	1815	3.2						light grey, soft, moderately stiff , dry, fine grain, low plasticity, high diletancy, road cut
HS TP 6C	450713	798441	1815	1						dark grey, stiff, massive, dry, coarse, low plasticity, high diletancy, has planty root on the top of sandy soil, well sorted, poorly graded

ID	Coordinates (Adindan) X	Y	elevation	depth (m)	UCS (MPa)	specific soil density (g/cm³)	plastic limit of soil (%)	liquid limit of soil (%)	plasticity index (%)	Description
HKUTP 1A	414714	809382	1812	0.5	1.5	2				yellowish brown, moderately stiffe, dry, fine, low plasticity, medium diletancy, residual soil
HKUTP 1B	414714	809382	1812	2		1.8				light grey, slightly stiff, massive, dry, low plasticity, medium diletancy, some concretion, silty to sandy
HKUTP 1C	414714	809382	1812	0.5	1.25	2.1	35	39	4	yellowish brown, moderately stiff, homogenous, dry, fine, low plasticity, medium, diletancy, all of the three samples a, b, c are residual and a slope cut for ponding
HKUTP 2A	390938	807704	1807	0.6						black, stiff, fissured, dry, fine, high plasticity, low diletancy, have concretion, residual soil
HKUTP 2B	390938	807704	1807	4.4						yellowish, stiff, fissure, dry, fine, moderately plastic and diletancy, have concretion, silty clay, residual
HKUTP 3A	395346	812399	1838	0.5						light grey, less stiff, fissured, dry, fine, low plasticity, high diletancy, residual soil, erosion cut
HNTP 1	461192	826605	1634	4						yellowish, soft, slightly stiff, heterogenous, dry, fine grained, low plasticity, high diletancy, have concretion, poorly sorted and graded, lacustrine deposit near to Lake Shalla and overlain by transported sediment
HNTP 2A	467318	810669	2013	3	2	2				yellowish, firm, homogenous, moist, fine to medium, low plasticity, high diletancy, has concretion, silty to sandy residual
HNTP 2B	467318	810669	2013	1	2.1	2.1				dark, firm, fissured, dry, fine, high plasticity, low diletancy, clay residual
HNTP 2C	467318	810669	2013	0.5	1.5	2.1				light grey, soft massive, dry, fine to medium, medium plasticity and diletancy, show concretion residual
HNTP 5A	458357	801916	1914	1.2	1.75					dark to brown, soft to massive, dry, fine, high plasticity, low diletancy, silty soil, overlain by 0.25 m thick pyroclastic deposit
HNTP 5B	458357	801916	1914	1.2	1.75					light grey, fine, soft, massive, dry
HMTP 1A	429214	855594	1833	0.5		2				light grey, stiff, fissured, dry, fine, low plasticity, high diletancy, have concretion, plant root observed residual soil

ID	Coordinates (Adindan) X	Coordinates (Adindan) Y	elevation	depth (m)	UCS (MPa)	specific soil density (g/cm³)	plastic limit of soil (%)	liquid limit of soil (%)	plasticity index (%)	Description
HMTP 1B	429214	855594	1833	2.5		2.32	26	43	17	yellowish grey, moderately stiff, fissured, dry, fine, to medium grained, moderately plastic and diletancy, have some concretion, residual
HATP 1A	424008	805769	1912	0.04		2				yellowish grey, less stiff, homogenous, dry, fine to medium, low plasticity, high diletency, have concretion, residual/lacustrine
HATP1B	424008	805769	1912	0.06		1.9				yellowish, less stiff, massive structure, dry, fine to medium, low plasticity, high diletancy, have some concretion, residual lacustrine
HKETP 1A	488490	837261	2490	2						light grey to brown, stiff, fissure, dry, fine to medium, low plasticity, high diletancy, have concretion
HKETP 1B	488490	837261	2490	1						light grey, stiff, fissured, dry
HKETP 2	497263	842673	2582	1.5	0.5					dark to light grey, moderately stiff, massive, fine, medium to high plasticity, low diletancy, moist, residual soil
HDTP 1	495073	829069	2744	2.3	2	2.4	34	49	15	reddish, less stiff, fissured, moist, fine, low plasticity, high diletancy
HTTP 1A	430307	859381	1869	0.9						light grey, stiff, masive, dry, fine, moderately plastic and diletancy, has some concretion, clay silt, residual
HTTP1B	430307	859381	1869	1.6						yellowish, stiff, massive, moist, fine, moderately plastic and diletancy, silty clay, residual
HTTP 2A	430322	863598	1870	1.1	2.75	2.3				yellowish, stiff, layering, dry, coarse, low plasticity, highy diletancy, have concretion, poor sorting, gap graded, sandy gravel, alluvial
HTTP2B	430322	863598	1870	0.4	2.5	2	31	39	4	light grey, stiff, fissured, dry, fine to moderate, medium plasticity, medium diletancyhave concretion, silty clay,
HTTP 2C	430322	863598	1870	0.8	2.5	1.9				dark brown, stiff, fissure, dry, fine, high plasticity, low diletancy, have some concretion, silty to clay, road cut, gully, residual
HTTP 3A	440155	874337	2045	0.5						light grey, moderately dense, fissured, dry, fine, low plasticity, high diletancy, has concretion, silty clay

ID	Coordinates (Adindan) X	Y	elevation	depth (m)	UCS (MPa)	specific soil density (g/cm³)	plastic limit of soil (%)	liquid limit of soil (%)	plasticity index (%)	Description
HTTP 3B	440155	874337	2045	2.6						yellowish, stiff, dry, fine, moderately plastic, and diletancy, road cut, clay silty, residual
HKTP 4A	473371	783641	2628	0.5	1.5					dark grey, fine, low plasticity, high diletancy, homogenous, use the area of the soil for irrigation purpose,
HKTP 4B	473371	783641	2628	3.5	2.25					reddish, silty clay, massive, moist, fine to medium grain size, medium plasticity and diletancy
HHTP 1	840320	375491	2318	5	1.5					light grey, soft, fissured, moist, high plasticity, low diletancy, residual soil, slope cut
HHTP 2	370276	856785	2509	2		2.6				reddish brown, stff, massive, dry, fine, moderately plastic and moderately diletancy, exposed along road cut and slope cut
HGJTP 1	370275	856781	2501	2		2.3	51	70	19	reddish brown, stiff, massive, dry, fine, highly plastic and low diletancy, slope cut, river valley
HHTP 3	375256	832018	2213	5		2.6				reddish brown, stiff, massive, fine to medium grained, moderately plastic and diltancy, residual soil
HAGTP 1	378533	812540	2202	2	2.5	2.3				light grey, soft, fissured, moist, fine, high plasticity, low diletancy, residual, slope cut
HSHTP 1	377952	775321	1879	4						grey, stiff, fissured, dry, fine to medium grained, high plasticity, low diletancy and has some concretion, residual soil, along road cut
HSTP 2	367757	782360	1842	2	3.5	2.3				reddish, dry, stiff, fissured, fine grained, moderately plastic, no concretion and has moderate diletancy, residual lateritic soil, gully
HAR 1	386902	780423	1728	5		2.3				yellowish grey, stiff, massive, fine grain size, low plasticity, high diletancy and has some concretion, exposed along kula River Kula cut, residual, slope cut
HDOTP 1	403039	875574	2646	1.5		2.3				reddish, soft, massive, moist, fine high plasticity, low diletancy and no concretion clay soil, residual soil, river valley
HFOTP 2	337823	869146	2890	2.5		2.6				reddish, stiff, massive, moist, fine grained, high plasticity, low diletancy, have concretion clay soil, residual soil

Annex No. 4 Soil property data (Part 4)

ID	Coordinates (Adindan)		elevation	depth (m)	UCS (MPa)	specific soil density (g/cm³)	plastic limit of soil (%)	liquid limit of soil (%)	plasticity index (%)	Description
	X	Y								
HGJTP 1A	385604	861711	2944	2	2.5					reddish, soft, massive, moist, fine grained, highly plastic, low diletancy, low concretion, clay soil, residual soil, slope cut
HGJTP 1B	385604	861711	2944	3	2.5	2.4				yellowish, soft, massive, moist, fine grained, low plasticity, high diletancy, has concretion, clay soil, residual soil, gully
HFOTP 1	349906	862304	1562	3.5						dark grey, less stiff, massive, moist, fine grained, highly plastic, low diletancy, has concretion, residual soil alon road cut
HGJTP 2	363012	867673	2029	4		2.6				reddish, soft, massive, moist, fine grained, highly plastic, low diletancy, have no concretion, residual soil, along road cut
HHOTP 1	351613	851894	1929	2.5	2	2.4				reddish, soft, massive, moist, highly plastic, low diletancy, have no concretion, clay soil, along road cut
HGIT 1	354387	825093	2085	2		2.2				dark grey, stiff, fissured, dry, fine, highly plastic, low diletancy, has some concretion, residual, gully
HGJT 3	384721	880110	2734	2.5		2.5				reddish brown, stiff, fissured, dry, fine grained, highly plastic, low diletancy, clay soil, road cut
HGITP 2	355302	818397	2269	2.5		2.5				reddish, soft, massive, moist, fine grained, highly plastic, low diletancy, have no concretion, residual soil, along road cut

ID	Coordinates (Adindan)		Purpose	Operated by	Status	Accesibility
	X	Y				
HSQ 1	455572	787566	Construction	machine	existing	good
HSQ 2	456992	776682	Construction	machine	existing	good
HSQ 3	457023	775968	Construction	machine	existing	good
HSQ 4	468752	787348	road fill	machine	existing	good
HSQ 6	450713	798441	road fill	machine	existing	good
HSQ 7	446366	800938	Construction	manual	existing	good
HAQ 1	437022	809418	road fill	manual	existing	good
HAQ 2	429534	806824	Construction	manual	existing	good
HAQ 3	432660	805800	Construction	machine	existing	good
HAQ 8	437691	804895	Construction	machine	existing	good
HNQ 1	481769	804562	Construction	manual	existing	good
HNQ 2	460902	806665	Construction	manual	existing	good
HNQ 3	464027	820355	road aggregate	machine	existing	good
HKQ 6	494689	775297	road aggregate	machine	existing	good
HZQ 1	461513	877400	Construction	manual	existing	good
HZQ 2	463859	877253	road aggregate	machine	existing	good
HDQ 1	494224	814067	Construction	manual	existing	good
HAWQ3	445375	777967	road aggregate	manual	existing	good
HAWQ 4	445467	779559	road aggregate	machine	existing	good
HAWQ 5	444348	780530	road aggregate	machine	existing	good
HCQ 1	491231	878196	road construction	manual	existing	good
HAWQ 1	441555	773969	Construction	manual	existing	good
HKUQ 1	396908	803684	Construction	manual	existing	good
HKUQ 2	397590	805825	Construction	machine	existing	good
HKUQ 3	396616	809165	Construction	manual	existing	good
HKUQ 4	399500	828489	Construction	manual	existing	good
HKUQ 5	403248	825322	road construction	machine	existing	good
HSQ 2	456992	776682	Construction	manual	existing	good
HSQ 3	457023	775968	Construction	machine	existing	good
HSQ 4	468752	787348	road fill	machine	existing	good
HHQ 2	380108	838135	Construction	machine	existing	good

ID	Coordinates (Adindan)		Purpose	Operated by	Status	Accesibility
	X	Y				
HAGQ 2	382175	807364	road fill	machine	existing	good
HAGQ 1	374487	814007	road fill	machine	existing	good
HHQ 3	375205	840242	road fill	machine	existing	good
HHQ 4	376864	846546	road fill	machine	existing	good
HAGQ 5	363677	805821	road fill	manual	existing	good
HARQ 1	360166	795889	Construction	machine	existing	good
HARQ 2	359434	800024	Construction	machine	existing	good
HwQ 1	399342	840516	road fill	machine	existing	good
HTQ 3	428651	883986	Construction	manual	existing	good
HDOQ 1	407002	865192	road fill	manual	existing	good
HTQ- 2	425772	884585	Construction	manual	existing	good
HDOQ 2	408493	869594	road fill	manual	existing	good
HDOQ 3	404784	871255	road fill	manual	existing	good
HDOQ 4	392350	864237	road fill	machine	existing	good
HFOQ 1	360360	870873	Construction	machine	existing	good
HFOQ 2	356455	867915	Construction	machine	existing	good
HGIQ 1	349350	825201	road construction	manual	existing	good
HHQ 6	369867	836569	Construction	manual	existing	good
HHQ 7	366704	837857	Construction	manual	existing	good
HHOQ 1	356258	835965	road construction	machine	existing	good
HGIQ 2	348591	824037	Construction	manual	existing	good
HGJQ 2	382117	881997	road fill	machine	existing	good
HGJQ 3	385135	878985	road construction	machine	existing	good
HGJQ 1	386188	864255	road fill	machine	existing	good
HHQ 8	372279	833418	road construction	machine	existing	good